

UNIVERSIDADE DE LISBOA
FACULDADE DE CIÊNCIAS
DEPARTAMENTO DE FÍSICA



**Mining the Brain to Predict Gait Characteristics:
A BCI study**

Inês Isabel Rodrigues Domingos

Mestrado Integrado em Engenharia Biomédica e Biofísica
Perfil em Sinais e Imagens Médicas

Dissertação orientada por:
Professor Guang-Zhong Yang
Professor Alexandre Andrade

2018

“Never give up on what you really want to do. The person with big dreams is more powerful than one with all the facts.”

— Albert Einstein

Acknowledgements

First, I would like to thank to the Erasmus+ Program and to the University of Lisbon for given me the financial support to carry this project in London.

I must acknowledge Professor Guang-Zhong Yang and Dr Fani Deligianni, for the warm welcome in the Hamlyn Centre group and for all the academic support. It was as honour to work under their supervision. I must also acknowledge my internal supervisor, Professor Alexandre Andrade, for the support during my thesis.

I would also like to acknowledge Jian-Qing Zheng, Jahanshah Fathi, Miao Sun and Dan-Dan Zhang for their help and contribution.

A big thank you to my friends, Mariana and Joana, for sharing this amazing experience with me and for always being there when I needed.

This journey would not have been possible without the support of my family. To my grandparents, thank you for supporting me through all these years.

Finally, I must express my very profound gratitude to my biggest support in life, my parents, who supported me emotionally and financially. Without them, this thesis wouldn't have been possible. I owe everything I am today, and everything I accomplished, to them. They are the ones who always encouraged me to follow my dreams and taught me not to be afraid to dream bigger and to fight for what I want. Thank you for raising me in the best way possible and for always believing in me.

Abstract

Gait adaptation is one of the most relevant concepts in gait analysis and its neuronal origin and dynamics has been extensively studied in the past few years. In terms of neurorehabilitation, gait adaptation perturbs neuronal dynamics and allows patients to restore some of their motor functions. In fact, lower-limbs robotic devices and exoskeletons are increasingly used to facilitate rehabilitation as well as supporting daily life functions. However, their efficiency and safety depend on how well they can detect the human intention to move and adapt the gait.

Motor imagery (MI), an emerging practise in Brain Computer Interface (BCI), is defined as the activity of mentally simulating a given action, without the actual execution of the movement. MI classification performance is important in order to develop robust brain computer interface environments for neuro-rehabilitation of patients and robotic prosthesis control.

In the first section of this thesis, it was performed a number of motor imagery tasks along with actual movements of the limbs to compare the classification performance of a dry 16-channel and a wet, 32-channel, wireless (Electroencephalography) EEG system. Results showed the feasibility of home use of dry electrode systems with a small number of sensors, and the possibility to discriminate between left and right MI tasks for both arms and legs, with a relatively high accuracy.

The second part of this thesis presents a gait adaptation scheme in natural settings. This procedure allows the monitorization of subjects in more realistic environments without the requirement of specialized equipment such as treadmill and foot pressure sensors. Gait characteristics were extracted based on a single RGB camera, and EEG signals are monitored simultaneously. This method demonstrated that it is possible to detect adaptation steps with more than 90% accuracy, when subjects tries to adapt their walking speed to a higher or lower speed.

Key words: BCI, EEG, Electroencephalography, Gait, Gait adaptation, Motor Imagery, Neurorehabilitation.

Resumo

A locomoção é uma das atividades mais comuns e relevantes da vida quotidiana, sendo que envolve a ativação dos sistemas nervoso e músculo-esquelético. Os distúrbios da locomoção são comuns principalmente na população idosa, sendo que frequentemente estão associados a uma diminuição da qualidade de vida. A ocorrência destes distúrbios aumenta com a idade, estimando-se que aproximadamente 10% das pessoas com idades entre 60 e 69 anos sofram de algum tipo de distúrbio da locomoção, enquanto esse número aumenta para mais de 60% em pessoas com idade superior a 80 anos. Os padrões da locomoção são influenciados por doenças, condições físicas, personalidade e humor, sendo que um padrão anormal ocorre quando uma pessoa não é capaz de andar da maneira usual, maioritariamente devido a lesões, doenças ou outras condições subjacentes. As causas dos distúrbios da marcha incluem condições neurológicas e músculo-esqueléticas. Um grande número de condições neurológicas pode causar um padrão de marcha anormal, como por exemplo um acidente vascular cerebral, paralisia cerebral ou a doença de Parkinson. Por outro lado, as causas músculo-esqueléticas devem-se principalmente a doenças ósseas ou musculares.

A avaliação ou análise da marcha, inclui a medição, descrição e avaliação das variáveis que caracterizam a locomoção humana. Como resultado, este estudo permite o diagnóstico de várias condições, bem como avaliar a progressão da reabilitação e desenvolver estratégias de intervenção. Convencionalmente, a marcha é estudada subjetivamente com protocolos observacionais. No entanto, recentemente foram desenvolvidos métodos mais objetivos e viáveis. Os métodos de análise da marcha podem ser classificados em laboratoriais ou portáteis. Embora a análise baseada em laboratório utilize equipamentos especializados, os sistemas portáteis permitem o estudo da marcha em ambientes naturais e durante atividades da vida diária. A análise laboratorial da marcha é baseada principalmente em informações de imagem e vídeo, embora sensores de piso e placas de força também sejam comuns. Por outro lado, os sistemas portáteis consistem em um ou vários sensores, ligados ao corpo.

A adaptação da locomoção é um dos mais relevantes conceitos na análise da mesma, sendo que a sua origem e dinâmica neuronal têm sido amplamente estudadas nos últimos anos. A adaptação da marcha reflete a capacidade de um sujeito em mudar de velocidade e direção, manter o equilíbrio ou evitar obstáculos. Em termos da reabilitação neurológica, a adaptação da locomoção interfere na dinâmica neuronal, permitindo que os pacientes restaurem certas funções motoras. Atualmente, os dispositivos robóticos para membros inferiores e os exoesqueletos são cada vez mais usados não só para facilitar a reabilitação motora, mas também para apoiar as funções da vida diária. No entanto, a sua eficiência e segurança depende da sua eficácia em detetar a intenção humana de mover e adaptar a locomoção. Recentemente, foi demonstrado que o ritmo auditivo tem um forte efeito no sistema motor. Consequentemente, a adaptação tem sido estudada com base em ritmos auditivos, onde os pacientes seguem tons de estimulação para melhorar a coordenação da marcha.

A imagem motora (MI), uma prática emergente em BCI, ou interface cérebro-máquina, é definida como a atividade de simular mentalmente uma determinada ação, sem a execução real do movimento. O desempenho da classificação da MI é importante para desenvolver ambientes robustos de interface cérebro-máquina, para neuro-reabilitação de pacientes e controle de próteses robóticas. O desempenho da classificação da MI é importante para desenvolver ambientes robustos de interface cérebro-máquina, para neuro-reabilitação de pacientes e controle de próteses robóticas, uma vez que, estudos anteriores, concluíram que realizar uma sessão de MI ativa parcialmente as mesmas regiões cerebrais que o desempenho da tarefa real. Inicialmente, as tarefas de MI centravam-se apenas nos movimentos dos membros superiores, no entanto, recentemente, estas começaram também a focar-se nos movimentos dos membros inferiores, de modo a estudar a locomoção humana. A deteção da intenção motora em tarefas de MI enfrenta vários desafios, mesmo para duas classes (esquerda / direita,

por exemplo), sendo que um dos principais desafios se deve ao número, localização e tipo de elétrodos de EEG usados.

Recentemente, um número crescente de estudos investigou a atividade cerebral durante a locomoção humana. Esses estudos, baseados maioritariamente no EEG, encontraram várias relações entre regiões cerebrais e ações ou movimentos específicos. Por exemplo, concluiu-se que a atividade cerebral aumenta durante a caminhada ou a preparação para caminhar e que a potência nas bandas μ e β diminui durante a execução voluntária do movimento. Em termos de adaptação da marcha, foi demonstrado que a atividade eletrocortical varia de acordo com a tarefa motora executada. Recentemente, as Interfaces Cérebro-Máquina permitiram o desenvolvimento de novas terapias de reabilitação para restaurar as funções motoras em pessoas com deficiências na locomoção, envolvendo o SNC para ativar dispositivos externos.

Na primeira parte desta tese, foram realizadas várias tarefas de MI, juntamente com os movimentos reais dos membros inferiores, de modo a comparar o desempenho da classificação de um sistema wireless de 16 elétrodos secos com um sistema wireless de 32 elétrodos com gel condutor. A extração e classificação das características do sinal foram também avaliadas com mais de um método (LDA e CSP). No final, a combinação de um filtro beta passa-banda com um filtro RCSP mostrou a melhor taxa de classificação. Embora durante a aquisição do EEG todos os canais tenham sido utilizados, durante os métodos de processamento, foram escolhidas duas configurações específicas, onde os elétrodos foram selecionados de acordo com sua posição relativamente ao córtex motor. Desde modo, infere-se que uma seleção cuidada da localização dos elétrodos é mais importante do que ter um denso mapa de elétrodos, o que torna os sistemas EEG mais confortáveis e de fácil utilização. Os resultados mostram também a viabilidade do uso doméstico de sistemas de elétrodos secos com um reduzido número de sensores, e a possibilidade de diferenciar entre as tarefas de MI (esquerda e direita), para ambos os membros, com uma precisão relativamente alta.

Por outro lado, a segunda parte desta tese apresenta um esquema de adaptação da marcha em ambientes naturais. De modo a avaliar a adaptação da marcha, os sujeitos seguem um tom rítmico que alterna entre três modos distintos (lento, normal e acelerado). As características da locomoção foram extraídas com base numa câmara RGB, sendo que os sinais de EEG foram monitorados simultaneamente. De seguida, estas características bem como as informações do tempo de reação foram utilizadas para extrair as etapas de adaptação da marcha versus etapas de não adaptação. De modo a remover os artefactos presentes no EEG, devidos maioritariamente ao movimento do sujeito, o sinal foi filtrado com um filtro passa-banda e sujeito a uma análise de componentes independentes (ICA). Posteriormente, as características de adaptação da marcha do EEG foram investigadas com base em dois problemas de classificação: i) classificação dos passos em direito ou esquerdo e ii) etapas de adaptação versus não adaptação da marcha. As características foram extraídas com base em padrões espaciais comuns (CSP) e padrões espaciais comuns regularizados (RCSP). Os resultados mostram que é possível discriminar com sucesso a adaptação versus não adaptação com mais de 90% de precisão. Este procedimento permite a monitoração dos participantes em ambientes mais realistas, sem a necessidade de equipamentos especializados, como sensores de pressão. Este método demonstrou que é possível detetar a adaptação com mais de 90% de precisão, quando os participantes tentam adaptar sua velocidade de marcha para uma velocidade maior ou menor.

Palavras-chave: Adaptação da locomoção, BCI, EEG, Eletroencefalografia, Imagem motora, Locomoção, Neuroreabilitação.

Table of contents

List of Figures	IX
List of Tables	XII
Abbreviations and Symbols.....	XIII
1. Introduction	1
2. Background	4
2.1 Gait.....	4
2.1.1 Gait Cycle	5
2.1.2 Abnormal Gait.....	6
2.1.3 Gait Analysis.....	6
2.2 Gait Adaptation	9
2.2.1 Gait Rehabilitation and Robotics.....	9
2.2.2 Robotic Rehabilitation Devices	10
2.3 Neurophysiology of gait and gait adaptation	11
2.3.1 EEG in Gait Analysis.....	11
2.3.3 Brain Rhythms	13
2.3.4 Motor Cortex.....	13
2.3.6 EEG Advantages and disadvantages	17
2.3.7 BCI in gait rehabilitation	17
2.4 BCI analysis.....	18
2.4.1 History of BCI.....	19
2.4.2 Feature extraction	20
2.4.3 Common Spatial Pattern (CSP).....	21
2.4.4 Classification in BCI	22
2.4.5 BCI Open-source Software Platforms	26
2.5 Motor Imagery	29
2.6 Artefacts Removal.....	30
2.6.1 Artefacts Removal during walking.....	31
3. Pre-processing for BCI.....	32
3.1 Filtering	32
3.2 Artefacts Removal based on Independent Component Analysis (ICA)	33
3.2.1 Independent Component Analysis.....	33
3.3 Results	37
3.3.1 Artefacts Removal based on ICA during Motor Imagery	37

3.3.2 Artefacts Removal based on ICA during Gait Adaptation.....	38
3.4 Discussion.....	39
4. Analysis of EEG signals based on time locked events.....	40
4.1 Methods.....	40
4.2 Results.....	40
4.2.1 Power Spectrum Analysis.....	40
4.3 Conclusions.....	43
5. Motor imagery and simple movements - EEG feature extraction and classification.....	44
5.1 Experimental design.....	44
5.1.1 Experimental Setup.....	44
5.1.2 Channels Locations.....	45
5.2 Analysis.....	46
5.2.1 Feature extraction and classification.....	46
5.3 Results.....	47
5.4 Discussion.....	53
6. Detection of intention to adapt the gait.....	54
6.1 Experimental Setup.....	54
6.2 Analysis.....	55
6.2.1 Gait Features Extraction.....	55
6.2.2 Movement Artefact Removal.....	57
6.2.3 EEG Feature Extraction.....	57
6.3 Results.....	58
6.4 Discussion.....	63
7. Conclusions.....	64
8. References.....	66
9. Appendix.....	75
A. Preprocessing for BCI.....	75
B. Analysis of EEG signals based on time locked events.....	77
C. Peak Detection method.....	78

List of Figures

2.1. Inverted Pendulum Principle	4
2.2. Terminology of the phases of the gait cycle. Adapted from [1].	5
2.3. Measures during a gait cycle. Adapted from [1].	5
2.4. Approximate plot of an action potential and its various phases.	12
2.5. The international standard electrode montage (10-20 system).	13
2.6. Topography of the motor cortex and its different areas.	14
2.7. Diagram of a BCI system.	19
2.8. Linear Discriminant Analysis.	23
2.9. Support Vector Machine.	23
2.10. Multilayer Perceptron composed by three layers.	23
2.11. OpenVibe Acquisition server.	26
2.12. OpenVibe scenario.	26
3.1. Motor imagery data with bandpass filtering at 1-30 Hz.	32
3.2. Gait adaptation with bandpass filtering at 3-45 Hz.	32
3.3. Scalp Topographies of the ICA components.	34
3.4. ICA components activations.	34
3.5. ICA components during motor imagery (subject 2), with the dry system.	37
3.6. ICA components during motor imagery (subject 3) with the wet system.	37
3.7. EEG signal after ICA (subject 3), with the wet system.	38
3.8. ICA components during gait adaptation (subject 3).	38
3.9. EEG signal before ICA (subject 3).	39
3.10. EEG signal after ICA (subject 3).	39
4.1. Scalp distribution of power during left hand motor imagery for different brain rhythms.	41
4.2. Scalp distribution of power during right hand motor imagery for different brain rhythms.	41
4.3. Scalp distribution of power during left leg motor imagery for different brain rhythms.	41
4.4. Scalp distribution of power during right leg motor imagery for different brain rhythms.	42
4.5 Scalp distribution of power during left leg movement for different brain rhythms.	42
4.6 Scalp distribution of power during right leg movement for different brain rhythms.	42

5.1. Visual Stimulus Presentation.	44
5.2. Visual stimulus timing diagram.	44
5.3. EEG electrode placement for the 16 channels g.Nautilus system used during the experiment based on the International 10-20 system.	45
5.4. Left: EEG electrode placement for the 32 channels g.Nautilus system used during the experiment based on the International 10-20 system (configuration 1). Right: EEG electrode placement for the 32 channels g.Nautilus system used during the experiment based on the International 10-20 system (configuration 2).	45
5.5. Average testing accuracy of the classifications results of left versus right (L/R) MI of the hands and legs and simple movements of the legs, based on the dry system.	48
5.6. 10-fold cross-validation generalization loss of the classifications results for the right versus left MI of the hands and legs and simple movements of the legs, based on the dry system.	48
5.7. Average testing accuracy of the classifications results of left versus right (L/R) MI of the hands and legs and simple movements of the legs, based on the wet system.	50
5.8. 10-fold cross-validation generalization loss of the classifications results for the right versus left MI of the hands and legs and simple movements of the legs, based on the wet system.	50
5.9. Average testing accuracy across subjects as more RCSP components are chosen from the most significant to less significant eigenvalues, based on the dry electrodes system.	51
5.10. Generalisation loss for different numbers of RCSP components, from the most significant to less significant eigenvalues, based on the dry electrodes system.	51
5.11. Average testing accuracy across subjects as more RCSP components are chosen from the most significant to less significant eigenvalues, based on the wet electrodes system.	52
5.12. Generalisation loss for different numbers of RCSP components, from the most significant to less significant eigenvalues, based on the wet electrodes system.	52
6.1. Channels locations according to the 10-20 EEG system.	54
6.2. Experimental design.	54
6.3. (Left) OpenPose output. (Right) OpenPose 2D keypoint detection.	55
6.4. Gait feature extraction.	56
6.5. Average testing accuracy of the classifications results of left versus right (L/R) steps and adaptation versus non-adaptation (A/NA) steps, based on CSP and RCSP feature extraction.	59
6.6. 10-fold cross-validation generalization loss of the classifications results of left versus right (L/R) steps and adaptation versus non-adaptation (A/NA) steps, based on CSP and RCSP feature extraction.	60

6.7. Generalisation loss for different numbers of CSP components, from the most significant to less significant eigenvalues.	60
6.8. Average testing accuracy across subjects as more CSP components are chosen from the most significant to less significant eigenvalues.	61
6.9. Generalisation loss for different numbers of RCSP components, from the most significant to less significant eigenvalues.	61
6.10. Average testing accuracy across subjects as more RCSP components are chosen from the most significant to less significant eigenvalues.	62
6.11. RCSP filters for the five most significant components of one of the subjects.	62

List of Tables

2.1. Summary of several studies on gait and gait adaptation using different imaging modalities and their key contributions.	15
2.2. Summary of several BCI platforms and their main features.	27
3.1. Independent Components. ICs and corresponding 2D topographies, continuous data map and activity power spectrum.	36
5.1. Average testing accuracy of the classifications results of left versus right (L/R) MI of the hands and legs and simple movements of the legs, based on the dry system.	47
5.2. 10-fold cross-validation generalization loss of the classifications results for the right versus left MI of the hands and legs and simple movements of the legs, based on the dry system.	47
5.3. Average testing accuracy of the classifications results of left versus right (L/R) MI of the hands and legs and simple movements of the legs, based on the wet system.	49
5.4. 10-fold cross-validation generalization loss of the classifications results for the right versus left MI of the hands and legs and simple movements of the legs, based on the wet system	49
6.1. Behavioural analysis of adaptation. Steps statistics (step duration, adaptation time and number of adaptation steps) according to the music tone frequency (slow, normal or fast).	58
6.2. Classification results for the right versus left gait cycles and for the adaptation versus non-adaptation steps, based on CSP and RCSP. The results are shown across different sizes of sliding window (w) with a range from 90 to 60 samples.	58
6.3. 10-fold cross-validation generalization loss of the classifications results for the right versus left gait cycles and for the adaptation versus non-adaptation steps, based on CSP and RCSP. The results are shown across different sizes of sliding window (w) with a range from 90 to 60 samples.	59
6.4. Paired t-test to compare the methods used (LDA and SVM with different values of sliding windows) based on CSP and RCSP.	63

Abbreviations and Symbols

ALS	Amyotrophic Lateral Sclerosis
AP	Action Potential
AR	Autoregressive
BCI	Brain-Computer-Interface
BSS	Blind Source Separation
BWS	Bodyweight Support
CCSP	Composite Common Spatial Pattern
CNS	Central Nervous System
COM	Centre of Mass
CPGs	Central Pattern Generators
CSP	Common Spatial Pattern
EEG	Electroencephalography
EMD	Empirical Mode Decomposition
ERD	Event-Related Desynchronization
ERS	Event-Related Synchronization
FES	Functional Electrical Stimulation
FFT	Fast Fourier Transform
fMRI	Functional Magnetic Resonance Imaging
fNIRS	Functional Near-Infrared Spectroscopy
HMM	Hidden Markov Model
IC	Independent Component
ICA	Independent Component Analysis
IMU	Inertial Measurement Unit
IP	Inverted Pendulum
KNN	K Nearest Neighbour
LDA	Linear Discriminant Analysis
MEG	Magnetoencephalography
MI	Motor Imagery
NN	Neural Network
PCA	Principal Component Analysis
PLV	Phase Locking Value
RBF	Radial Basis Function

RCSP	Regularised Common Spatial Pattern
RGB	Red-Green-Blue
RT	Reaction Time
SMA	Supplementary Motor Area
SMR	Sensorimotor Rhythm
SNR	Signal-to-Noise Ratio
SSA	Singular Spectrum Analysis
SVM	Support Vector Machine

1. Introduction

Walking is a common and important activity of daily life and involves the activation of the nervous and musculoskeletal systems. Gait has an important role in the quality of life and independence of people, mainly in the ones suffering with gait impairments. Gait disorders are common in the elderly population and are frequently associated with a poor quality of life. The occurrence of gait disorders increases with age. It is estimated that approximately 10% of people between the ages of 60 and 69 years suffer from any kind of gait disorder, while this number increases to more than 60% in people over 80 years. Moreover, gait patterns are also highly influenced by diseases, physical conditions, personality and mood. Abnormal gait is an altered gait pattern which occurs when a person is not able to walk in the usual way, mainly due to injuries, diseases or other underlying conditions. The causes of gait disorders include neurological and musculoskeletal conditions. An extensive number of neurological conditions can cause an abnormal gait pattern, like stroke, cerebral palsy or Parkinson disease. On the other hand, musculoskeletal causes are mainly due to bone or muscle diseases.

The evaluation of gait, or gait analysis, includes the measurement, description and assessment of variables that characterize human walking. As a result, the study of gait, allows the diagnostic of several conditions, and it is also useful to evaluate rehabilitation progression and to develop intervention strategies. Conventionally, gait is studied subjectively with observational protocols. However, in the past few years, more objective and feasible methods have been developed. Gait analysis methods can be classified in laboratory-based analysis and wearable methods. While laboratory-based analysis uses specialized facilities and equipment, wearable systems allows the study of gait in natural environments and during daily life activities. Laboratory-based analysis is mainly based on image and video information, although floor sensors and force plates are also quite common. On the contrary, wearable systems consists in one or multiple sensors, attached to the body.

An emerging practise in BCI is motor imagery, which is defined as the activity of mentally simulating a given action, without the actual execution of the movement. This technique is extensively used in rehabilitation, for example, for persons with motor deficits, since numerous studies found that performing a MI session activates partially the same brain regions as the performance of the real task. Initially, MI focused mainly in hand and arm movements, but recently, studies also started to embrace legs and feet movements, in order to study human gait. Research teams are also trying to combine BCI with exoskeleton robots. The detection of motor intention in MI tasks faces several challenges, even for just two classes movements (left/right, for example). One of the main challenges is due to the number, placement and type of EEG electrodes. Electrodes can be either wet or dry. Wet electrodes require the application of conductive gel that improves the signal quality. However, they require long preparation times and impede the use of the technology at everyday scenarios. Dry electrodes may overcome this problem, reducing montage times and subject discomfort but the signal quality is poorer. The use of fewer channels helps to decrease the computational and montage complexity and develop methods that allow real-time feedback to the user. Artefact removal is an additional challenge in intention detection, since the EEG data is highly corrupted with noise. In order to decrease the artefacts contamination, chapter three illustrates the pre-processing methods for artefact removal in BCI used, namely filtering and the ICA techniques. Later, chapter four illustrates the analysis of EEG signals based on time locked events.

In this thesis, chapter five presents a motor imagery study, where the EEG feature extraction and classification is studied based on MI and simple movements. Several two-classes experiments that include MI of the hands, legs and actual movements of the legs based on a Graz-BCI stimulation paradigm were evaluated. EEG data was acquired from both a dry 16-channel and a 32-channels wet system, to compare their offline classification performance. Feature extraction and classification were

also evaluated with more than one method. In the end, the combination of a beta bandpass filter with a Regularised Common Spatial Pattern (RCSP) filter has shown the best classification rate. Although during the EEG acquisition all the channels have been used, during processing methods, two channels configurations have been chosen, where electrodes were selected according to their position relativity to the motor cortex. This showed that a careful selection of electrode location is more important than having a dense map of electrodes, which makes EEG systems user-friendly and more reliable.

Chapter six is focused mainly in gait and gait adaptation. Gait adaptation is crucial in walking, since it reflects the ability of a subject to change speed and direction, to keep balance or avoid obstacles. Deficiencies in gait adaptation may reflect several conditions, such as aging and neurological diseases like stroke and Parkinson disease. Furthermore, gait adaptation may also suggest appropriate interventions for gait rehabilitation. Adaptation of gait has a strong role in neurorehabilitation, since it is able to change neuronal dynamics, allowing patients to restore motor functions. Recently, it has been shown that the auditory rhythm has a strong effect on the motor system. Consequently, gait adaptation studies have been focusing in auditory rhythms, where patients couple heel strikes and pacing tones to improve gait coordination.

In the field of gait rehabilitation, robot-assisted training has shown to be an emerging technique since it offers a safer and more intensive rehabilitation to patients with motor disabilities than conventional therapies. Several robotic devices were specially designed to aid the rehabilitation of limbs, such as the LokomatTM and LOPESTM devices. These systems have shown that patients trained with robotic devices combined with regular physiotherapy showed more promising outcomes than patients trained only with regular physiotherapy.

In the past few years, an increasing number of studies investigated brain activity during human locomotion. These studies, mainly using EEG, have found several relations between brain regions and specific actions or movements. For example, it has been found that cerebral activity increases during walking or preparation for walking and that the power in the μ and β bands decreases during a voluntary execution of movement. In terms of gait adaptation, it has been shown that the electrocortical activity changes according to the motor task executed. Recently, Brain Computer Interfaces have emerged as a new rehabilitation therapy to restore motor functions in people with gait deficiencies, by involving the CNS to activate external devices. BCIs have been widely studied mostly in the field of post-stroke gait therapy. This growth of this technology is mainly due to the capability of directly control rehabilitation devices and to provide feedback to the user based on brain activity.

Recently, steady state visual evoked potentials (SSVEPs) have been proposed to control lower-limb exoskeletons. However, SSVEPs is an indirect way of interfacing brain signals with machine and they do not reflect real human intention and motor control. On the other hand, intention detection of movement and gait adaptation is well accepted as the best way to successfully integrate a lower limb robotic system. Nevertheless, this depends on decoding EEG signal mainly from motor, premotor and frontal cortex.

As previously said, chapter six, evaluates gait adaptation where subjects follow a rhythmic tone that alternates between three modes of slow, normal and fast pace. The EEG signal is simultaneously recorded via wireless devices. Here, contrary to previous studies, no treadmill or specialized equipment is used, allowing the investigation of gait adaptation in more natural settings. Gait characteristics are captured based on a single RGB camera. Subsequently, gait characteristic and reaction time information are used to extract gait adaptation steps versus non-gait adaptation steps. EEG is pre-processed with a bandpass filter and independent component analysis (ICA) to remove motion related artefacts and subsequently the signal is epoched based on right/left heel strikes. Finally, EEG gait adaptation characteristics are investigated based on two classification problems, with two classes: i) right versus left gait cycle classification and ii) adaptation versus non-adaptation steps. Features were extracted based on common spatial patterns (CSP) and regularized common spatial patterns (RCSP). Results show that

it is possible to successfully discriminate adaptation versus non-adaptation with more than 90% testing accuracy.

2. Background

2.1 Gait

Locomotion is defined as the capability of an organism to move between places. It is a complex sequence of repetitive movements, which requires the activation of a neural mechanism and the musculoskeletal system. In particular, human locomotion is a process in which the upright and moving body is sustained by the two legs, alternatively, to maintain balance, while advancing. During this process, humans' limbs follow different configurations of movement. Consequently, gait may be defined as the pattern of how a person walks, or as the bipedal forward propulsion of the human body with alternate movements of different parts of the body.

Gait can be explained based on the Inverted Pendulum (IP) principle [3] [4]. This model has been extensively used to describe human locomotion, mainly in the fields of robotics and biomechanics [5] [6]. The IP model states that the leg acts like a pendulum, describing an arc. During single support, the stance leg is relatively straight and supports the centre of mass (COM), located near the hip, and the ground reaction force is directed from the centre of pressure to the COM. The COM moves in a sequence of arcs described by each single support phase. This model also states that walking can be performed without muscle actuation, since no work is performed in the COM.

In 1953, Saunders and Inman recognised several elements of gait, namely the pelvic rotation, pelvic tilt, knee and hip flexion, knee and ankle interaction and lateral pelvic displacement. This elements may be useful to determine whether a pattern is normal or pathological [7]. Several factors may contribute to locomotor disabilities or gait malfunctions, for instance, abnormal gait patterns may be due to early medical conditions, such as cerebral palsy, or to later injuries or illnesses, such as stroke, Parkinson or traumatic brain injuries. Gait disorders are common in the elderly population and are frequently associated with reduced mobility, regular falls, depressed mood and consequently a poor quality of life. It is evident that the occurrence of gait disorders increases with age. It is estimated that around 10% of people between the ages of 60 and 69 years suffer from any kind of gait disorder and this number increases to more than 60% in people over 80 years [8].

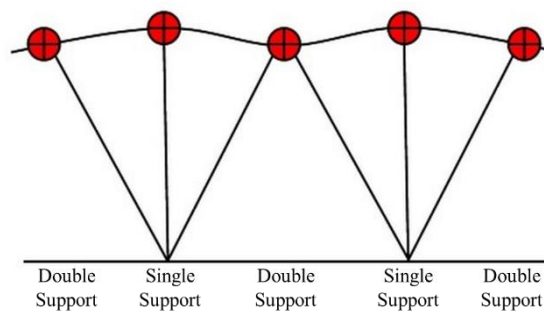


Figure 2.1. Inverted Pendulum Principle. The IP principle states that the stance leg acts like a pendulum, describing an arc. During single support, the stance leg is relatively straight and supports the COM, represented in red. The COM moves in a sequence of arcs described by each single support phase. Adapted from [2].

2.1.1 Gait Cycle

The gait cycle is the time interval between two consecutive events of the actions of walking and may be allocated between two distinct phases: the stance and swing phase. The first phase, which represents approximately 60% of the gait cycle, is divided into initial contact or heel strike, loading response, mid-stance, terminal stance and pre-swing. The second phase is divided into initial swing or toe-off, mid-swing (tibia vertical) and terminal swing (figure 2.1). The heel strike is a short period that starts when the foot touches the ground. The ankle moves from a neutral to a plantar flexion and the knee flexion begins. In the loading response phase, or foot flat, the body continues in pronation to absorb the impact of the foot. During mid-stance the body is supported by one single leg and moves forward. Afterwards, the heel leaves the floor, which marks the beginning of the terminal stance. In the pre-swing/toe-off phase, the hip becomes less extended and the toes leave the ground. In the mid-swing phase, the hip and the knee flexes. Lastly, in the terminal swing phase there is an extension of the knee followed by a neutral position of the ankle [9]. The gait cycle may also be described using a basic terminology, using some important measures, as the walking speed, cadence (number of steps per unit of time), walking base width (measured from midpoint to midpoint of both heels), step length and stride length (linear distance walked during one gait cycle), like is shown in figure 2.2 [10] [1].

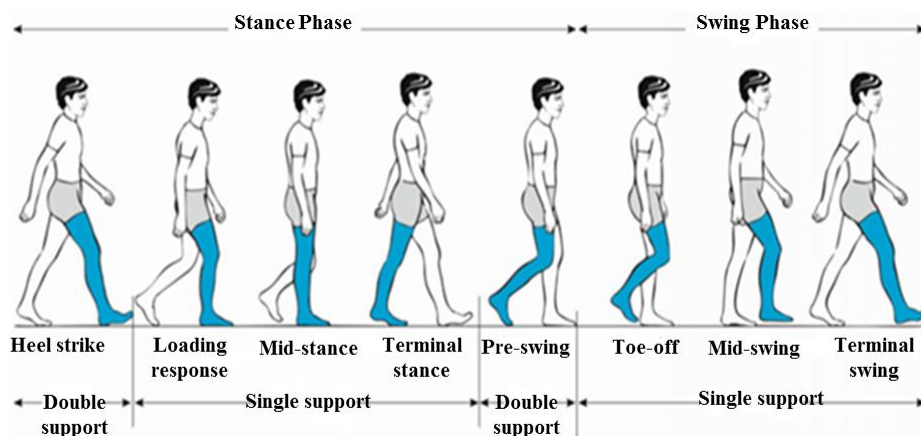


Figure 2.2. Terminology of the phases of the gait cycle. The gait cycle may be allocated between two distinct phases: the stance and swing phase. The first phase is divided into heel strike, loading response, mid-stance, terminal stance and pre-swing. The second phase is divided into toe-off, mid-swing and terminal swing. Adapted from [1].

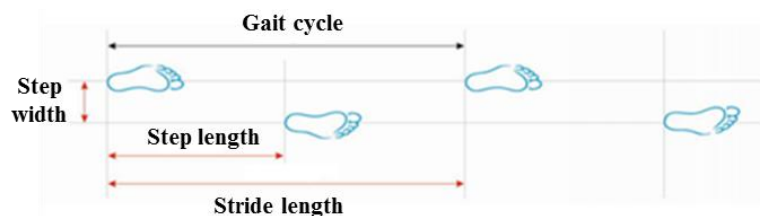


Figure 2.3. Measures during a gait cycle. The gait cycle may be described using a basic terminology, using the walking speed, cadence, walking base width, step length and stride length. Adapted from [1]

2.1.2 Abnormal Gait

Pathological or abnormal gait is an altered gait pattern and occurs when a person is not able to walk in the usual way, due to injuries, diseases or other underlying conditions. The changes in gait patterns can be divided into neurological or musculoskeletal causes. The musculoskeletal causes of abnormal gait patterns are mainly due to bone or muscle diseases or conditions like hip, knee, foot and ankle pathologies, injuries, leg length inconsistency or pain (antalgic gait). On the contrary, a wide number of neurological conditions can also cause an abnormal gait patterns, like stroke, cerebral palsy and Parkinson disease.

Pathological gait due to neurological conditions is mainly divided in hemiplegic, diplegic, Parkinsonian, ataxic, sensory, myopathic and neuropathic gait. The most common neurological origin pathological gait is the hemiplegic gait, which is usually the result of a stroke. This type of gait is mainly characterized by the loss of function in some muscles of one leg, while the other leg remains normal or practically normal. Here, the lower limb rotates internally, and the affected leg moves in a semicircle (circumduction). Contrary to the hemiplegic gait, the diplegic gait is associated with a spasticity of both legs and is mainly characterized by a hip and knee flexion and by an extreme tension of hip adductors. This type of gait is a common manifestation of cerebral palsy. Parkinson disease may be recognized by the Parkinsonian gait, which is characterized by the reduced arm swing and the slow movements. In this case, people are bent with the head and neck forward and walk with small steps. Ataxic gait is described by an incoordination of steps, with a variable foot placement. This gait is usually seen in cerebral diseases, but it may also be identified in patients with alcohol dependency. People who suffer from sensory disturbances tend to present a sensory gait, which is characterized by high steps and by an exacerbated force of the foot on the ground, in an attempt to gain sensory feedback. The myopathic gait occurs due to a weakness on one side of the pelvis which leads to a drop in the pelvis while walking (Trendelenburg sign). This gait is perceived in patients with muscular dystrophy. Lastly, the neuropathic gait is seen in patients with a weakness of foot dorsiflexion, also called, foot drop. The patients lift their legs high while walking, so that the foot does not drag on the floor [9].

2.1.3 Gait Analysis

Gait analysis is defined as the methodical study of human locomotion. This systematic evaluation of bipedal locomotion comprises the measurement, description, and assessment of variables that characterize human walking. As a result, it is possible to identify the gait phase and kinetic parameters of human gait and assess the musculoskeletal functions and disease progression [11]. Pathological gait may reflect an extensive number of underlying medical conditions, like Parkinson, stroke or multiple sclerosis. It is important to mention that the study of gait, not only allows the diagnoses of certain pathologies, but it is useful to study intervention strategies and rehabilitation. Besides the clinical applications, gait analysis can also be used in the areas of sports, forensics and comparative biomechanics, in order to study the gait of animals and understand the locomotion patterns of different species.

Gait analysis has caught the interest of numerous researchers, since it is an essential method to study human locomotion. The way a person moves the body through the two phases of the gait cycle, provides information to diagnose a gait abnormality. This process is known as observational gait analysis. Several parameters are evaluated during observational gait analysis, namely the step and stride length, speed, trunk rotation and arm swing. Conventionally gait analysis is conducted subjectively with observational protocols. However, this traditional way keeps updating and have been replaced by more objective and feasible methods that use optical tracking, cameras, force plates and wearable sensors, in specialized laboratories for this type of analyses.

These instruments are used to evaluate basic gait parameters, such as stride length, velocity and cadence, the forces and movements of the joints, the muscle activity and the velocity and acceleration of the body. The stride length is defined as the distance between two successive placements of the same foot and comprises two step lengths, right and left. In abnormal gait, the right and left steps show different lengths. The cadence is the number of steps in a certain amount of time and is usually expressed in steps per minute. The velocity is the distance walked in a given time and is expressed in meters per seconds. These parameters change according to certain conditions or locomotor disabilities. Gait symmetry is another useful indicator of normal or abnormal gait. In healthy subjects, it is expected the gait to be symmetric, while in abnormal or pathological locomotion, the gait is asymmetrical [12].

The methods used to study gait analysis can be classified in laboratory-based analysis or non-wearable methods and wearable methods. Laboratory based analysis required the use of specialized facilities and equipment. On the contrary, wearable systems allow the study of gait in a more natural environment and during everyday activities.

In terms of laboratory-based analysis, a substantial part of the methods used is based on image and video information from video sequences. Multi-camera systems are the state-of-the-art in measuring lower limb kinematics . They are usually based on the tracking of reflective skin markers. Although, these systems are very accurate, their use is limited in large clinics and specialised laboratories. The use of floor sensors is also very common. The sensors are placed in the floor or instrumented treadmill and gait is evaluated when the subject walks, exerting a force or pressure in the sensors. Floor sensors can be divided in force platforms or pressure sensors. The later does not allow a direct measurement of the force. The force exerted on the floor is designated by Ground Reaction Forces (GRFs) and is considered in several gait analysis studies because they are related to the load exerted to the joints [13]. GRFs can also be measured with pressure insoles, which are devices that record and measure the pressure distribution under the foot. This method allows a complete measure of the GRFs outside the laboratory and without the use of force plates [14] [15].

Wearable sensors' configurations consist from one or multiple sensors, which are attached to the body, to measure acceleration, pressure or angular rate. The recent technological advances in wireless communication and wearable sensing technologies, allows small, lightweight and continuous monitoring devices for gait analysis, in a wide range of environments. In 2005, Jovanov *et al* designed a device that can be combined into a Wireless Body Area Network, a technology for computer-assisted physical rehabilitation and ambulatory monitoring [16]. Later, in 2008, a wearable system called "*GaitShoe*" was developed to offer gait analysis outside the laboratories, using multiple sensors, accelerometers and gyroscopes. This wireless device was built to perform gait analysis in any environment and during extended periods, without disturbing the subject [17]. Lately, inertial sensors have also been successfully used to study human gait. These sensors can be attached to any part of the body and use a group of accelerometers, gyroscopes and magnetometers to measure the velocity, acceleration, orientation and gravitational forces. One of the most common sensors in this field is the Inertial Measurement Unit (IMU), which comprises several sensors in a single device. Anna et al, in 2013, proposed a system, with inertial sensors, to evaluate gait symmetry and normal gait. This study was validated against kinematic measurements in a specialized laboratory, showing a good correlation between the methods [18]. More recently, in 2017, Tunca et al developed a study proposing an IMU-based gait analysis device, which is able to identify several neurological conditions related to gait abnormalities in a natural environment [19]. Goniometers are another type of wearable sensors used to evaluate gait. These sensors are used to measure the angles of different joints, such as ankles, knees or hips. The most common type are the flexible strain gauge goniometers, which are based on the flexion of the sensor [20]. Lately, some digital goniometers have also been designed to measure human joints positions [21]. These sensors have a limited usage due to the complexity of how to balance the number of sensors required with the amount of information captured, since the sensors capture much more

information than is actually needed. To avoid these problems, studies have been developed in order to integrate all the capabilities into a single wireless sensor. Recently, the team from The Hamlyn Centre (Imperial College London) developed an innovative way to acquire gait data and to detect walking gait impairment, based on just one sensor attached to the ear of the patient, called ear-worn Activity Recognition (e-AR) sensor. The validation of the sensor was done using a force-plate instrumented treadmill. This technology promises to allow patients to be more independent while their condition is monitored 24/7 [22] [23]. In a recent study (2017), The Hamlyn Centre group also proposed an innovative integrated approach, using the e-AR sensor combined with a single video camera, to estimate the interaction of ground reaction forces and ankle dynamics during normal and abnormal walking [24]. Recently, Yang *et al* proposed a video acquisition system with a single camera to evaluate human gait function. The results showed that the portable camera and the system were able to effectively detect gait events, offering a useful and inexpensive solution for gait analysis outside a specialized laboratory [24] [25] [26].

2.2 Gait Adaptation

Gait adaptation involves the ability to change walking direction and/or speed to avoid obstacles, for example. Deficiency in walking adaptation indicates a risk factor of falling in the elderly population or patients with Parkinson or stroke. Moreover, the understanding of gait adaptation may suggest suitable interventions for an effective gait rehabilitation.

Gait adaptation plays an important role in neurorehabilitation since it perturbs neuronal dynamics and allows patients to restore motor function. Additionally, intention detection of movement and gait adaptation is a successful way to integrate a lower limb robotic system in patient's rehabilitation.

Numerous researches have shown that auditory rhythm has a deep effect on the motor system. These studies show that there is a strong connectivity across cortical, subcortical, and spinal levels between the auditory and motor systems [27]. Based on these evidences, several gait adaptation studies focus on auditory rhythms, where patients try to couple heel strikes and pacing tones, improving the gait coordination. Consequently, gait adaptation based on split-zone treadmill exercises and auditory rhythm has shown to improve gait symmetry in patients with stroke, cerebral palsy and Parkinson disease [27] [28] [29] and is an effective way to adapt stride frequency and improve gait coordination in people after stroke [30].

2.2.1 Gait Rehabilitation and Robotics

The main goal of gait rehabilitation is to help a patient to recover the locomotor abilities, after suffering an injury, illness or disease, in order to enhance the quality of life. Gait training focus mainly in re-training the nervous system, re-building the muscle strength and improving balance. From a clinical perspective, the key to gait recovery is neuroplasticity, which is defined as an adaptive alteration in brain structure in response to a modification in the environment with a consequent change in function [44]. Following a neurological injury, gait rehabilitation has shown to have numerous therapeutic benefits. Several studies proved that gait rehabilitation should focus on repetitive movement patterns, since repetitive practice fortifies the neural connections involved in a motor task through reinforcement learning. It was also proved that the effectiveness of the practice is higher when it task-specific [45].

Gait rehabilitation modalities can be divided into conventional manual gait rehabilitation, bodyweight support (BWS) treadmill gait rehabilitation and robot-assisted gait rehabilitation. Conventional gait rehabilitation is performed by a physical therapist who develop exercises to strength and practice one movement at time. In this type of rehabilitation, the patient can use parallel bars for an extra support while walking, which allows then to put more weight on their legs and progressively recover the walking ability. A more sophisticated therapy developed for the purpose of gait rehabilitation is partial bodyweight support combined with treadmill training. In this kind of therapy, the patient is partially suspended with a proper system in order to maintain the upright posture and balance during treadmill walking. As soon as the patient coordination and balance begin to improve, the amount of support can decrease gradually. BWS allows the patient to develop more effective movement strategies since it reduces the demands on muscles. This controlled environment may also increase patient confidence, since it provides a secure way to practice walking [46]. An emerging technique in field of gait rehabilitation is the robot-assisted training. Robotic devices offer a safer and more intensive rehabilitation to patients with motor disabilities [47].

2.2.2 Robotic Rehabilitation Devices

Conventional gait rehabilitation, usually, requires several therapists together to manually assist the legs and torso during gait training, which can be quite intense and exhaustive, and it cannot be carried out for a long period. Robotic rehabilitation can provide greater duration of reliable and repetitive motor practise, replacing the physical effort of a therapist. Additionally, robotic rehabilitation can precisely measure and track patient's motor recovery along rehabilitation. Robotic gait technology has shown to have positive effects on clinical outcomes of patients with stroke, spinal cord injury and Parkinson disease, when incorporated into a multi-modality rehabilitation approach, with conventional physiotherapy [48] [49] [50].

Regarding robotic devices designed for the lower limbs, treadmill robotic gait training devices were the first to be designed, specifically the LokomatTM (Hocoma) [51] and the Lower Extremity Powered Exoskeleton (*LOPES*TM) [52]. The aim of these devices is to promote normal gait patterns, guiding the lower limbs through programmed gait cycles. In a research that evaluated the effectiveness of robotic-assisted gait training (Lokomat device), in patients with stroke, the results showed that patients trained with the robotic device combined with regular physiotherapy showed more promising outcomes than patients trained only with regular physiotherapy [53].

2.3 Neurophysiology of gait and gait adaptation

Locomotion is the result of a complex combination that involves not only the muscles, bones and joints but also involves the brain, spinal cord and peripheral nerves. Movements are generated by specific arrangements of nerve cells named Central Pattern Generators (CPGs). These cells contain the necessary information to activate the motor neurons, in order to generate motor patterns. CPGs that generate rhythmic movements, such as locomotor CPGs are localized in the spinal cord [31].

Although CPGs play an important role in walking function, human walking is significantly influenced by the supraspinal centres. The motor cortex have been identified to have a particular importance in gait regulation, specifically in the supplementary motor area and the prefrontal cortex [32]. The cerebellum has also been known to control posture and gait. Lesions in this area may cause incoordination of the muscles involved in locomotion, and may result in irregular gait patterns [33].

2.3.1 EEG in Gait Analysis

Carlo Matteucci and Emil Du Bois-Reymond, who firstly registered the electrical signals arousing from muscle nerves, established the concept of neurophysiology. However, was Hans Berger who discovered the existence of human EEG signals.

The central nervous system (CNS) is mainly composed by nerve and glia cells. Nerve cells consists in axons, dendrites and cell bodies. CNS activity is mostly related with the synaptic currents verified between axons and dendrites, or dendrites and dendrites of cells. An action potential (AP) is the information transmitted by a nerve cell. These potentials arise from a transfer of ions through the membrane, which means that the membrane potential suffers a temporary change during an action potential.

Excitable cells have voltage-gated channels, particularly, sodium (Na^+) and potassium (K^+) channels. These channels open and close according to the membrane voltage. APs are produced due to the action of both sodium and potassium ions and, usually, Na^+ has a higher concentration outside the cell and lower inside. The opening of sodium channels, with positive charge, depolarizes the membrane potential, turning the membrane potential more positive and consequently, producing a spike. Then, after the spike, the membrane potential repolarizes. Later, the potential decreases to values lower than the resting potential, returning to normal after a period. After an AP, the cell membrane cannot immediately produce a second AP, since the nerves need nearly two milliseconds before another stimulus (refractory period) [34]. The amplitude of an AP, for a human being, extends from approximately -60 mV to 10 mV. APs may be originated from different types of stimulus, such as light, pressure or chemical. Particularly, APs from the nerve cells on the CNS are mainly originated due to chemical stimulus in the synapses. These stimuli need to be higher than a certain level in order to produce an AP. The currents generated in the dendrites, during synaptic excitations, in the cerebral cortex generate a magnetic and an electrical field. An EEG signal is the measurement of these currents, which can be detected with electrodes placed on the scalp.

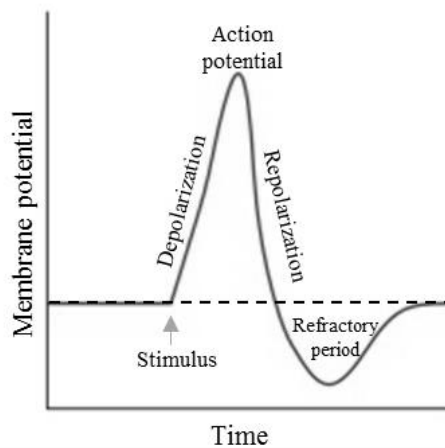


Figure 2.4. Approximate plot of an action potential and its various phases. A stimulus is applied raising the membrane potential abruptly. After the stimulus, the membrane potential rapidly rises to a peak potential. Later, the potential drops and the resting potential is re-established.

2.3.2 EEG Recording and Measurement

The growing knowledge of the human body is mainly due to the use of signals and images, which allow the diagnose of a vast range of conditions and diseases. Like previously said, the first neural electrical activities were registered using a galvanometer. Later, more recent systems used a set of electrodes, amplifiers, filters and a needle register. Therefore, in order to analyse the EEG signals, the signals need to be in a digital form, which requires sampling, quantization and encoding of the signals. The conversion from analogue to digital is achieved using analogue to digital converters (ADC's).

The electrodes used in the EEG recording are crucial for the acquisition of high-quality data. Different type of electrodes can be used, such as disposable electrodes, needle electrodes, reusable disc electrodes and electrode caps.

Usually, EEG is recorded with wet (gel-based) electrodes, in order to have a low electrode-skin impedance. In most EEG recordings, passive electrodes are used. These electrodes are easy to manufacture and maintain and have a low price. However, they require special skin preparation to reduce the impedance. On the other hand, active electrodes, requires no skin preparation. These electrodes have an amplifier inside and the gel is inserted between the electrode and the skin. Although, gel-based active electrodes have a strong signal quality, the main disadvantage is the long montage time and the need to wash the cap and the user's hair after the recording. During long recordings, gel may also dry out, resulting in a poor signal quality. Dry electrodes eliminate the need for gel, enabling a faster setup time and users' comfort during the recordings. The main disadvantage is the electrode-skin impedance, which may lead to a significant increase in the noise and interference. Recently, active electrodes enable scalp EEG measurement with dry electrodes, improving user comfort and long-term monitoring [35].

The conventional electrode position, also called the 10-20 system, describes the conventional electrode positioning for 21 electrodes. This system places the electrodes considering the relationship between their location and the corresponding cerebral cortex areas. To guarantee the correct electrode positioning, two anatomical reference points are considered. These points are the depressed area between the eyes (nasion), and the lowest point of the skull, located in the posterior part of the head (inion), like is shown in figure 2.5

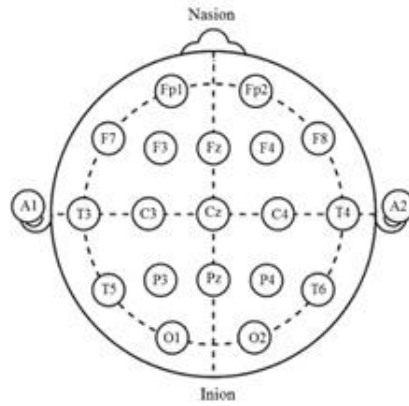


Figure 2.5. The international standard electrode montage (10-20 system). This system places the EEG electrodes considering the relationship between their location and the corresponding cerebral cortex areas, based on two anatomical marks (nasion and inion).

2.3.3 Brain Rhythms

Conventionally, the frequency range of an EEG signal varies from 0.5 Hz to 100 Hz, depending on the brain activity and physiological state of the subject. A rhythmic or repetitive neural activity in the CNS is called a neural oscillation or a brainwave. It is possible to identify five major brain waves types, mainly distinguished by their frequency ranges (delta, theta, alpha, beta and gamma waves).

Delta (δ) waves have a frequency of oscillation between 0.5-4 Hz and tend to be the highest in amplitude. These waves appear mainly during deep sleep. Theta (θ) are located in the range of 4-7.5 Hz and occur most often in sleep but are also dominant in deep meditation. Alpha (α) waves are originated in the occipital lobe mainly during an awake and restless state with closed eyes, being reduced with open eyes or during sleep. These waves are in the frequency range of 8-13 Hz. There is an alpha rhythm called mu rhythm (μ), located in the frequency range of 7.5 and 12.5 Hz and found over the motor cortex. This rhythm is observed mainly in resting conditions and is suppressed when a person executes or observes another person executing a motor action. Beta waves (β) have a range between 14-26 Hz and dominate our normal waking state of consciousness. These waves are also associated with attention states, like active thinking. Finally, the frequencies above 30 Hz corresponds to gamma waves (γ), the waves with the highest amplitudes. The occurrence of these waves is rare. A particular brain wave is the sensory motor rhythm, which is located in the range of 13 to 15 Hz. When the sensory or motor areas are activated, for example, during motor tasks or motor imagery, the amplitude of this rhythm usually decreases. The changes in the μ and β rhythm amplitudes are denoted as event-related desynchronization (ERD) and event-related synchronization (ERS). These changes are normally associated with movement, motor imagery and sensation.

2.3.4 Motor Cortex

The motor cortex is a region of the cerebral cortex responsible for the execution of voluntary movements, planning and movement control. This region is located in the frontal lobe, anterior to the central sulcus, and is composed by three different areas: the primary motor cortex, the premotor cortex and the supplementary motor area (SMA). The primary motor cortex is located in the precentral gyrus and is the main contributor in generating neural impulses. This area contains pyramidal neurons, or upper motor neurons, which are the first primary output of the motor system. These neurons, form connections with lower motor neurons, which directly innervate the skeletal muscles, to produce a movement. Although the exact functions of the SMA and the premotor cortex are not yet fully

understood, it is thought that the SMA is mainly involved in movement planning and in the execution of sequences of movements. The premotor cortex is responsible for the preparation for movement, the incorporation of sensory cues during movement and the selection of actions based on behavioural context. Usually, the posterior parietal cortex is also considered to be part of the group of motor regions. Regarding motor actions, it is responsible for transforming multisensory information into motor commands and is responsible for some aspects of motor planning [36].

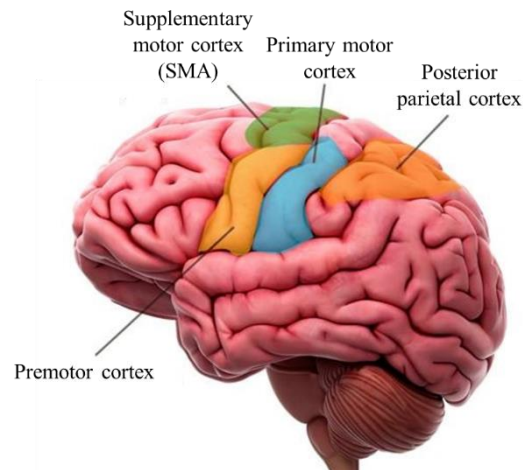


Figure 2.6. Topography of the motor cortex and its different areas. The motor cortex is composed by the supplementary motor cortex (green), the primary motor cortex (blue) and the premotor cortex (yellow). Usually, the posterior parietal cortex (orange) is also considered a part of the motor cortex.

2.3.5 Brain activity during gait and gait adaptation

Recently, a growing number of studies investigate brain activity during human locomotion, particularly there has been an increasing interest in the use of EEG. Preceding studies found that cerebral activity increases during walking or preparation for walking and there is a significant activation of the sensorimotor area, during isolated leg or foot movements [37] [38]. Moreover, it is also reported that gait cycle phase is coupled with electrocortical activity during treadmill walking [15] and with the kinematics of the legs [39]. In previous studies, it was also reported that the power in the μ and β bands decreases during a voluntary execution of movements [40], while β band power increased is related to movement suppression [41]. Additionally, high γ amplitudes (60–80 Hz), located in central sensorimotor areas increase during walking, when compared to standing and even higher γ (70–90 Hz) amplitudes are modulated accordingly to the gait cycle, in the same areas [42]. It is also believed that neuronal activity has different functional roles according to the frequency ranges, which may provide finer details on which brain network features are important in gait control and allow the development of better and more specialised treatments [43]. In summary, EEG oscillations are mostly verified during movement conditions, while the suppression of the μ and β bands, which have their amplitude modulated during the gait cycle phase.

Regarding gait adaptation, it has been shown that the electrocortical activity observed differs according to the motor task executed. For example, if a subject walks in a narrow beam instead of a regular treadmill, the electrocortical activity shows a larger theta power in specific regions of the brain and a reduced alpha and beta-band power in the area of the sensorimotor cortices [44]. In another study, was showed an increased event-related potential (ERP) in the prefrontal cortex when a subject is stepping over obstacles [45]. In addition, it has been shown that there are two oscillatory networks

involved in gait adaptation. A motor μ and β decrease with movement execution and a frontal β band, which increases with cognitive control [46].

Recently, it also became possible to study gait control with real time imaging, with the development of functional near-infrared spectroscopy (fNIRS). This technique showed that there is also a cortical involvement during tasks related to walking. For instance, when switching from a rest state to gait initiation, the activity of the premotor and prefrontal increases while continuous walking does not produce any cortical activation [47]. Furthermore, the prefrontal cortex has a bigger activation during precision stepping when compared to normal gait [48]. An earlier study, using single photon emission computed tomography (SPECT) showed an activation in multiple brain areas including the supplementary motor area, medial sensorimotor cortex, striatum, and cerebellum, which suggests that these regions may be involved in human gait [49]. Table 2.1 summarizes the results of several studies on gait and gait adaptation using different imaging modalities.

Table 2.1. Summary of several studies on gait and gait adaptation using different imaging modalities and their key contributions.

Paper	Imaging Modality/ Number of Subjects	Pre-processing methods	Experimental Conditions	Gait	Key Contribution
Alcock et al, 2018 [50]	- , 33	-	Instrumented walkway	Gait adaptation	The greatest temporal-spatial adaptations were verified when participants crossed tall obstacles. Subjects adapted a wider step when crossing tall obstacles.
Bruijn et al, 2015 [51]	EEG, 10	<ul style="list-style-type: none"> - High-pass filter (3 Hz) - Band-stop filter (50, 100, 150, and 250 Hz) - Channel rejection - ICA 	Treadmill walking	Stabilized and normal gait	Increased beta band activity in the left premotor cortex during stabilization of gait.
Dixon et al, 2018 [52]	- , 35	-	Brick walkway and flat surface	Gait adaptation	Subjects increased hip flexion at foot-strike, while decreasing ankle dorsiflexion, stability, symmetry, and consistency on uneven, compared to flat, surface. Older adults showed a larger increase in knee flexion. Only young adults modified their hip abduction angles.
Fernandez et al, 2017 [53]	- , 14	-	Pressure sensors walking	Gait adaptation	Involvement of the right cerebellar hemisphere in gait adaptation
Fukuyama et al, 1997 [49]	SPECT, 14	-	Natural walking	Normal gait	Activation in the SMA, primary sensorimotor area, striatum, cerebellar vermis and visual cortex.
Gilbertson et al, 2005 [41]	EMG, 10	- Bandpass filter (16-300 Hz).	Isolated movements	-	β band power increased is related to movement suppression

Haefeli et al, 2011 [45]	EEG/MEG, 12	<ul style="list-style-type: none"> - EEG: bandpass filter (1-30 Hz); - Ocular artefacts removal; - EMG: bandpass filter (30-300 Hz). 	Treadmill walking	Gait adaptation	Increased ERP in the prefrontal cortex of the right hemisphere and a greater limb muscle EMG activity, during swing over obstacles when compared to normal walking.
Koenraadt et al, 2014 [48]	fNIRS, 11	-	Treadmill walking	Normal and precision gait	Bigger activation of the prefrontal cortex during precision stepping when compared to normal gait.
Martelli et al, 2016 [54]	- , 18	-	Active walking (A-TPAD device)	Gait adaptation	Adaptation of the balance recovery is verified only for perturbations sent along the AP directions;
Muller-Putz et al, 2007 [37]	EEG, 8	- Visual artefact detection.	Foot movements (active, passive and imagined)	-	Significant activation of the sensorimotor area during isolated leg or foot movements.
Presacco et al, 2011 [39]	EEG, 6	<ul style="list-style-type: none"> - Channel rejection - Signals decimated by a factor of 5 (to 100 Hz) and band-pass filter (0.1–2 Hz). 	Treadmill walking	Normal and precision gait	Involvement of a fronto-posterior cortical network in the control of precision and normal walking.
Seeber et al, 2015 [42]	EEG, 10	<ul style="list-style-type: none"> - Bandpass filter (1-200 Hz), notch filter (50 Hz and multiples); - Channel rejection; - Artefact rejection based on frequency spectral decomposition. 	Active walking (<i>Lokomat</i> TM device)	Normal gait	High γ amplitudes (60–80 Hz), located in central sensorimotor areas increase during walking, when compared to standing, and even higher γ (70–90 Hz) amplitudes are modulated accordingly to the gait cycle.
Sipp et al, 2013 [44]	EEG, 26	- ICA.	Treadmill walking	Gait adaptation	The electrocortical activity shows a larger theta power in specific regions (anterior cingulate, anterior parietal, superior dorsolateral-prefrontal, and medial sensorimotor cortex) and a reduced alpha and beta-band power in the sensorimotor cortices, when a subject walk in a narrow beam instead of a regular treadmill
Suzuki et al, 2004 [47]	fNIRS, 9	-	Treadmill walking	Gait adaptation	The prefrontal and premotor cortices are involved in adaptation of the locomotor speed on the treadmill.
Wagner et al, 2016 [46]	EEG, 18	<ul style="list-style-type: none"> - High pass filter (1 Hz) and low pass filter (200 Hz); - Channel rejection; - ICA. 	Treadmill walking	Gait adaptation	There are two oscillatory networks involved in gait adaptation. A motor μ and β decrease with movement execution and a frontal β band, which increases with cognitive control.

Wieser et al, 2010 [38]	EEG, 20	<ul style="list-style-type: none"> - Bandpass filter (1.5-30 Hz); - Visual artefact detection; - ICA. 	Assisted legs movements (<i>Erigo</i> device)	-	The primary somatosensory cortex, primary motor cortex and SMA play an essential role in cortical control of human gait.
-------------------------	---------	----------------------------------------------------------------------------------------------------------------------------------------	------------------------------------------------	---	--------------------------------------------------------------------------------------------------------------------------

2.3.6 EEG Advantages and disadvantages

Although several other methods to study brain functions exist, like functional magnetic resonance imaging (fMRI), magnetoencephalography (MEG) or fNIRS, EEG still has a lot of advantages. One of the main advantages is the hardware cost, which is significantly lower than other techniques. Another important aspect is that EEG has a very high temporal resolution. EEG is non-invasive and is quite tolerant during subject movements. This technique is also a useful tool to follow brain changes during life. When compared to other techniques, EEG is a quite simple equipment. Whereas fMRI and MEG need highly specialised infrastructures and equipment, EEG can be used at home and in natural environments, due to the small size and simple acquisition procedures. Like any other technique, EEG also has disadvantages like the low spatial resolution on the scalp and the poor signal-to-noise ratio (SNR). In addition, it cannot identify exact locations in the brain, and requires a correct and precise placement of electrodes around the scalp.

2.3.7 BCI in gait rehabilitation

Recently, brain-computer interfaces have been used as a rehabilitation therapy to restore the motor functions in people with gait impairments. This is accomplished by involving the CNS to activate external devices, according to the detected intention to walk [55]. Specifically, there has been a huge interest in the use of BCIs in post-stroke gait therapy [56] [57].

This technology can be used in two different approaches. It can be used to control directly the rehabilitation devices or to provide feedback to the user based on brain activity. The feedback is provided by output of rehabilitation devices, for example, the movement of a prosthetic limb, activated with brain activity. Later, when brain activation associated with motor intention is measured the information is extracted and used as a signal to control external devices. These approaches include mainly SMR [58]. For the purpose of BCI, the better neural control signal is found in the range of 8-13 Hz (μ -rhythm), which is found in the central sensory-motor areas [59].

BCI can also be combined with functional electrical stimulation (FES), allowing a more intentional control of relevant muscles. A study led by Takahashi, tested the viability of an ERD-modulated FES system, when compared with FES without ERD, to drive FES to the tibialis anterior muscle in a stroke patient. The results showed an augmented EMG activity in the muscle, and an increased dorsiflexion, after BMI-FES when compared to the isolated FES, which suggests that the coupling between motor intent and stimulation may have beneficial effects [60].

2.4 BCI analysis

A Brain-Computer Interface is a system that acquires and analyses brain signals, translating them into commands that are related to an external device, in order to carry a desired action. This system is completely independent of peripheral nerves and muscles, since it uses only the brain signals produced by the CNS. The most common brain signals used to control a BCI are the electrical signals from brain activity, which are measured with electrodes on the scalp, although other signals can be used. The purpose of a BCI is to identify characteristics of brain signals, indicating what the user wants the BCI to do and translate these measurements into the desired device commands. The brain-signal characteristics used for this purpose are called features or signal features.

A BCI system is composed by four different components, namely the signal acquisition, the feature extraction, the feature translation and the device output. The first step of a BCI system is the signal acquisition, which is the measurement of the brain signals. The second step is the feature extraction, which extracts signal features that expresses what the user wants to do. The signals recorded from the brain typically contain noise and irrelevant information, so it is important to distinguish pertinent signal characteristics that have correlate strongly with the intention of the user. The most common signal features used are amplitudes, latencies of event-evoked potentials or frequency power spectra. Feature extraction may be divided into three distinct steps: the signal conditioning, the extraction of the features and the feature conditioning. The first step, the signal conditioning or pre-processing, improves the signal, eliminating some artefacts or irrelevant information or enhancing the most relevant features. Before the feature extraction, the signals are also segmented into consecutive sample blocks. After the signal conditioning, the feature extraction, extracts the chosen features. The last step, the feature conditioning, also known as post-processing, prepares the feature vector for the feature-translation step. After the extraction of the features, it is mandatory to translate them into appropriate device commands (feature translation). This step is accomplished using the translation algorithm. The central component of an effective translation algorithm is an appropriate model. A model is a mathematical concept of the relationship between independent variables (brain signal features) and dependent variables (the user's intent). In the end of the process, the BCI system have to output a command into an external device, such as a cursor control, a robotic limb operation or other assistive device [61].

BCI systems can be categorized in open or closed-loop BCI systems, whether they provide or not feedback to the user. In an open-loop BCI, the participant does not receive feedback regarding the neural activity. On the contrary, in a closed-loop BCI, the user receives real-time feedback of the neural activity, which is useful to verify if the BCI has the desired output. An open and closed-loop BCI systems are illustrated in figure 2.5.

When talking about BCI, the applications that come to mind are mostly clinical applications. This means that the main possible BCI users are people who are severely disabled or paralyzed, such as people with cerebral palsy, spinal cord injuries or amyotrophic lateral sclerosis (ALS). One of the possible uses of BCI is communication, for example, for people who suffer from "locked in" syndrome. Another main goal of BCI is to re-establish the motor control in paralyzed patients or the possibility to control the environment for disabled people. The restoration of independent locomotion is also a promising application of BCIs for paralyzed people. In addition, BCI systems may also be used in therapy, to help people who suffered a trauma to relearn motor function. On the other hand, for non-clinical applications, BCI also has an extensive range of applications, for example, training and education or gaming and entertainment.

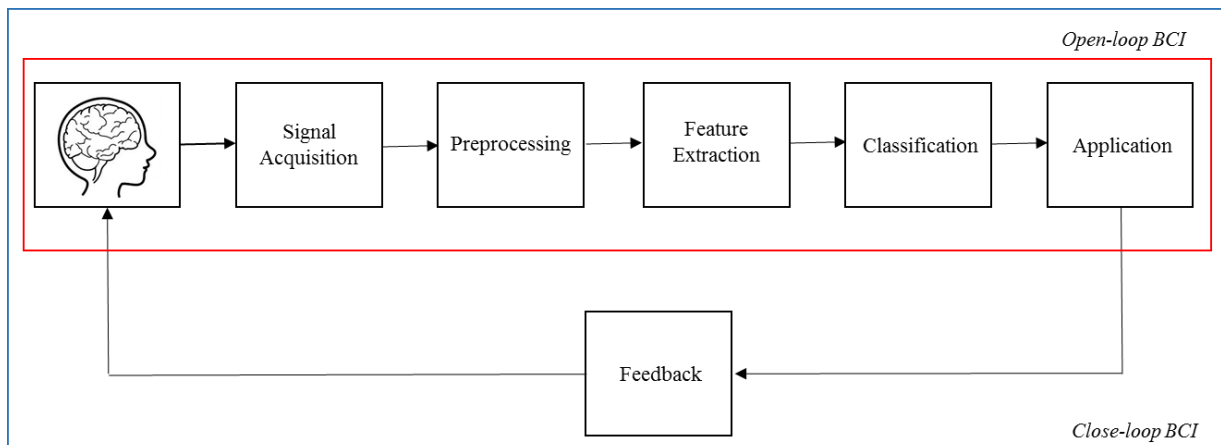


Figure 2.7. Diagram of a BCI system. Open-loop BCI represented in red and closed-loop BCI represented in blue.

2.4.1 History of BCI

Over the past years, increased BCI research has been determined by an enhanced understanding of the several brain functions and by a potent computer equipment. The term brain-computer interface dates to 1977, when Jacques Vidal developed a BCI system based on visual evoked-potentials [62]. Later, in 1999, Chapin et al determined that motor cortex neurons can directly control a specific device [63]. Since then, there has been an increased interest in this technology, mainly to restore the motor capacities of severely disabled patients, particularly the ones suffering from ALS, stroke, cerebral palsy and spinal cord injury [64].

BCI's can be categorized into two categories, whether they use non-invasive or invasive methods for electrophysiological recordings. Non-invasive BCI's use EEG recordings from the surface of the head, to control external devices, like computer cursors. Although this method provides an advantageous solution for paralyzed people, the neural signals have a limited bandwidth. Some systems are based on visual evoked potentials (VEPs), such as the P300 evoked potential, which occurs approximately 300 milliseconds after a significant event or stimulus. It is generated when a subject tries to discriminate stimulus. The first use of the P300 potential was described by Farwell and Donchin, with a P300-based spelling device. In this study, the letters of the alphabet are displayed on a computer screen and the subject focuses attention on the characters he wishes to communicate [65].

Another BCI system uses the sensorimotor rhythms (SMRs). These rhythms do not require a specific stimulus and change with movement or even with the imagination of a specific movement. These rhythms were first used in 1991 to control a cursor, where subjects learned to change μ rhythm amplitude in order to reach a specific target [66]. Later, in 2008, it was shown that an asynchronous EEG-based BCI, allows subjects to control a wheelchair [67].

Although BCI systems may represent a huge advantage for disabled people, operating an EEG-based-BCI requires some practice, that can take many days, since the visual feedback is the crucial part of the training [68]. Some techniques have been developed to provide feedback to the BCI users. For example, virtual reality systems are advantageous to provide a useful feedback for BCI training [69]. In addition to electrophysiological measures, different techniques have been explored, for instance, functional magnetic resonance, magnetoencephalography and fNIRS [70] [71] [72]. Contrary to non-invasive BCI's, invasive approaches use microelectrodes implanted in cortex to record the activity of single brain cells.

Although the greater part of the research in this area has been made with animals, more recent studies have focused on human users. For example, Hochberg et al, aimed to restore the motor functions

in paralysed humans using microelectrodes implanted in motor cortex [73]. Different studies have shown that user can also control a cursor rapidly and accurately, with electrocorticographic activity recorded from the surface of the brain [74].

2.4.2 Feature extraction

Like previously said, the brain characteristics used in BCI, to translate a user's intent, are called signal features. Most BCIs extract several features simultaneously, which is referred as feature vector. Consequently, the feature extraction is defined as the process of discriminating the signal characteristics from unnecessary content and compact these features in a vector to be interpreted by a computer. In order to be effective for a BCI application, these features should be based on temporal, spatial or spectral characteristics.

To identify temporal features, the methods of peak-picking/integration and correlation/template matching can be used. The Peak-Picking technique determines the minimum or maximum values of a signal, in a determined time block, after a stimulus, using the value as the feature for the time block considered. A more elaborated technique than the simple peak-picking is the integration, where the signal can also be integrated or averaged over the time block. This method was used by Farwell and Donchin, in 1988, during the development of the first P300-based BCI [65]. On the other hand, the Template-Matching uses the similarity or correlation of a response to a predefined template as a feature. The output value will be high when the response correlates with the template, and low when the segments differ from each other. In 2007, Krusienski et al used a μ -rhythm matching filter to control a BCI [75].

Since brain activity oscillations are modulated in the form of amplitudes and frequencies, there is a great advantage of tracking the changes of this parameters, to extract spectral features. Although the most common spectral features extraction method is the Fast Fourier Transform (FFT), the band power and the autoregressive (AR) modelling can also be used. The band power method tracks amplitude modulations, at a specific band (frequency). Firstly, the frequency chosen is isolated, applying a bandpass filter, which produces a sinusoidal signal. Then, the absolute value is calculated, to produce only positive values and lastly, with a low-pass filter, the peaks are smoothed. The FFT method represents an implementation of the discrete Fourier transform. The FFT characterizes the frequency spectrum of a digital signal with a frequency resolution of FFT-points, or sample rate. Kelly et al used a method based on FFT in an independent BCI [76]. The AR modelling, like the Fourier transform, is used to calculate the frequency spectrum of a signal. However, in this method, the signal is generated passing white noise through an infinite impulse response (IIR) filter. Burke et al, applied the AR modelling for feature extraction during BCI analysis [77].

In terms of time-frequency features, the wavelet analysis produces a time-frequency representation of the signal. When compared to FFT, wavelet analysis designs a filter to achieve an enhanced time-frequency resolution. Qin et al developed a wavelet-based time-frequency analysis method for classification of MI tasks for BCI applications [78].

Lastly, the similarity features can be divided in three different methods, namely the Phase Locking Value (PLV), the coherence and the Mahalanobis Distance. The phase locking value (PLV) represents the value of the mean phase difference between two signals, that occupy the same frequency range. PLV is useful to calculate the phase relationship among different EEG electrodes. The PLV ranges from zero, when the phase is not coupled, to one, when the signals are phased locked with each other. Wei et al showed that coupling measures quantified by PLV are appropriate methods for feature extraction in BCIs [79]. The coherence is the measurement of the amplitude correlation between two signals in the same frequency band. The value also varies from zero (no coherence) to one (highest coherence). To estimate the coherence, it is necessary a large number of observations. Therefore, this method is not

suitable for online BCI applications. Lastly, the Mahalanobis Distance measures the similarity between signal features and predefined distributions of those features.

2.4.3 Common Spatial Pattern (CSP)

2.4.3.1 CSP algorithm

The Common Spatial Pattern method was suggested for the first time, for classification of EEG data, during imagined hands movements by H. Ramoser [80]. This algorithm extracts spatial filters that maximize the discriminability between two classes [81]. CSP uses spatial filters s that maximize the following equations:

$$J(s) = \frac{s^T X_1^T X_1 s}{s^T X_2^T X_2 s} = \frac{s^T C_1 s}{s^T C_2 s} \quad (2.1)$$

X_i denotes the matrix $k \times n$ for class i , where k is the number of samples and n is the number of channels. C_i is the covariance matrix of the EEG signal from class i . This problem is transformed to a standard eigenvalue problem by noting that it is equivalent to maximizing the next function derived based on the Lagrange method:

$$L(\lambda, s) = s^T C_1 s - \lambda(s^T C_2 s - 1) \quad (2.2)$$

The derivative of L with respect to the filter s equal 0, and therefore:

$$C_2^{-1} C_1 s = \lambda s \quad (2.3)$$

The spatial filters that extremize equation 3 are the eigenvectors of $M = C_2^{-1} C_1$, corresponding to the largest and lowest eigenvalues.

2.4.3.2 Regularized CSP (RCSP)

Although CSP is known to be very popular and effective, it is also very affected with the noise and may overfit regularly, especially with small datasets [82]. Recently, to overcome these disadvantages of the CSP method, there has been a vast interest in adding prior information to the CSP learning process, using regularization terms [83] [84] [85]. The process of adding prior information into the CSP method can be achieved with two distinct manners. It can be done either at the covariance matrix estimation or at the level of the objective function, which imposes prior information on the spatial filters [81].

So far, several RCSP algorithms were developed, namely, the composite CSP (CCSP), the regularized CSP with generic learning approach, the regularized CSP with diagonal loading and the invariant CSP. The goal of the composite CCSP, proposed by Kang et al [84], is to perform subject-to-subject transfer, which regularizes the covariance matrix using other subjects' data. The Regularized CSP with generic learning approach was proposed by Lu et al [83] and aims to regularize the covariance matrices using data from other subjects. The Regularized CSP with diagonal loading approach uses the Ledoit and Wolf's method to decrease the covariance matrix towards the identity matrix [86]. Lastly, the invariant CSP, regularizes the CSP objective function, to make filters that are invariant to a specific noise source. In this case, additional EEG measurements have to be performed in order to acquire the EEG signals and their covariance matrix. The present algorithm was proposed by Blankertz *et al* [87].

Recently, Lotte *et al* [81] proposed four new algorithms for CSP regularization: a CSP regularized with selected subjects, a Tikhonov and a weighted Tikhonov regularized CSP and a spatially regularized CSP. The Regularized CSP with selected subjects is similar to CCSP, with the difference

that it only uses the data from selected subjects instead of using all the subjects. To select the right number of subjects an algorithm was developed to select the subject to add or remove, to increase the accuracy of the BCI training. The CSP with Tikhonov Regularization is based on a regularization form, firstly introduced for regression problems, consisting in penalizing solutions with large weights [88]. The CSP with weighted Tikhonov Regularization is similar to the CSP with Tikhonov Regularization, although it assumes that to classify a specific mental state, some channels are more important than others are. With weighted Tikhonov Regularization, different channels have different penalties, depending if they are likely to be useful or not. The Spatially Regularized CSP intends to use the spatial information of the EEG electrodes, obtaining filters for which neighbouring electrodes have relatively similar weights.

2.4.4 Classification in BCI

In order to have the desired output, the BCI systems has to identify brain patters produced by the user and translate them into commands. Usually, this pattern recognition depends on classification algorithms. The main classification algorithms used in BCI research can be separated into four different groups: linear classifiers, neural networks (NN), nonlinear Bayesian classifiers and Nearest Neighbour classifiers, although a combination of more than one classifier can also be used.

2.4.4.1 Linear Classifiers

These classifiers represent discriminant algorithms that use linear functions to discriminate between classes, being the prevalent type of classifiers used in BCI research. Linear classifiers can be divided into two main categories, namely the Linear Discriminant Analysis (LDA) and Support Vector Machine (SVM).

LDA is based on a hyperplane that separates the data that represent different classes. This algorithm assumes a normal distribution of the data, with equivalent covariance matrix for both classes. The hyperplane is found by searching the projection that exploits the distance between the means of the two classes, minimizing the interclasses variance. The biggest advantages of this technique are the simplicity and the reduced computational power needed, what makes it appropriate for online BCI. On the other hand, the main disadvantage is that on nonlinear EEG, the linearity can provide poor results. LDA has been used mainly in MI-based BCI and P300 speller.

On the other hand, SVM, also uses hyperplanes to categorize classes, although the hyperplane maximizes the boundaries. Due to this maximization, this technique has good generalization properties. SVM also allows the existence of outliers since it uses a regularization parameter. This classifier uses the ‘Kernel trick’ to create nonlinear decision boundaries. This consists in assigning the data to another space, using a kernel function $K(x, y)$. Usually, the kernel function used in BCI research is the Gaussian or Radial Basis Function (RBF) Kernel, defined by equation (2.4), where x and y represent the two samples and σ represents a free parameter.

$$K(x, y) = \exp\left(\frac{-|x - y|^2}{2\sigma^2}\right) \quad (2.4)$$

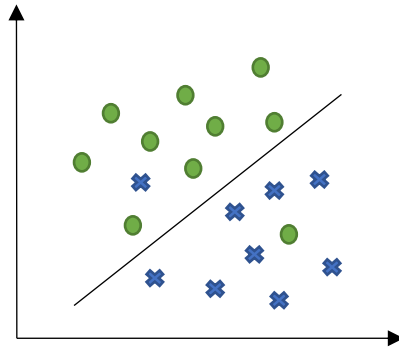


Figure 2.8. Linear Discriminant Analysis. LDA is based on a hyperplane that separates two classes, represented in blue and green.

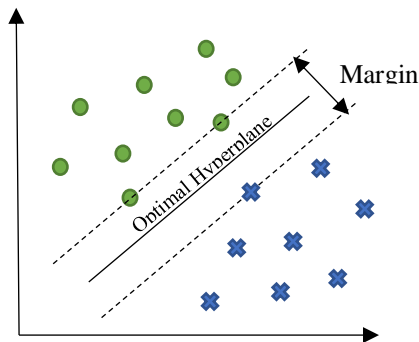


Figure 2.9. Support Vector Machine. SVM finds the optimal hyperplane for generalization, between two classes, represented in blue and green.

2.4.4.2 Neural Networks

The second main category of classifiers are the Neural Networks, which are computing systems based on biological neural networks. This means that NN are an association of numerous artificial neurons, which allows to create nonlinear decisions. The most commonly used NN for BCI research is the Multilayer Perceptron, composed by a variable number of neurons' layers (input layer, one or several hidden layers and an output layer). This technique is very flexible, since it can classify a variable number of classes and consequently adjust to a great variety of problems. Figure 2.10 represents a neural network composed with three different layers.

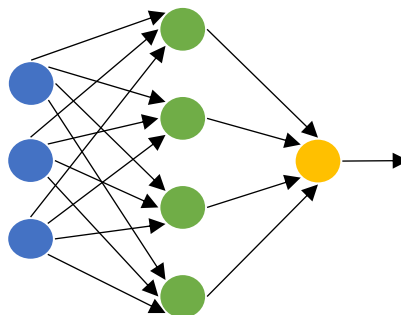


Figure 2.10. Multilayer Perceptron composed by three layers. Input layer (blue), hidden layer (green) and output layer (yellow).

2.4.4.3 Nonlinear Bayesian classifiers

The third category of classifiers includes the Nonlinear Bayesian classifiers (Bayes quadratic and Hidden Markov Model). Both classifiers produce nonlinear decision boundaries. Although these classifiers perform a more effective rejection of samples than discriminant classifiers, non-linear classifiers are not widespread as linear classifiers or NN among BCI research.

The Bayesian approach uses the concept of maximum likelihood to combine prior knowledge with newly acquired knowledge to produce a posterior probability, this means that it produces the model parameters that are most likely to be correct based on the available data. This classifiers has been applied successfully in motor imagery experiments [89].

Hidden Markov Model (HMM) classifiers represent a probabilistic mechanism that gives the probability of observing a certain sequence of feature vectors. Later, the mechanism can model the probability of observing the feature vector. This model is appropriate for time series classification, for instance, to the classification of raw EEG signals [90].

2.4.4.4 Nearest Neighbour classifiers

The last category includes the Nearest Neighbour classifiers, namely the k Nearest Neighbours and the Mahalanobis distance. These classifiers aim to assign a feature vector to a class based on its nearest neighbours.

The goal of k Nearest Neighbours is to allocate to a hidden point, the dominant class amongst its k nearest neighbours. This technique is used only in BCI systems with low-dimensional feature vectors. With a high value of k and sufficient training samples, this algorithm is capable to produce nonlinear decision boundaries, since k NN can approximate any function.

In terms of the Mahalanobis distance, these classifiers assume a Gaussian distribution $N(\mu_c, M_c)$, for each sample of the class c . Later, a feature vector x is allocated to the class that matches to the nearest sample. Although this classifier is barely used in BCI, it is appropriate for multiclass and asynchronous BCI systems. It can be mathematically represented by equation (2.5).

$$d_c(x) = \sqrt{(x - \mu_c)M_c^{-1}(x - \mu_c)^T} \quad (2.5)$$

2.4.4.5 Recently Developed Classifiers

Although the previous classifiers are still used regularly, new algorithms have been designed and tested to classify EEG signals during BCI operations. These recently developed classifiers are divided into four categories: adaptive classifiers, matrix and tensor classifiers, transfer learning and deep learning [91].

Adaptive classifiers were proposed in the mid-2000s and are shown to be useful for offline analysis. These classifiers re-estimate each parameter (weight attributed to each feature in a hyperplane) over time, as the new data become available, allowing the classifier to track changes in the feature distributions [92].

Matrix and tensor classifiers can be subdivided into Riemannian geometry-based classification (RGC) and feature extraction and classification using tensors. RGC consists in mapping the data directly into a geometrical space with an appropriate metric. In this space, data can be manipulated for several purposes, such as averaging, smoothing and classifying. This method is based on the hypothesis that the

power and the spatial distribution of EEG sources can be considered fixed for a specific given mental state. Tensors, or multi-way arrays, provides a representation of EEG data for feature extraction, clustering and classification in BCI. This method is based on the generation of higher-order structured tensors from lower order data formats. The representation of BCI data with tensors is useful in attenuating the problems with small sample sizes, since the information about the structure of data is usually essential in tensors. Although tensors may represent a promising technique, this method requires more research in order to be applicable in practice.

Transfer learning focuses on a set of methodologies where a model developed for a specific task is reused for a model on a second task. This method is particularly relevant in situations where exists abundant labelled data for one task and data are rare or expensive to acquire for the second task. The effectiveness of the method depends on how well-related the tasks are. Transfer learning has been mainly used during motor imagery tasks.

Deep learning consists in a machine learning algorithm that uses a cascade of multiple layers of nonlinear processing units for feature extraction, where each successive layer uses the output from the previous layer as input. This learned features are related to increasing levels of concepts. This method is also able to learn in supervised (classification) and unsupervised (pattern analysis) manners [93]. Deep learning models are inspired by the information communication patterns in biological nervous systems.

2.4.5 BCI Open-source Software Platforms

Over the past few years, computer power and complexity has increased and is, currently, enough for the majority of BCI requirements. Although MATLAB (The Mathworks, Inc.) is one of the most widespread platforms to develop a huge variety of scientific problems, software platforms specifically designed to the BCI research have been developed.

In the present study, it was used OpenVibe, due to its numerous advantages, such as the user-friendly interface and the capability of real-time processing and visualisation of brain signals. OpenVibe platform includes two main user dedicated tools, namely, the acquisition server (figure 2.11) and the designer (figure 2.12). The acquisition server provides a user interface to connect the acquisition devices and to forward the acquired signals to OpenVibe applications in a standardized format. The acquisition server connects with the acquisition devices using modules called drivers. The designer allows the user to create scenarios with a graphical language, used in all steps of the BCI [94]

Table 2.2 summarizes several BCI platforms, their key features and their advantages compared to the other platforms.

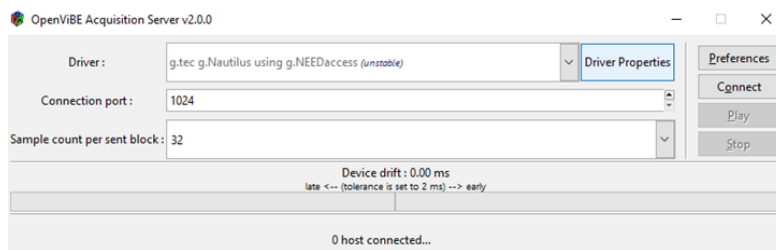


Figure 2.11. OpenVibe Acquisition server. The acquisition server provides a user interface to connect the acquisition devices.

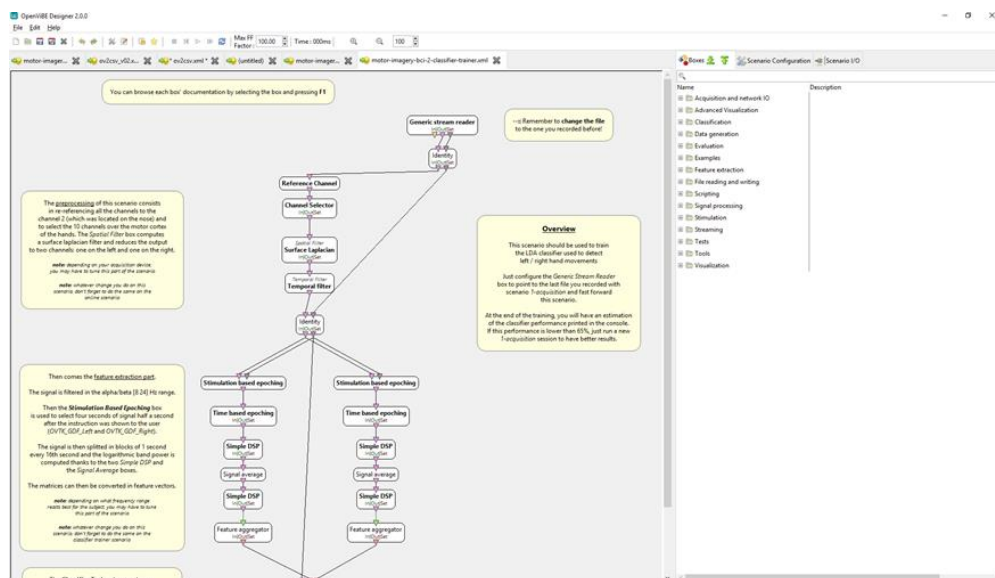


Figure 2.12. OpenVibe scenario. The designer allows the user to create scenarios with a graphical user interface.

Table 2.2. Summary of several BCI platforms and their main features.

Software	Design Goal	Main Features	Programming Language	Advantages
OpenVibe [94]	Acquisition, processing and visualization of cerebral data. Set of software modules that can be easily integrated to develop fully functional BCIs.	Can be integrated with high-level applications such as virtual reality environments.	Graphical language	Allows users to create hardware-independent scenarios. Offers a wide range of visualization widgets such as raw signal display or time-frequency maps. Includes sample scenarios for BCIs or neurofeedback applications.
BCI2000 [95]	Data acquisition, stimulus presentation and brain monitoring applications.	Customizable auditory/visual stimulation that is synchronized with acquisition of brain signals and other inputs	C++, Matlab and Python compatibility.	Support for different data acquisition hardware Does not rely on third-party software
TOBI [96]	Facilitates distributed BCI research and interoperability between different BCI systems and platforms.	Set of interfaces which connect parts of different BCI systems.	C/C++ and Matlab	Connect different BCI systems with a minimum of additional work.
BCILAB [97]	Rapid prototyping, real time testing, offline performance evaluation of new BCI applications, and comparative evaluation of BCI methods	Emphasis on combining recent methods in machine learning, signal processing, statistical modelling, and electrophysiological imaging. Provides several frameworks to speed up incorporation and testing of new BCI methods	Graphical and scripting (Matlab) user interface.	Strong focus on recently published methods. High level of automation. Linkage to EEGLAB
BCI++ [98]	Based on a sophisticated graphics engine which allows a rapid development of BCI systems.	Consists of two functional modules that split the development of a BCI system into two parts. The first module is called HIM (Hardware Interface Module) and handles signal processing. The second module provides a graphical user interface (GUI).	C/C++ and Matlab	HIM supports several acquisition devices
xBCI [99]	Data processing, data acquisition, data visualization, experiment control, real time feedback presentation	Easy-to-use system development. Extendable and modular system design (functional modules can be added by users).	GNU C/C++	Supports multiple operating systems. Does not depend on any commercial software products
BF ++ [100]	Provide tools for the implementation, modelling and data analysis of BCI systems.	Create unique methods, terminologies, and tools independent from the specific protocols such as P300 or SSVEP.	C++	Support for several file formats (BCI2000, GDF, Brain Vision Analyzer, MEG)

<p>Pyff [101]</p>	<p>Development of BCI feedback and stimulus applications as fast and easy as possible.</p>	<p>Comes with a variety of ready-to-use experimental paradigms. Can be used as a platform to run neuroscientific experiments independent from BCI systems.</p>	<p>Python</p>	<p>Not tied to a special operating system.</p>
<p>BioSig [102]</p>	<p>Data acquisition, artefact processing, quality control, feature extraction, classification, modelling, and data visualization.</p>	<p>A real-time BCI system implemented in Matlab (rtsBCI).</p>	<p>C/C++ and Matlab</p>	<p>Tools for different application areas (neuroinformatics, BCI, neurophysiology, psychology, cardiovascular systems, and sleep research) Almost fully automated data analysis</p>

2.5 Motor Imagery

An important practice in the field of BCI research is the modulation of SMR through motor imagery. Motor imagery based BCI relies on the concept of simulating an action mentally, without the actual performance of the movement. Numerous studies showed that MI stimulates the same brain regions as the execution of the actual movement [103] [104]. MI patterns have been found not only in healthy people, but also in patients suffering from ALS, spinal cord injury and stroke [105] [106] [37] [107]. This technique can be used in patients without motor function since it does not need a motor input.

Firstly, the studies involving MI focused mainly in the upper limbs movements, although, more recently, those studies also started to consider the lower limbs, in order to study and evaluate the human gait. In 2007, Baker *et al* conducted an experiment with fourteen healthy subjects who performed both MI and actual walking tasks. The results showed a high association between the imagined and the actual walking, proving that MI uses similar cerebral resources as actual gait [108]. Neuroimaging studies proved that MI is associated with the activation of several cerebral areas, such as the SMA, the inferior parietal cortex, the primary motor cortex, the inferior parietal cortex, the cerebellum and the basal ganglia [109]. The activation in MI differs also from distinct body parts. MI of lower-limb and gait relies on a completely different cerebral network than MI of upper-limbs. MI of the upper-limbs movements activates mainly the premotor cortex including the inferior frontal gyri, middle frontal gyrus, and precentral gyrus. On the other hand, MI of lower limb involves essentially the SMA, cerebellum, putamen, and parietal regions [110].

MI has been widely used in neurological and post-stroke rehabilitation. Dickstein *et all* described the use of this technique to recover or improve walking ability in patients with hemiparesis, suggesting that MI may be suitable for the walking rehabilitation in patients after stroke and that imagery practice should rely on specific impairments during gait [111]. A different study concluded that MI is more effective when combined with physical practice, which means that MI promotes leaning by reinforcing processes at the cortical level [112]. Several studies also showed that different types of imagined movements have a different spatial distribution. For example, μ (8-12Hz) and β (18-26Hz) rhythms reveal different areas of ERD concerning each state [40].

Ramoser *et al* designed a spatial filter with the CSP method and demonstrated that this technique is useful to extract information from two classes of single-trial EEG [80].

MI faces a number of challenges associated with the detection of motor intention in MI tasks of upper and lower limbs even for just two classes [113] [114]. These challenges are, for example, the low signal decoding performance and a large inter-subject variability. The low processing speed limits the practical applications. This is due mainly because EEG signals are prone to contamination for a wide range of artefacts, such as blinking/movements of the eyes (EOG), heartbeats and electromyography (EMG). The number of channels also plays an important role in MI, since it is important to choose an optimal number of electrodes and their locations, to improve discrimination between classes. The use of small number of channels is advantageous since it helps to decrease the computational complexity and allows the development of methods for real-time feedback. Although MI-based BCI is still not use in the real-life environment, it has a higher classification accuracy, in the order of 90%, for the classification of imagined left and right-hand movements.

2.6 Artefacts Removal

During the recording of cerebral activity, EEG also records electrical activities that does not result from neurophysiological sources. This type of activity is named artefact. The main artefacts can be classified into patient-related or physiological artefacts and system or extraphysiologic artefacts. The physiologic artefacts are mainly caused by muscle activity, eye movements, pulse and respiration or skin artefacts. On the contrary, extraphysiologic artefacts are mainly due to electrodes, cable defects, electrical noise or movements in the environment. The huge variety of artefacts and their overlapping with the signal of interest makes difficult the task of recovering the EEG signal of neurophysiological origins. During BCI applications, artefacts can contaminate the EEG signal that the recovery of and worsen the classification sensitivity and specificity. Although, there is no common solution available for this problem, there is a wide range of methods used in artefact removal.

Artefact removal consists in cancelling or correcting the artefacts without distorting the signal. One of the most common techniques to handle artefacts is based on rejecting or cancelling the data epochs identified as artefactual. The major disadvantage of this method is that it also removes important neurophysiological information. This may reduce the statistical power of BCI methods to detect features. Therefore, with the increased development of signal processing techniques, several methods have been developed.

Another method for artefact removal is based on low, high or bandpass filters. Nevertheless, this method is only effective when the frequency band of the signals and the artefacts do not intersect. Usually, simple filtering is not considered for artefact removal, except for narrow band artefacts like the line noise (between 50 and 60 Hz). To make the process of artefact removal more efficient, several filtering techniques try to adapt the filter parameters. The principal filtering techniques used in this process are the adaptive filtering, the Wiener filtering and the Bayes filtering. An adaptive filter tries to adapt the filter parameters according to an optimization algorithm. Boudet et al, designed an adaptive filtering method based on CSP, to reduce ocular and muscular artefacts on EEG recordings [115] [116].

Linear regression methods were extensively used, particularly for eye interferences, due to their simplicity and the low computational power required. This technique assumes that each EEG channel comprises a clean EEG signal source and an artefacts source, available through a reference channel [117]. More advanced methods, such as blind source separation decompose the EEG data into other domains [118]. Assuming that the measured cerebral activity ($a(t)$) is represented by the sum of the actual cerebral activity ($c(t)$) and the noise ($d(t)$), the approach for artefact removal in EEG signals can be mathematically denoted by equation 2.1.

$$A = BC + D \quad (2.6)$$

Where A is the EEG data and n is the number of samples. B represent an unidentified mixing matrix, C is a matrix of unknown sources, and D is the noise matrix [119]. Blind source separation (BSS) aims to calculate the matrix C , from equation (2.6), from the observations in A , without a reference waveform. BSS techniques, such as ICA and PCA contemplate the information provided by all the channels [120]. Independent Component Analysis is the most common form of BSS used in removing artefacts from EEG data [121] [122]. This technique involves the extraction of maximally independent components (IC) from the EEG signal. Non-brain components are normally identified manually based on their frequency profile and their spatial distribution. Subsequently, they are removed and the EEG signal is reconstructed without their influence. ICA has several advantages compared to principal component analysis (PCA), which is based on an orthogonal decomposition of correlated variables in linearly, uncorrelated variables (Principal Components). This method was firstly proposed to remove ocular artefacts [123], but later it was shown that PCA cannot totally separate artefacts from cerebral activity, particularly when the amplitudes are similar [124].

Other source decomposition methods, decomposes each channel into waveforms, representing the signal or the artefacts. Wavelets and empirical mode decomposition (EMD) are examples of source decomposition techniques [125] [126] [127]. The Wavelet Transform is represented by the product of the signal $f(t)$ with the time scaled of the wavelet function $\Psi(t)$, called mother wavelet. The WT decomposes the signal into several coefficients, for different scales, representing the similarity of the signal with the wavelet, at that scale. WT was used alone to automatically identify and remove ocular artefacts [128] or in combination with other techniques, such as ICA, to enhance the pre-processing of EEG signals [129].

Empirical mode decomposition decomposes a signal into a sum of its basis functions, called intrinsic mode functions. These functions can be calculated applying the Hilbert transform. This technique is mainly used to nonlinear signal processing or non-stationary signals. EMD has been used to remove ocular artefacts [130] [131] and muscle artefacts [132]. In the past years, researchers also tried to combine the advantages of several methods, to improve artefact detection. Mijović et al combined EMD and ICA to remove artefacts from single-channel recordings and Castellanos et al used ICA enhanced with WT for artefact suppression [133] [134].

2.6.1 Artefacts Removal during walking

Recently, there has been a huge interest in recording EEG during locomotion. This process induces several challenges, mainly due to motion artefacts and head acceleration and deceleration. Studies have shown that there is a correlation between the EEG amplitude and the head acceleration, and that motion artefacts related to gait may occur in a systematic pattern. Independent Component Analysis has shown to be a reasonable technique to identify motion artefacts in scalp EEG [135]. In 2010, Gwin et al developed a channel-based artefact template regression method, with a spatial filter, to remove gait related movement artefacts, proving that EEG can be used to study human locomotion and that gait related artefacts can be minimized with a template regression procedure [136]. Recently, Oliveira et al proposed a channel rejection method to attenuate motion artefacts in EEG recording during walking activities. While, traditionally, bad channels are identified according to the range, standard deviation, kurtosis and correlation, this method aims to remove the channels carrying motion related artefacts that were not detected with the standard methods, for example, channels with artefacts locked to gait events [137]. In terms of real-time artefacts detection, Kim et al, developed a BCI system capable to detect gait phases and remove motion artefacts, while subjects walk in real environments. This study used human strides to train the BCI system, showing the possibility of using mobile and wireless BCI systems in real-life environments [138].

3. Pre-processing for BCI

3.1 Filtering

In order to use the EEG for further analysis, data should be pre-processed, in terms of filtering and artefact removal. EEG data was recorded from six healthy participants (3 males and 3 females, 25.5 ± 6.7453 years). It were used two g.tec Nautilus, EEG wireless acquisition systems with active-electrodes: a 16-channels dry electrodes cap (g.Sahara) and a 32-channels wet electrodes cap (g.ladybird), with a sampling frequency of 250 Hz, placed accordingly to the 10-20 system.

As previously mentioned, EEG signals may be extremely affected by noise and interference, which may result in artefactual recordings. Since most of the brain activity observed in the scalp has a frequency range of 3–40 Hz, it is useful to apply a bandpass filter to remove lower and higher frequencies. Usually, a notch filter is also applied, to reject the 60 Hz or 50 Hz power line noise.

For the motor imagery study, the EEG signal was filtered based on a bandpass Butterworth filter (order 4) at 1–30 Hz. For the gait adaptation part, it was used a bandpass impulse response (FIR) filter of 3–45 Hz to filter the EEG signal.

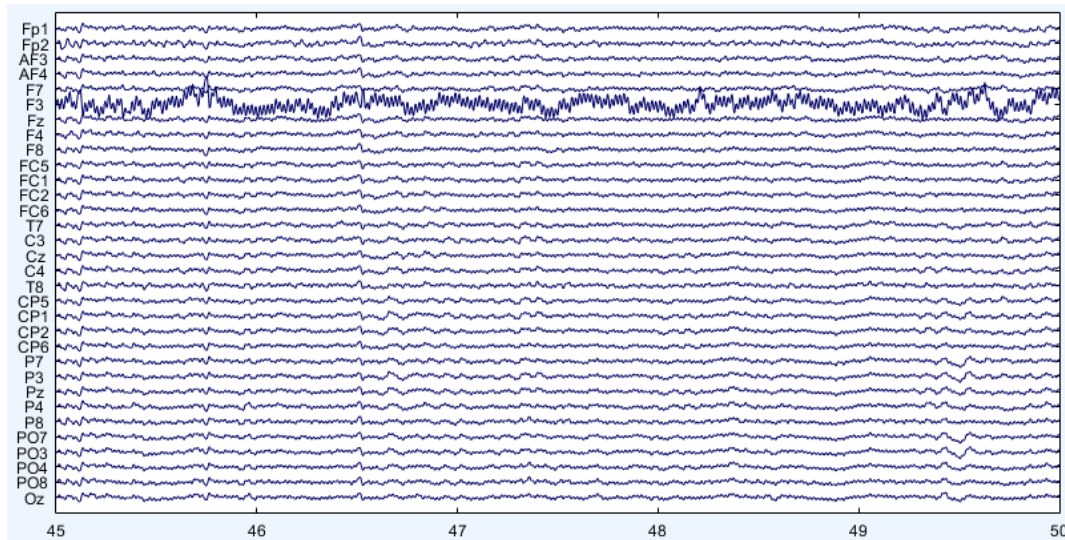


Figure 3.1. Motor imagery data with bandpass filtering at 1–30 Hz.

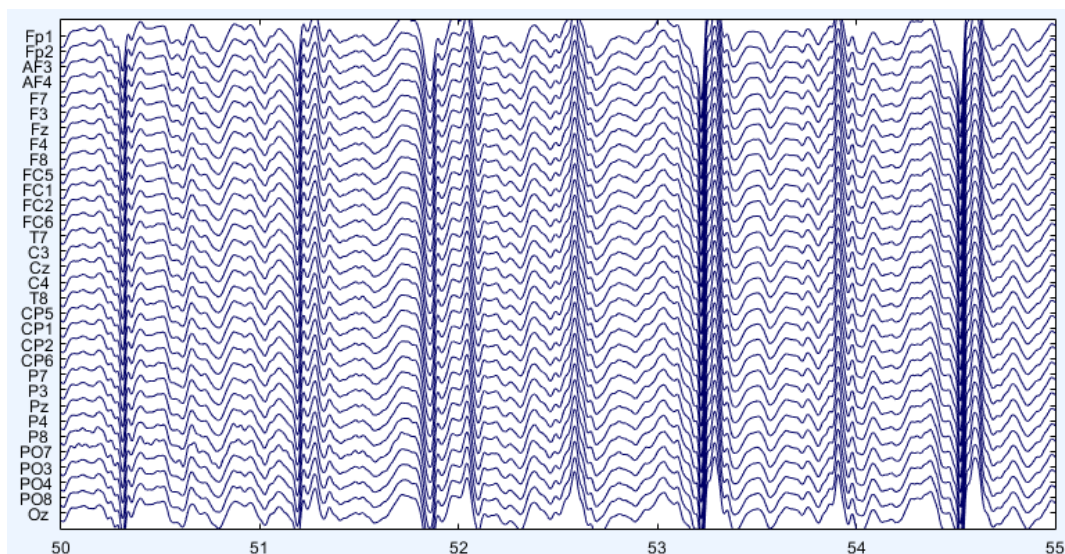


Figure 3.2. Gait adaptation with bandpass filtering at 3–45 Hz.

Comparing figures 3.1 and 3.2 it is possible to verify that in the case of motor imagery, the bandpass filtering technique is sufficient to remove most of non-physiological artefacts, while in the gait adaptation part, the EEG signal is still highly contaminated by noise and interference. Contrary to the motor imagery study, where subjects were seated and still, during gait adaptation, subjects were asked to walk at different speeds, which induces several artefacts in the EEG signal, mainly motion artefacts. Consequently, to remove the influence of motion components it was used ICA, a common approach to remove gait-related movement artefacts [136] [135].

3.2 Artefacts Removal based on Independent Component Analysis (ICA)

In this study, artefact removal was performed in Matlab R2017b (The Mathworks, Natick, MA), using scripts based on eeglab (Appendix A) [139]. The eeglab function runica.m performs the ICA decomposition using the Infomax ICA algorithm, proposed by Bell and Sejnowski, with the extended-ICA algorithm of Lee [140] [141]. ICA involves the extraction of maximally independent components. Motion components were identified manually based on their frequency profile and spatial distribution and, subsequently, were removed and the EEG signal were reconstructed without their influence.

3.2.1 Independent Component Analysis

As previously mentioned, ICA involves the extraction of maximally independent components from the EEG signal. Considering observations of random variables $(a_1(t), \dots, a(t))$, where t represents the time and B is an unknown matrix and assuming that the variables are generated as a linear combination of ICs:

$$\begin{pmatrix} a_1(t) \\ a_2(t) \\ \vdots \\ a_n(t) \end{pmatrix} = B \begin{pmatrix} c_1(t) \\ c_2(t) \\ \vdots \\ c_n(t) \end{pmatrix} \quad (3.1)$$

ICA consists in estimating the matrix B and the parameter $c_i(t)$ based only on the variable $a_i(t)$. In ICA, the number of ICs is the same as the number of observed variables. This technique is based on two main principles. The first principle states that ICA finds the matrix B so that for any $i \neq j$, the components c_i and c_j and the transformed components are uncorrelated. The second principle is called the Maximum Nongaussianity, which finds the local maxima of nongaussianity of a linear combination, assuming that the variance of c is constant.

Figure 3.3 represents the scalp map projections of the ICA components. The Scalp Topographies illustrates the effects that independent components have on each electrode. The effects of ICs are shown with a colour scale, where green represents no effect and red and blue represent positive and negative contributions, respectively.

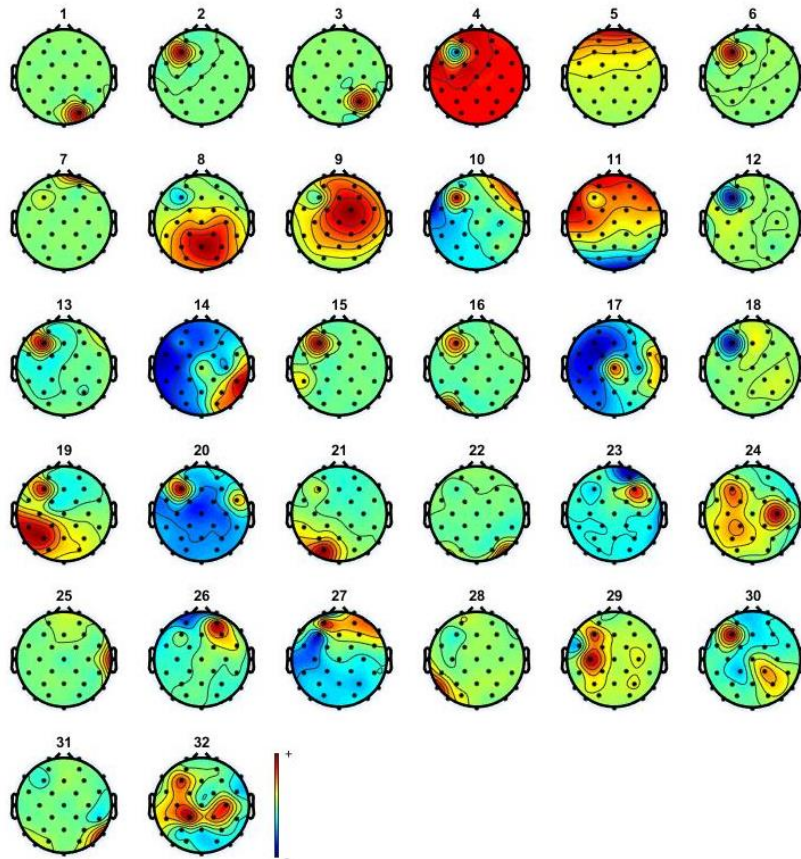


Figure 3.3. Scalp Topographies of the ICA components. Each scalp map illustrates the effects that independent components have on each electrode. The effect of independent components is represented with a colour scale, where green represents no effect and red and blue represent positive and negative contributions, respectively.

When looking for the ICA components to remove from the dataset, it is also useful to scroll through the ICA activations, which can identify components pointing for characteristic artefacts. As illustrated in figure 3.4, the first components reflect several types of artefacts and should be removed from the EEG dataset before further analysis.

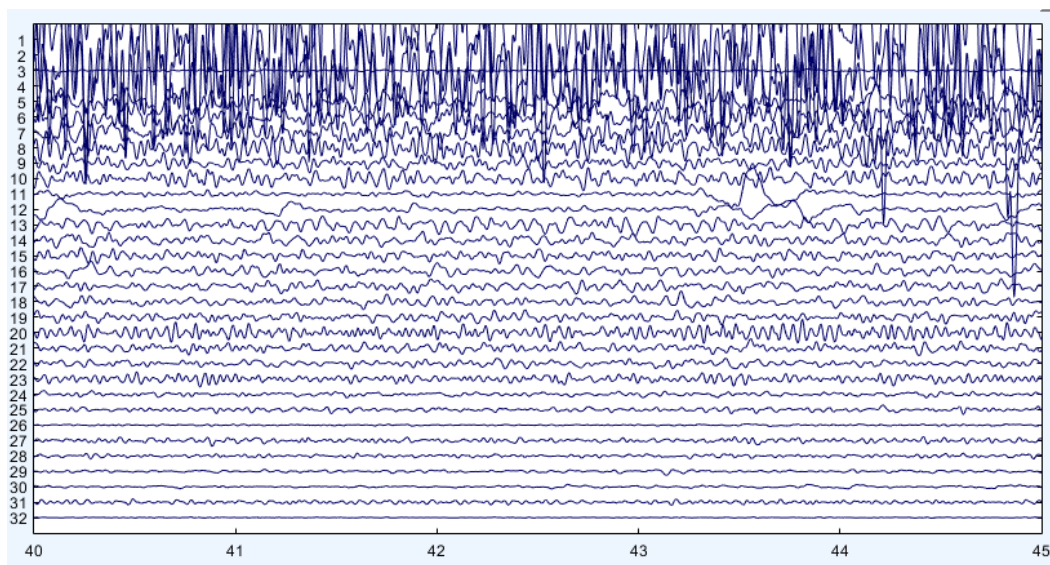


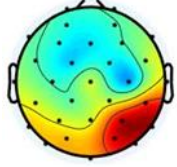
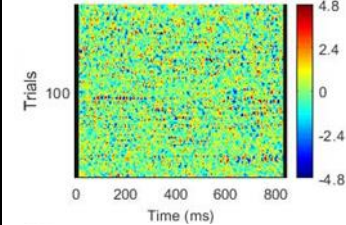
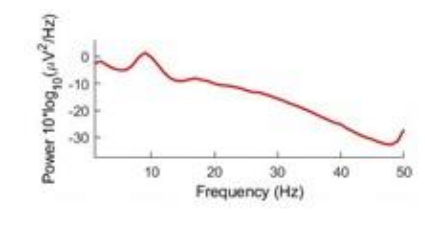
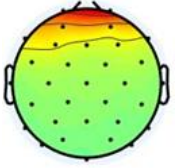
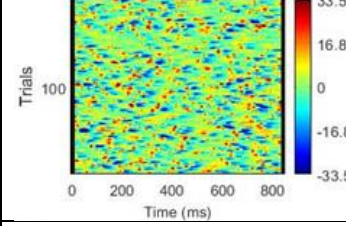
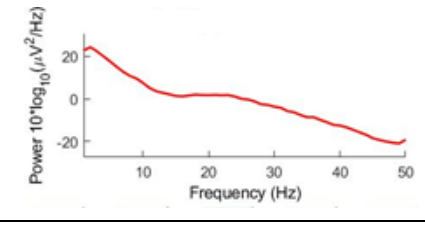
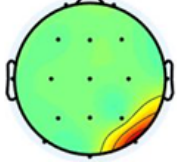
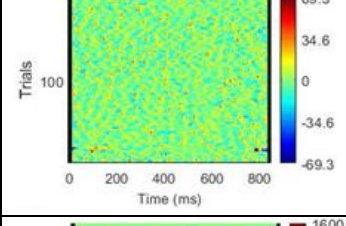
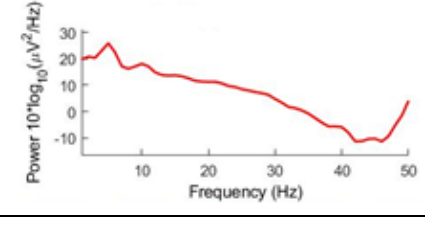
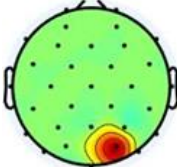
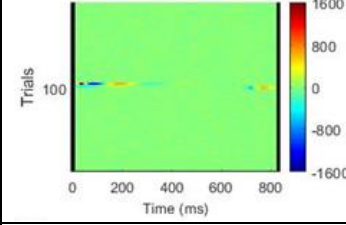
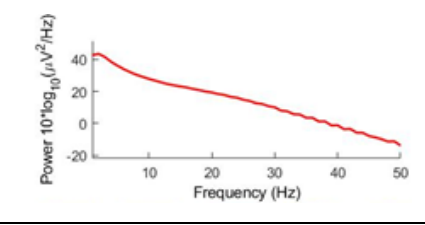
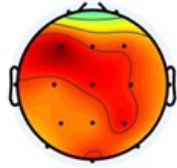
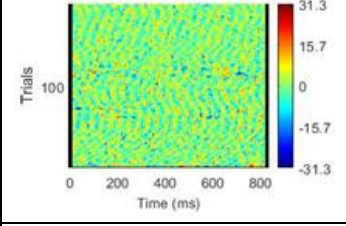
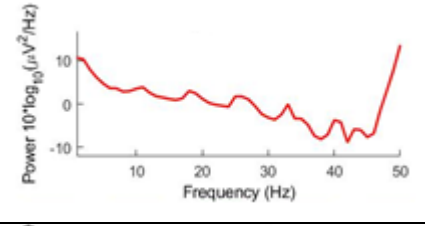
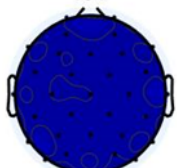
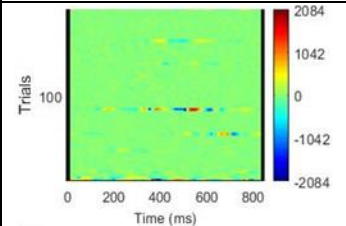
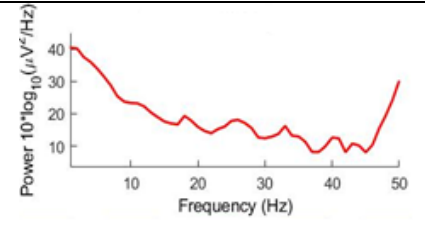
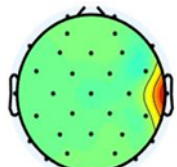
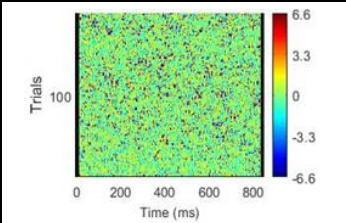
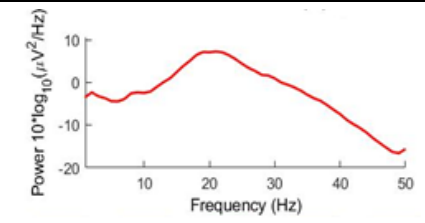
Figure 3.4. ICA components activations. These representation of components helps to identify components pointing for characteristic artefacts.

To identify the components to remove it is important to label each IC to distinguish them as brain or non-brain sources. ICs can be labelled as brain, muscle, eye or heart components, and channel or line noise. The main characteristic of brain components is that the scalp topography often looks dipolar, which means that brain components creates a positive potential on one side of the equivalent current dipole and a negative potential on the other. These components also tend to have a low power at higher frequencies and the power spectrum decreases as frequency increases. Additionally, in brain components the power spectrum usually has a peak between 5 and 30 Hz, with 10 Hz (alpha frequency) being the most common.

On the other hand, artefacts may be introduced by the muscle and eye movements, heart beat and so on. The muscle components represent the electrical fields generated by muscle activity. These activations usually are spread amongst higher frequencies (20 Hz and above). The eye components can be identified due to the characteristic scalp map, which shows a strong frontal projection. The decreasing EEG spectrum is also characteristic of an eye artefact. Power is also concentrated at low frequencies (below 5 Hz). Heart Components represent the electrical potentials generated by the heart. In this component, it is possible to observe a clear QRS complex in the data at about 1 Hz, in the component time series.

Independent Components representing channel noise are mainly characterized by the distinct scalp topography, which is only weighted on a single electrode. These components also show consistent artefacts in the component activations and the power spectrum is a decreasing curve. Furthermore, line noise is the contamination from the alternating current used in electronic equipment. These types of components are mostly identified due to a strong peak in power spectrum at 50 Hz or 60 Hz. Table 3.1 illustrates the 2D topographies, continuous data and activity power spectrum for each IC.

Table 3.1. Independent Components. ICs and corresponding 2D topographies, continuous data map and activity power spectrum.

ICA components	2D topography	Continuous data	Activity power spectrum
Brain component			
Eye component			
Heart Component			
Channel noise			
Line noise			
Muscle component			
Muscle component			

3.3 Results

3.3.1 Artefacts Removal based on ICA during Motor Imagery

Although during motor imagery, the bandpass filtering technique is sufficient to remove most of non-physiological artefacts, ICA was performed to ensure a complete removal of the artefacts from the EEG data. Figure 3.5 and 3.6 illustrates the scalp topographies for the dry and wet systems, respectively and figure 3.7 shows the EEG signal after pre-processing techniques.

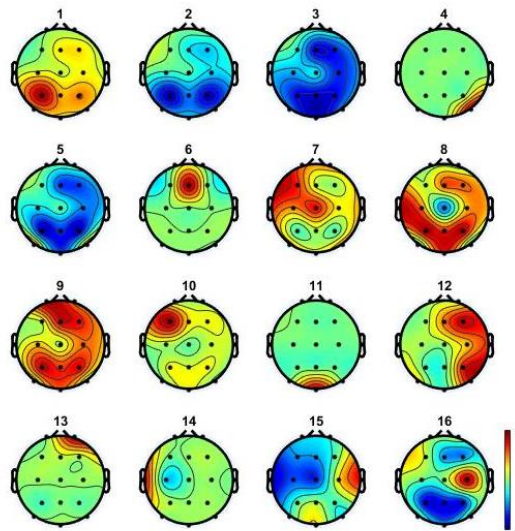


Figure 3.5. ICA components during motor imagery (subject 2), with the dry system.

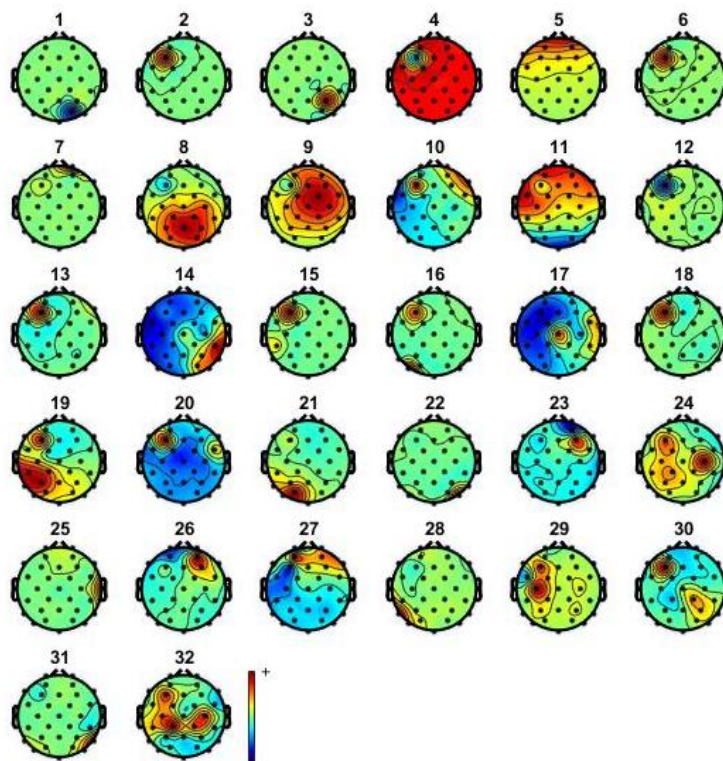


Figure 3.6. ICA components during motor imagery (subject 3) with the wet system.

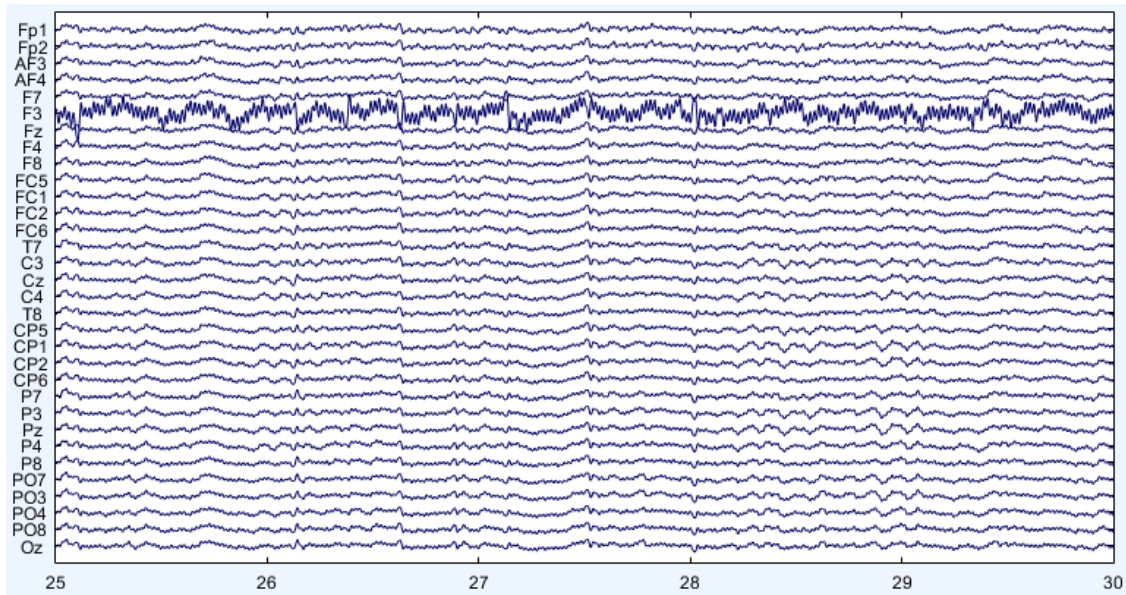


Figure 3.7. EEG signal after ICA (subject 3), with the wet system.

3.3.2 Artefacts Removal based on ICA during Gait Adaptation

As mentioned above, gait adaptation data is highly corrupted by noise and motion artefacts, as illustrated in figure 3.9. Scalp topographies (figure 3.8) show that the first components comprise mainly motion artefacts and should be removed. Figure 3.10 shows the reconstructed EEG signal after the removal of the artefactual components.

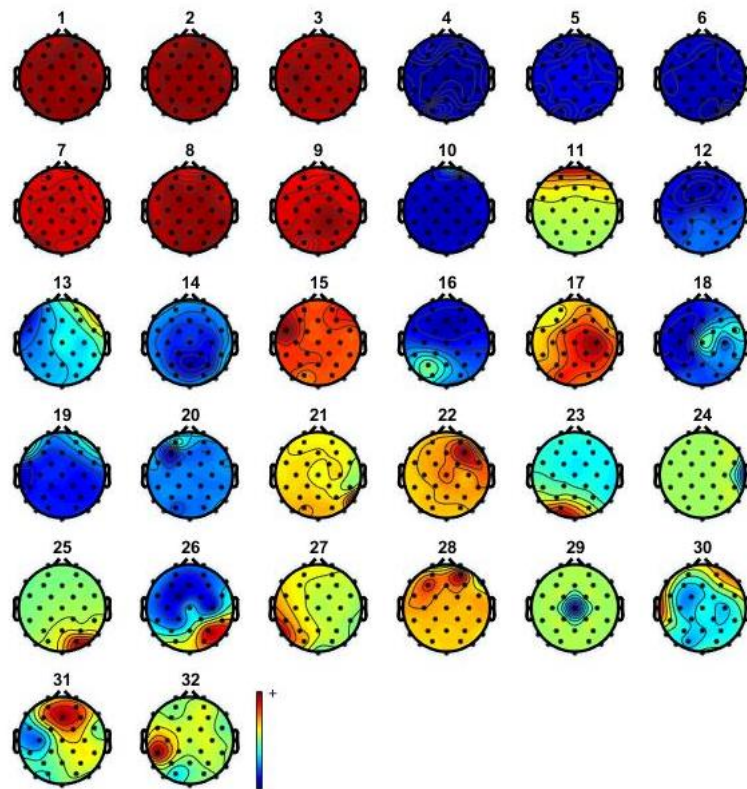


Figure 3.8. ICA components during gait adaptation (subject 3).

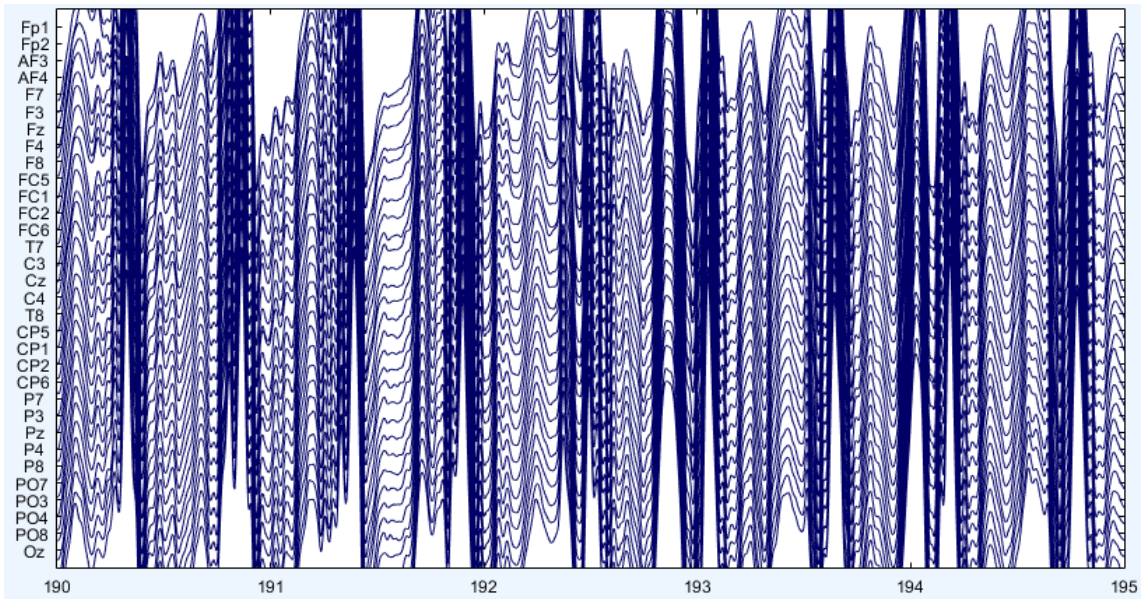


Figure 3.9. EEG signal before ICA (subject 3).

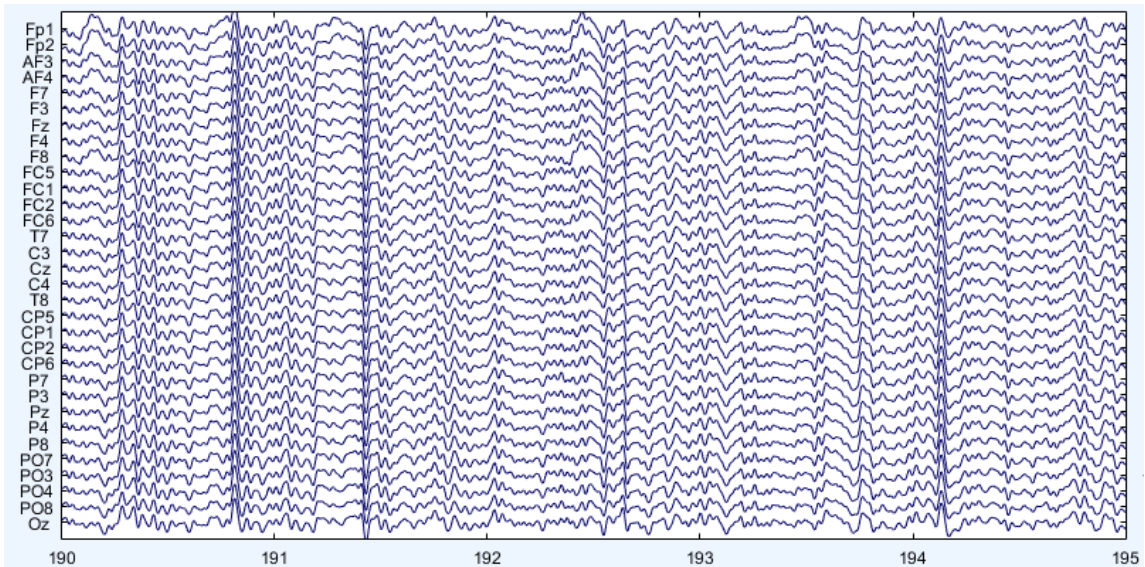


Figure 3.10. EEG signal after ICA (subject 3).

3.4 Discussion

Although there is not a standard solution for the removal of EEG artefacts, and especially motion artefacts, ICA is one of the most used techniques to remove gait-related movement artefacts. According to the previous figures, ICA seems to be useful to remove artefacts from the EEG data, both in the motor imagery and gait adaptation studies. During the MI study, the filtering technique removes most of non-physiological artefacts, while in the gait adaptation part, the EEG signal is still extremely contaminated by noise and interference. Consequently, ICA is used mainly to remove the influence of motion and gait-related components. Highly corrupted components are easy to identify, mainly during walking conditions (figure 3.8), due to the abundance of motion artefacts. These results suggest that motion artefacts can be minimized using ICA and filtering techniques, for posterior use with BCI analysis.

4. Analysis of EEG signals based on time locked events

As previously said, the changes in the μ (7.5-12.5 Hz) and β (14-26 Hz) rhythm amplitudes are denoted as event-related desynchronization (ERD) and event-related synchronization (ERS) and are mainly associated with movement and MI tasks. Movement or preparation for movement is typically accompanied by a decrease in mu and beta rhythms (ERD). On the opposite, rhythm increase (ERS) occurs after movement and with relaxation. Since ERD and ERS do not require actual movement and may occur with MI, they might support an independent BCI [40].

Therefore, the study of EEG data may also be analysed in terms of event related EEG dynamics, which allows the study of time locked events, like left/right motor imagery or movements. In order to do so, the data epochs, which are time locked to events of interest, should be extracted from the filtered data.

4.1 Methods

EEG data was recorded from six healthy participants, two females and four males (27.5 ± 7.58 years), with a 32-channels EEG wireless acquisition system (g.tec Nautilus) with active-electrodes (Ag/AgCl), and with a sampling frequency of 250 Hz. The EEG cap was placed accordingly to the 10-20 system, ensuring that each channel had less than 30Ω of impedance for all participants. EEG data was recorded with OpenVibe version 1.3 [94]. Similarly to the previous chapter, the analysis of EEG signals was performed in Matlab R2017b (The Mathworks, Natick, MA), using scripts based on eeglab (Appendix B).

EEG data was epoched based on two events (left and right motor imagery or left and right movements), and each epoch has the duration of three seconds, after the event (when the subject is performing the MI task). After the preprocessing of EEG data, each epoch file was studied separately by plotting power spectral maps.

4.2 Results

4.2.1 Power Spectrum Analysis

The power spectral maps show the activated parts on the brain during a specific event (i.e. motor imagery or actual movement), where each colored trace represents the spectrum of the activity of data channels. Here, the power spectrum is analysed at 4, 8, 14 and 26 Hz, in order to study the scalp distribution of power at different brain rhythms.

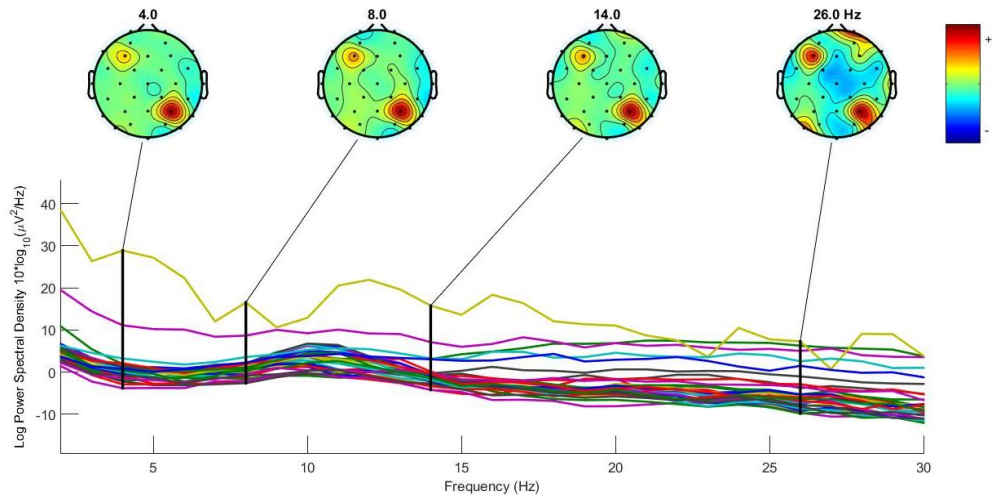


Figure 4.1. Scalp distribution of power during left hand motor imagery for different brain rhythms (Wet system, subject 3).

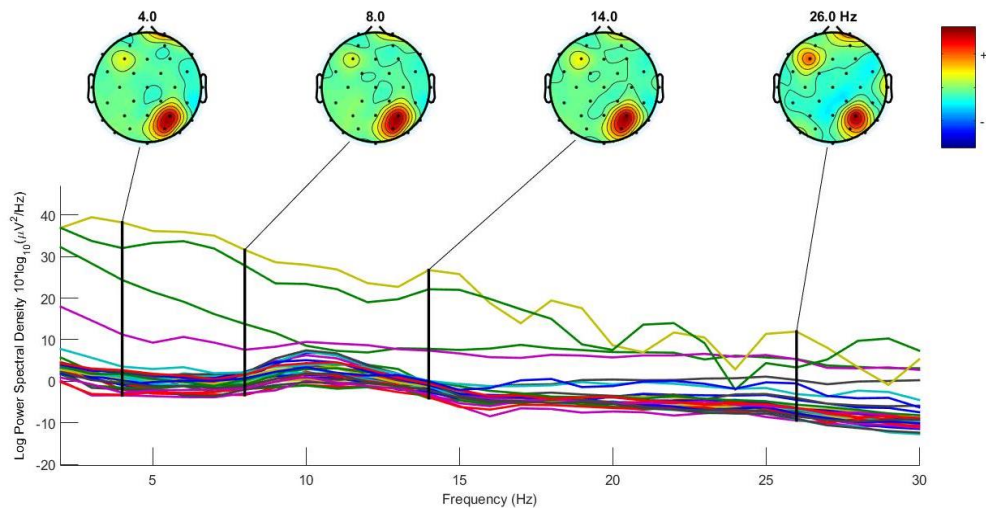


Figure 4.2. Scalp distribution of power during right hand motor imagery for different brain rhythms (Wet system, subject 3).

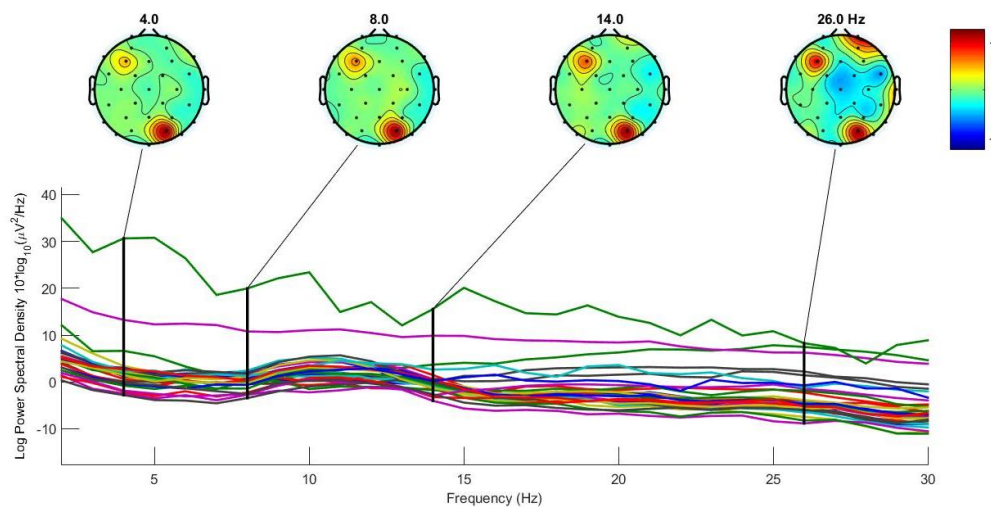


Figure 4.3. Scalp distribution of power during left leg motor imagery for different brain rhythms (Wet system, subject 3).

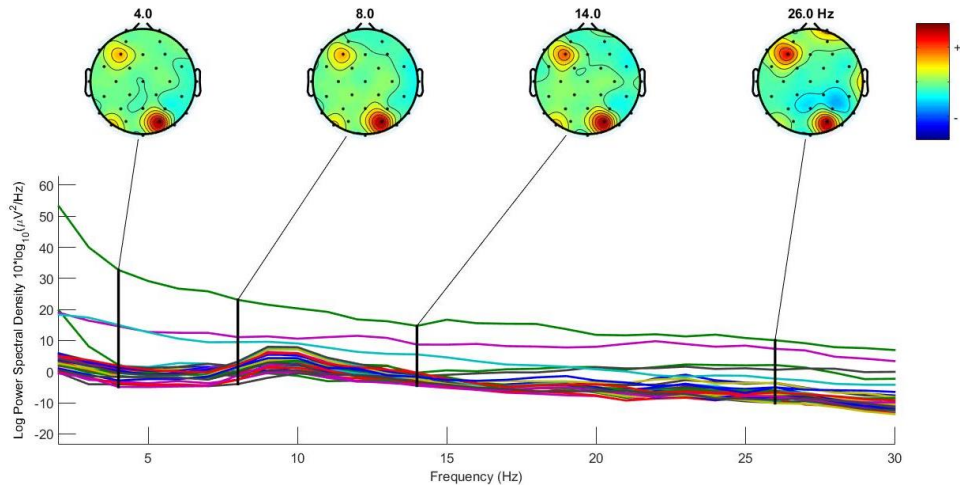


Figure 4.4. Scalp distribution of power during right leg motor imagery for different brain rhythms (Wet system, subject 3).

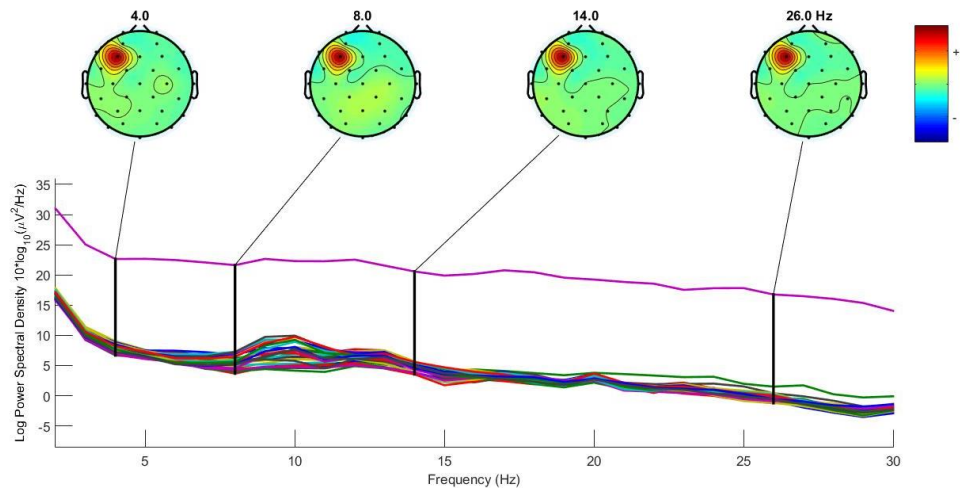


Figure 4.5 Scalp distribution of power during left leg movement for different brain rhythms (Wet system, subject 3).

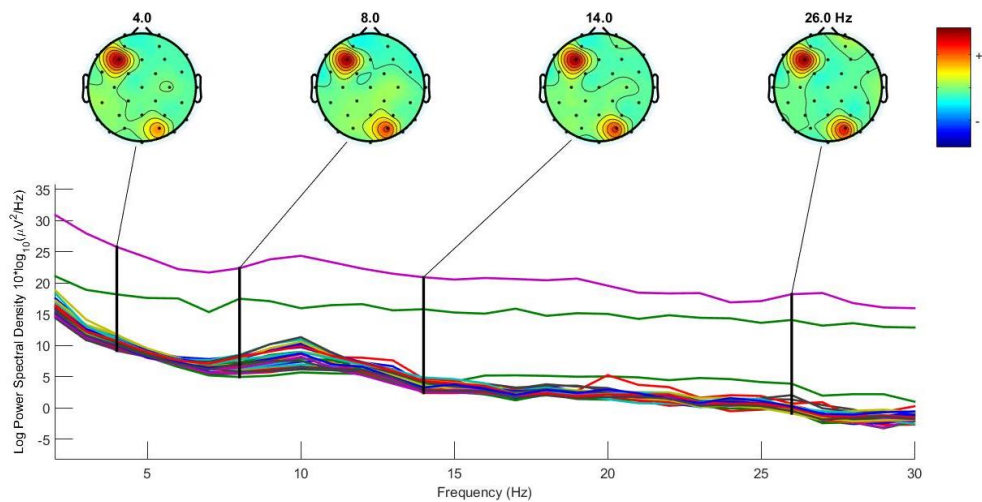


Figure 4.6 Scalp distribution of power during right leg movement for different brain rhythms (Wet system, subject 3).

4.3 Conclusions

From the spectral plots above, it can be seen that the spectral plot of left hand imagery shows an increase in the P4, F3 and Fp2 electrodes and a decrease in power in the area of the Cz, FC1 and FC2 electrodes at 26 Hz. During the right-hand MI task, the spectral power increases in the P4, PO4 and Fp2 electrodes. For the left leg MI, there is an increase in power in the PO4, F3 and 2 electrodes and a decrease in the area of Cz, Fz, FC1 and FC2 electrodes, at 26 Hz. On the contrary, for the right leg, there is an increase in the PO4, F3 and PO7 electrodes, with a decrease in power near the P4 electrode. In terms of legs movement, for the left leg, there is an increase in power in the F3, PO4 and electrodes and for the right leg, the increase is verified at the F3 and Fp2 electrodes.

5. Motor imagery and simple movements - EEG feature extraction and classification

5.1 Experimental design

5.1.1 Experimental Setup

EEG data was recorded from six healthy participants (3 males and 3 females, 25.5 ± 6.7453 years). None of the participants had previous motor imagery experience. It were used two g.tec Nautilus, EEG wireless acquisition systems with active-electrodes: a 16-channels dry electrodes cap (g.Sahara) and a 32-channels wet electrodes cap (g.ladybird), with a sampling frequency of 250 Hz. The EEG systems were placed accordingly to the 10-20 system. The study comprised three different experiments:

- i) A two-class MI task that involved imaginary movements of the left and right arms;
- ii) A two-class MI task that involved imaginary movements of the left and right legs;
- iii) A task with actual movements of the left and right leg while the subject was sited.

To collect the data for offline classification it was followed a Graz-BCI stimulus paradigm [142]. The cues were displayed with *Psychtoolbox-3* (Matlab R2017b), the EEG acquisition was made with OpenVibe 1.3 and the EEG analysis was performed with Matlab R2017b (The Mathworks, Natick, MA) [143] [144] [145] [94].

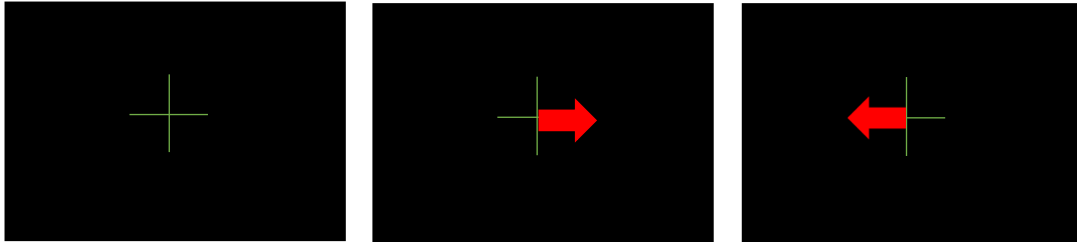


Figure 5.1. Visual Stimulus Presentation. The screen displays a green cross with a red arrow, pointing to the left or right. The direction of the arrow indicates if the subject should imagine/move the right or left limb.

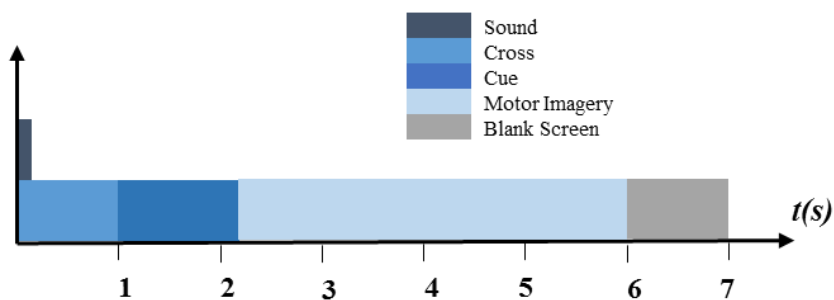


Figure 5.2. Visual stimulus timing diagram. A sound is emitted before the cue. After the cue, subjects should perform the motor imagery /movement for approximately four seconds. Motor imagery / movement is followed by a blank screen.

5.1.2 Channels Locations

Firstly, the testing accuracy was calculated considering all the channels, in both systems. Then, specific channels were selected based on their locations with respect to the motor cortex. For the dry cap, the testing accuracy was calculated selecting just a specific group of electrodes in the area of the motor cortex: F3, Fz, F4, T7, C3, C4, T8, P3, Pz and P4 (configuration 1). For the wet system, the testing accuracy was also calculated considering the same electrode configuration as the dry cap and a different configuration according to [146], where it was selected the channels F3, F4, FC5, FC6, C3 and C4 (configuration 2).

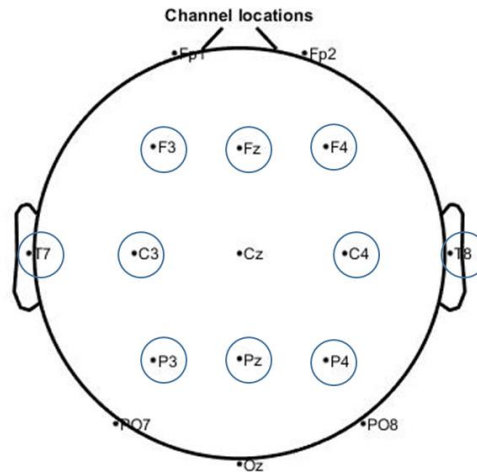


Figure 5.3. EEG electrode placement for the 16 channels g.Nautilus system used during the experiment based on the International 10-20 system. The channels selected are represented in blue.

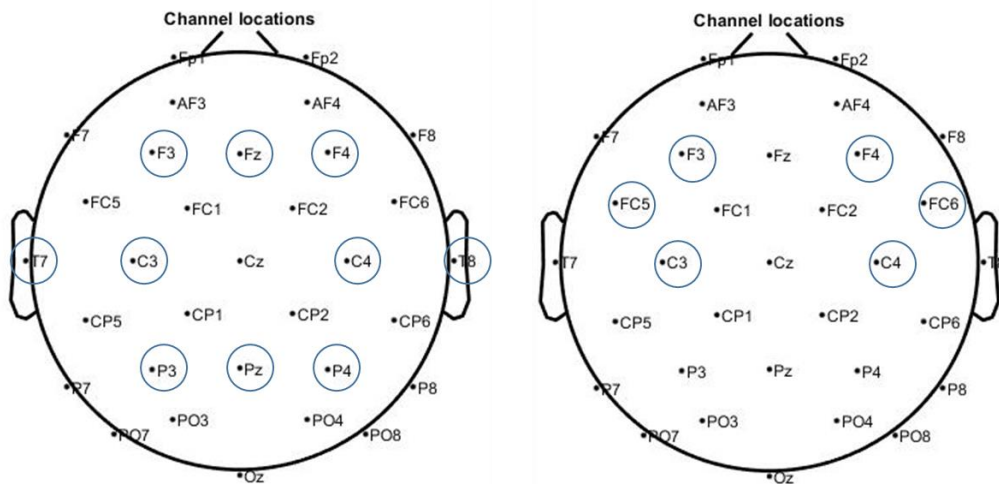


Figure 5.4. Left: EEG electrode placement for the 32 channels g.Nautilus system used during the experiment based on the International 10-20 system (configuration 1). Right: EEG electrode placement for the 32 channels g.Nautilus system used during the experiment based on the International 10-20 system (configuration 2). The channels selected are represented in blue.

5.2 Analysis

5.2.1 Feature extraction and classification

EEG feature extraction is investigated based on right versus left motor imagery of the hands and legs and simple movements of the legs (two classes classification).

Initially, the EEG signal was filtered based on a bandpass Butterworth filter (order 4) at 1-30 Hz, and, subsequently, it was used ICA to remove the influence of non-brain components (artefact removal). Later, the signal was also temporally filtered in the β band (12-30 Hz), since this frequency range has shown to improve the classification accuracy, according to [147].

Feature extraction and classification were performed in Matlab, using scripts based on eeglab [139]. For the feature extraction, it was selected 0.4 seconds of the signal, half a second after the cue. Features were extracted based on a Common Spatial Pattern filter, which increases the signal variance for one condition while minimizing the variance for the other condition. For comparison terms, features were also extracted based on a Regularized Common Spatial Pattern filter.

5.2.1.1 Feature Extraction based on Common Spatial Patterns

To extract classification features from the EEG data, it was used the Common Spatial Pattern algorithm, which extracts spatial filters that maximize the discriminability between two classes. The CSP training was performed with the function `learnCSP.m`, developed by Lotte et al [81].

5.2.1.2 Regularised Common Spatial Patterns (RCSP)

As mentioned before, although the CSP filters are an efficient way of extracting spatial filters that discriminate two classes, they are sensitive to noise and outliers. To minimize the influence of these outliers in extracting features based on the CSP algorithm it was used the regularization, particularly, with the Ledoit and Wolf's method [86], which regularizes the covariance matrix by shrinking it to identity. Here, the CSP training was performed with the function `learn_DL_CSPLagrangian_auto.m`, also developed by Lotte et al in the RCSP toolbox [81]. This function learns the regularized CSP filters based on diagonal loading, to discriminate between two mental states in EEG signals.

5.2.1.3 Classification

For the classification process, two algorithms were tested, namely, SVM based on radial basis function and linear discriminant analysis (LDA). SVM and LDA algorithms were implemented with the Matlab proper functions, `fitcsvm.m` and `fitcdiscr.m`, respectively.

5.3 Results

The classification results for the right versus left MI and simple movements tasks for both dry and wet systems, are shown in tables 5.1 and 5.3 and illustrated in figures 5.5 and 5.7. The 10-fold cross-validation generalization loss of the classifications results, are shown in tables 5.2 and 5.4 and illustrated in figures 5.6 and 5.8.

Table 5.1. Average testing accuracy of the classifications results of left versus right (L/R) MI of the hands and legs and simple movements of the legs, based on the dry system. The results are shown using the SVM and LDA algorithms, with CSP and RCSP approaches for feature extraction. The configuration 1 for electrodes placement is represented by *.

	Testing Accuracy (%)		
	MI hands	MI legs	Movement
SVM (CSP)	85.78 ± 8.44	86.50 ± 4.92	84.26 ± 7.30
LDA (CSP)	83.66 ± 7.78	85.50 ± 3.15	82.78 ± 8.62
SVM (RCSP)	86.74 ± 6.77	85.33 ± 5.39	83.86 ± 4.52
LDA (RCSP)	85.43 ± 7.30	84.11 ± 4.48	83.10 ± 5.51
SVM (RCSP)*	86.26 ± 7.38	84.95 ± 5.84	83.78 ± 3.90
SVM (RCSP) β	97.84 ± 1.18	96.47 ± 2.23	91.73 ± 4.26
SVM (RCSP) β*	96.84 ± 1.61	97.73 ± 2.12	91.88 ± 3.55

Table 5.2. 10-fold cross-validation generalization loss of the classifications results for the right versus left MI of the hands and legs and simple movements of the legs, based on the dry system. The results are shown using the SVM and LDA algorithms, with CSP and RCSP approaches for feature extraction. The configuration 1 for electrodes placement is represented by *.

	Generalisation Loss		
	MI hands	MI legs	Movement
SVM (CSP)	0.13 ± 0.07	0.13 ± 0.04	0.15 ± 0.06
LDA (CSP)	0.15 ± 0.08	0.15 ± 0.06	0.16 ± 0.06
SVM (RCSP)	0.13 ± 0.08	0.14 ± 0.06	0.16 ± 0.04
LDA (RCSP)	0.14 ± 0.07	0.16 ± 0.06	0.16 ± 0.03
SVM (RCSP) *	0.13 ± 0.07	0.14 ± 0.06	0.16 ± 0.05
SVM (RCSP) β	0.02 ± 0.01	0.02 ± 0.01	0.05 ± 0.02
SVM (RCSP) β*	0.01 ± 0.00	0.02 ± 0.01	0.05 ± 0.02

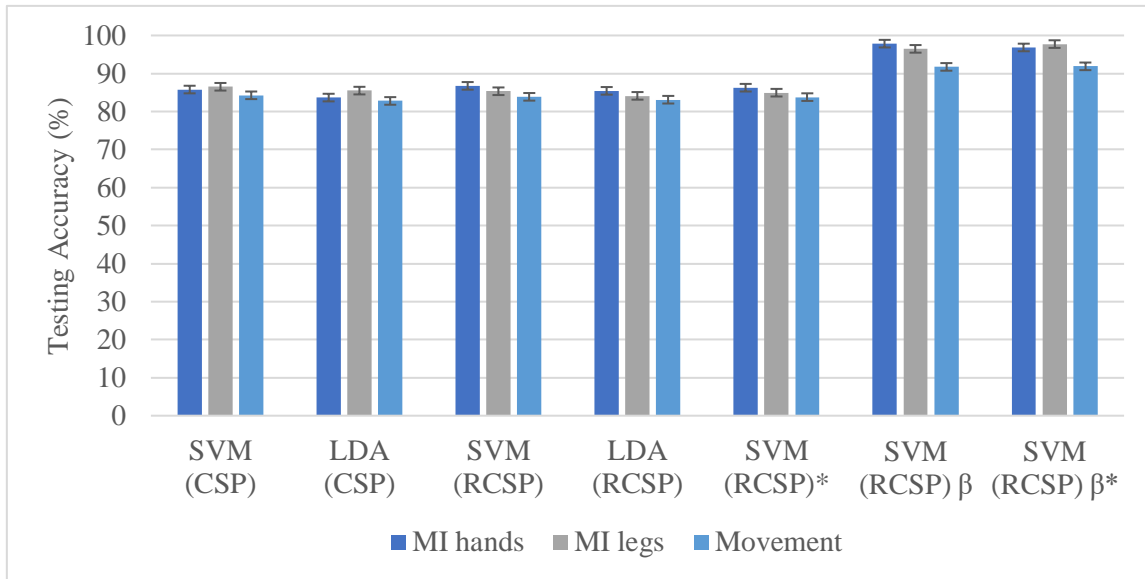


Figure 5.5. Average testing accuracy of the classifications results of left versus right (L/R) MI of the hands and legs and simple movements of the legs, based on the dry system. The results are shown using the SVM and LDA algorithms, with CSP and RCSP approaches for feature extraction. The configuration 1 for electrodes placement is represented by *.

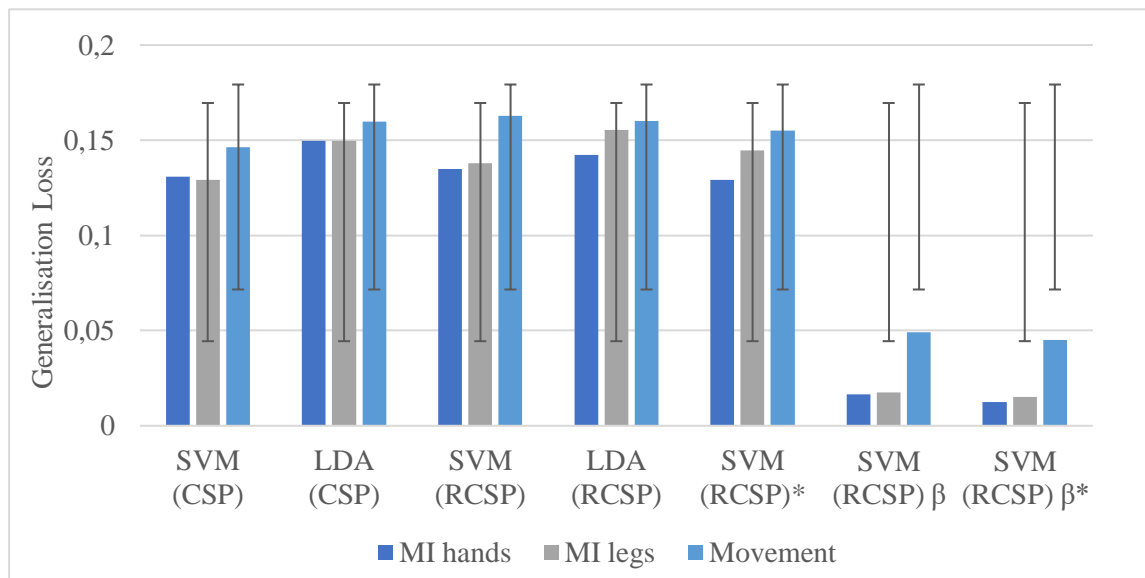


Figure 5.6. 10-fold cross-validation generalization loss of the classifications results for the right versus left MI of the hands and legs and simple movements of the legs, based on the dry system. The results are shown using the SVM and LDA algorithms, with CSP and RCSP approaches for feature extraction. The configuration 1 for electrodes placement is represented by *.

Table 5.3. Average testing accuracy of the classifications results of left versus right (L/R) MI of the hands and legs and simple movements of the legs, based on the wet system. The results are shown using the SVM and LDA algorithms, with CSP and RCSP approaches for feature extraction. The configuration 1 for electrodes placement is represented by * and the configuration 2 is represented by **.

	Testing Accuracy (%)		
	MI hands	MI legs	Movement
SVM (CSP)	95.24 ± 2.31	93.21 ± 6.08	98.02 ± 1.43
LDA (CSP)	95.11 ± 3.67	95.47 ± 3.42	97.93 ± 0.82
SVM (RCSP)	94.48 ± 5.61	93.83 ± 5.20	97.71 ± 2.78
LDA (RCSP)	91.97 ± 7.90	94.16 ± 3.02	97.87 ± 1.62
SVM (RCSP)*	94.29 ± 6.54	94.02 ± 6.00	98.18 ± 2.57
SVM (RCSP)**	93.36 ± 7.62	95.54 ± 4.49	97.63 ± 3.12
SVM (RCSP)* (β)	98.49 ± 0.51	99.90 ± 0.14	100.00 ± 0.00
SVM (RCSP)** (β)	98.49 ± 0.57	99.72 ± 0.40	99.82 ± 0.01

Table 5.4. 10-fold cross-validation generalization loss of the classifications results for the right versus left MI of the hands and legs and simple movements of the legs, based on the wet system. The results are shown using the SVM and LDA algorithms, with CSP and RCSP approaches for feature extraction. The configuration 1 for electrodes placement is represented by * and the configuration 2 is represented by **.

	Generalisation Loss		
	MI hands	MI legs	Movement
SVM (CSP)	0.05 ± 0.04	0.06 ± 0.05	0.01 ± 0.02
LDA (CSP)	0.03 ± 0.02	0.05 ± 0.04	0.02 ± 0.01
SVM (RCSP)	0.07 ± 0.07	0.04 ± 0.03	0.02 ± 0.02
LDA (RCSP)	0.08 ± 0.06	0.05 ± 0.05	0.02 ± 0.02
SVM (RCSP) *	0.07 ± 0.07	0.05 ± 0.04	0.02 ± 0.03
SVM (RCSP) **	0.06 ± 0.06	0.06 ± 0.05	0.02 ± 0.03
SVM (RCSP)* (β)	0.01 ± 0.00	0.00 ± 0.00	0.00 ± 0.00
SVM (RCSP)** (β)	0.01 ± 0.01	0.00 ± 0.00	0.00 ± 0.00

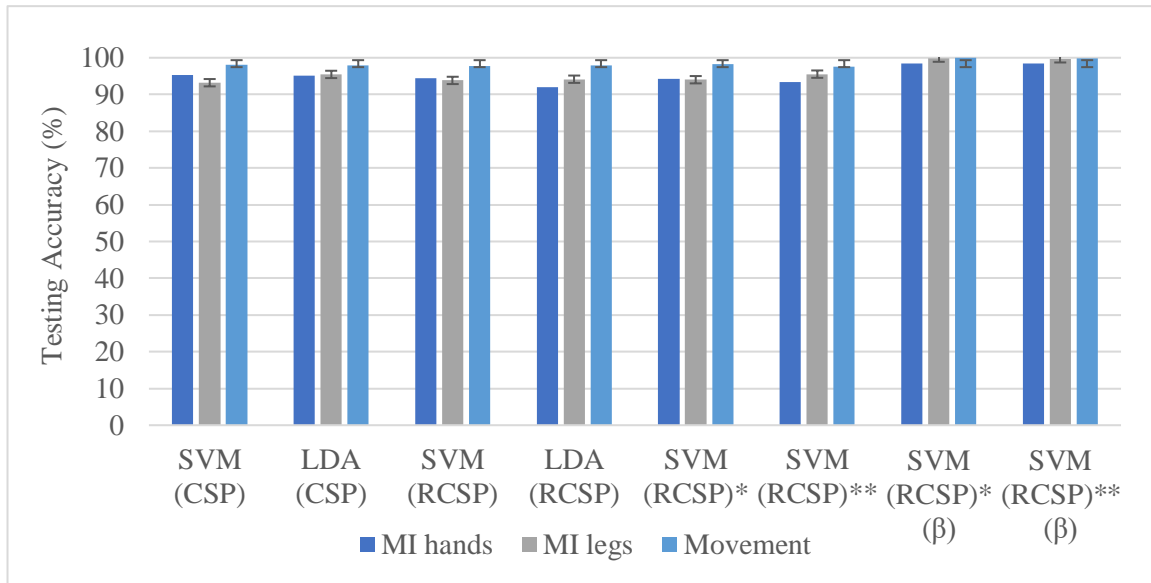


Figure 5.7. Average testing accuracy of the classifications results of left versus right (L/R) MI of the hands and legs and simple movements of the legs, based on the wet system. The results are shown using the SVM and LDA algorithms, with CSP and RCSP approaches for feature extraction. The configuration 1 for electrodes placement is represented by * and the configuration 2 is represented by **.

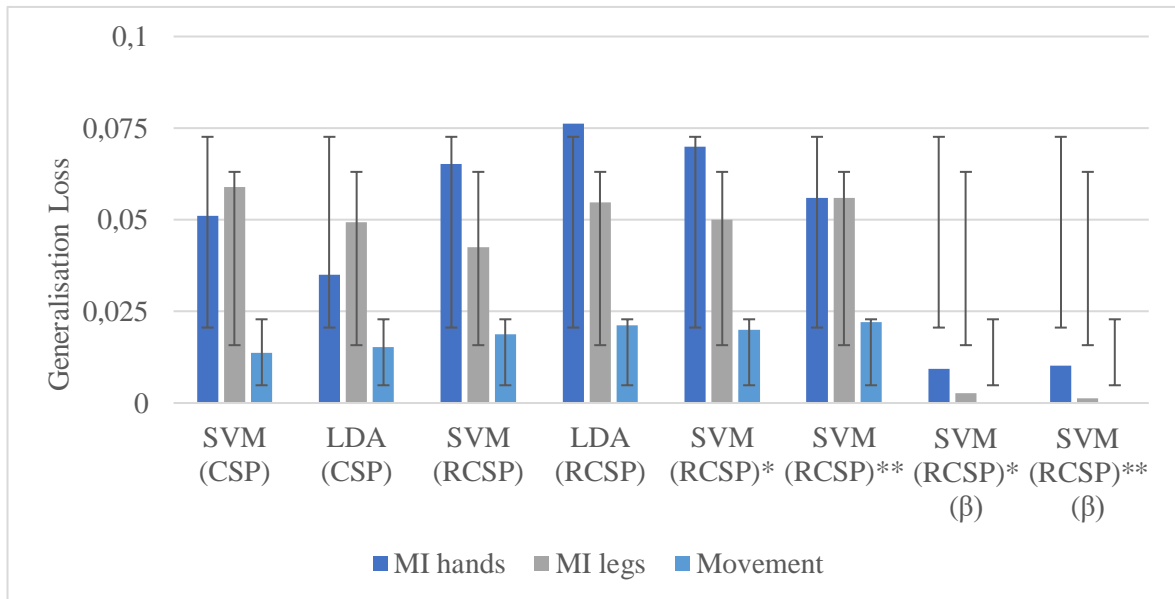


Figure 5.8. 10-fold cross-validation generalization loss of the classifications results for the right versus left MI of the hands and legs and simple movements of the legs, based on the wet system. The results are shown using the SVM and LDA algorithms, with CSP and RCSP approaches for feature extraction. The configuration 1 for electrodes placement is represented by * and the configuration 2 is represented by **.

Regarding the dry electrodes system, the highest classification accuracy ($97.84 \pm 1.18 \%$) was verified for the MI of the hands with the SVM classifier and the RCSP approach, considering all the channels and a temporal filter in the β band. On the other hand, considering the wet electrodes system, the best classification ($100.00 \pm 0.00 \%$) was obtained during simple movements of the legs, using the SVM classifier with the RCSP approach, based on configuration 1 for electrodes positioning and a β band temporal filter.

Figure 5.9-5.12 illustrate the analysis of the most significant RCSP components during MI and simple movements tasks. Classification was performed with the SVM classifier. The average across subjects is calculated, as more RCSP components are chosen, from the most significant to less significant eigen values. Figure 5.9 and 5.11 illustrate the testing accuracy, for the dry and wet systems, respectively. Figures 5.10 and 5.12, show the 10-fold cross-validation, generalisation loss.

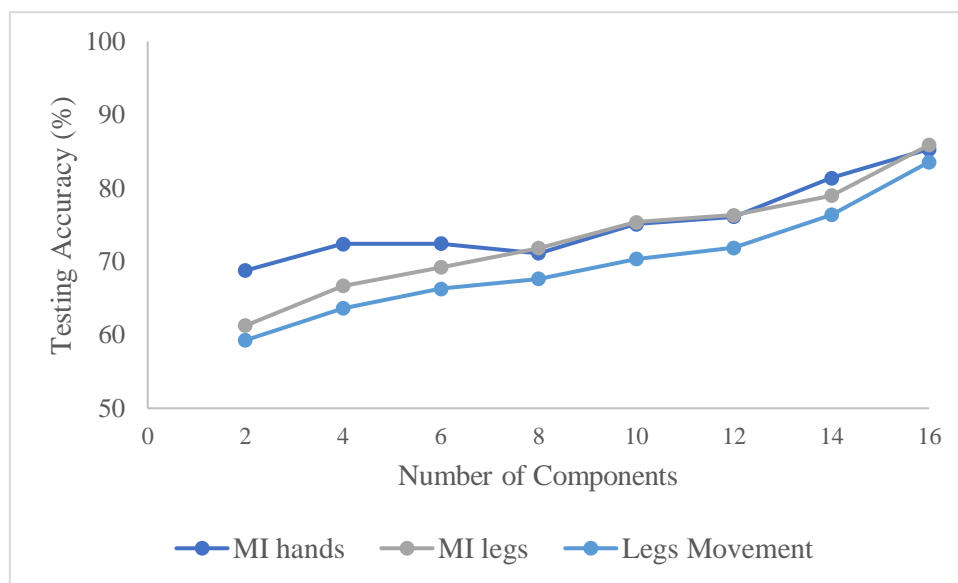


Figure 5.9. Average testing accuracy across subjects as more RCSP components are chosen from the most significant to less significant eigenvalues, based on the dry electrodes system.

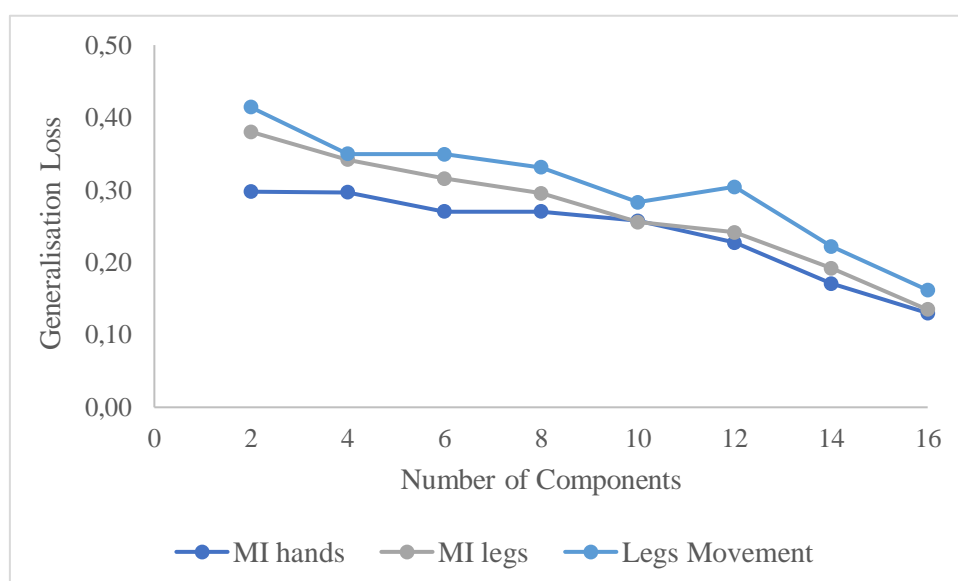


Figure 5.10. Generalisation loss for different numbers of RCSP components, from the most significant to less significant eigenvalues, based on the dry electrodes system.

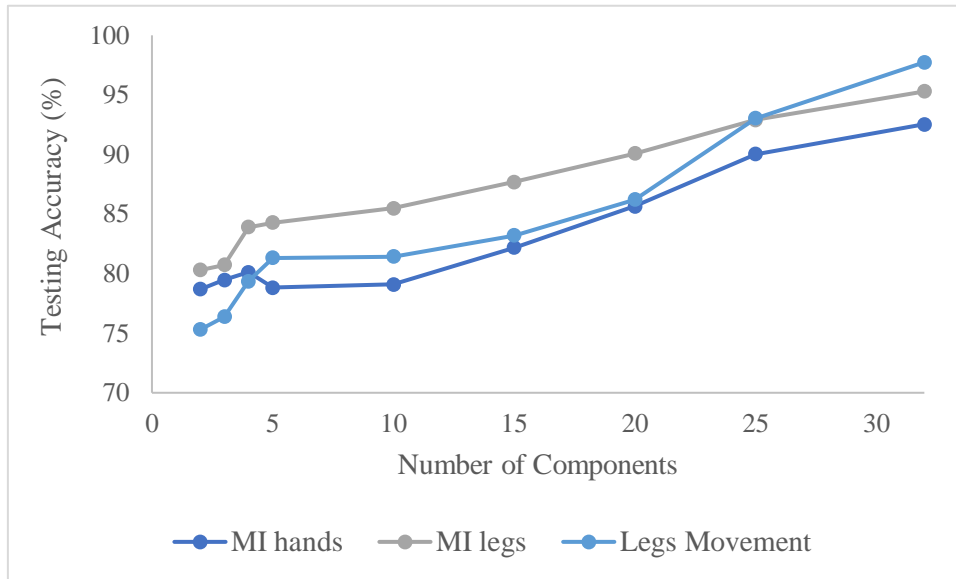


Figure 5.11. Average testing accuracy across subjects as more RCSP components are chosen from the most significant to less significant eigenvalues, based on the wet electrodes system.

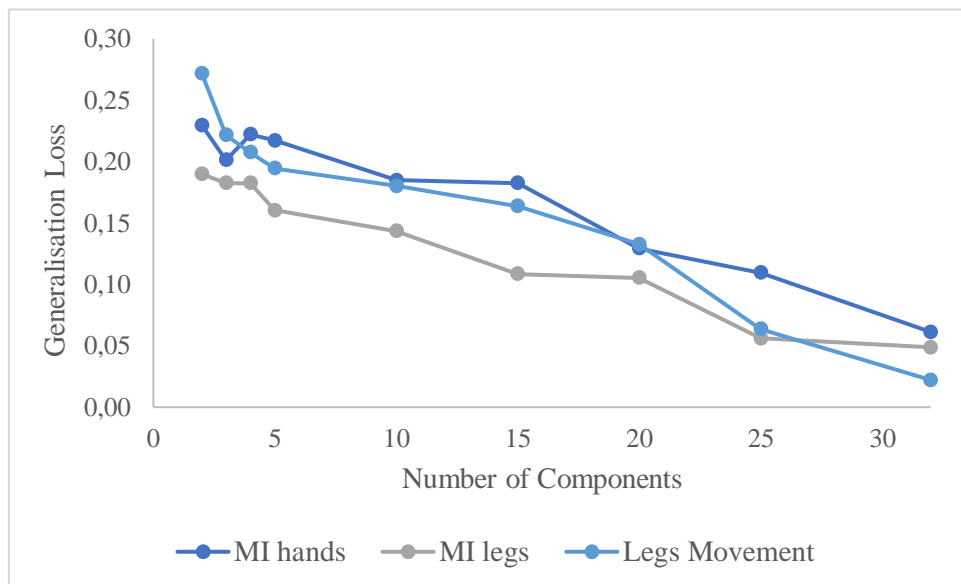


Figure 5.12. Generalisation loss for different numbers of RCSP components, from the most significant to less significant eigenvalues, based on the wet electrodes system.

According to the number of components selected, for the wet system, the error drops significantly for the first five components, but it drops at a slower rate as the number of components increase. As expected, the error is minimum when all the components are incorporated in the analysis. The classification increases abruptly for the first five components and continues to grow as more components are incorporated.

For the dry system, the error drops with a slower rate, when more components are incorporated, when compared to the wet system. For the MI and movements of the legs the error increases when 12 components are used. The classification also increases when more components are incorporated although it decreases for the MI of the hands when 8 and 12 components are used.

5.4 Discussion

According to the tables and figures above, it is possible to infer that the combination of a beta bandpass filter with a RCSP filter has shown the best classification rate. These results show that a careful selection of electrode location is more important than having a dense map of electrodes. Moreover, dry systems are more sensitive to interference and their signal-to-noise quality is low. Nevertheless, with an appropriate sensor selection process and feature extraction, their classification performance can increase. In order to make EEG systems user-friendly and more reliable, future work should focus on how to dynamically select the optimum EEG sensor configuration.

6. Detection of intention to adapt the gait

6.1 Experimental Setup

EEG data was recorded from six healthy participants, two females and four males (27.5 ± 7.58 years), with a 32-channels EEG wireless acquisition system (g.tec Nautilus g.ladybird) with active-electrodes (Ag/AgCl). This system records the EEG data with a sampling frequency of 250 Hz, and acceleration data in three axes (x, y, z).

The EEG cap was placed accordingly to the 10-20 system (figure 6.1), ensuring that each channel had less than 30Ω of impedance for all participants. EEG data was recorded with OpenVibe version 1.3 [94].

To conduct this study, participants were asked to walk according to a musical tone that changed between three modes, slow walking (0.875 Hz), normal walking (1.750 Hz) and fast walking (2.625 Hz). Each mode consisted of 20 trials, resulting in 60 adaptations randomly permuted. The overall experiment lasted for about 16 minutes. The experimental design is illustrated in figure 6.2. The stimulus (musical tone) was programmed and displayed with Psychtoolbox-3 [143] [144] [145]. The adaptation events (changes between musical tones) were sent to the EEG acquisition server via TCP/IP communication.

In order to record the participants while they were walking, a Logitech camera has been also used, recording the participants at 60 frames per second. To synchronize the camera recording with the EEG acquisition, each captured frame raised an event that was sent to the EEG acquisition server via TCP/IP communication. Video capturing and events' transmission was also implemented with Psychtoolbox-3.

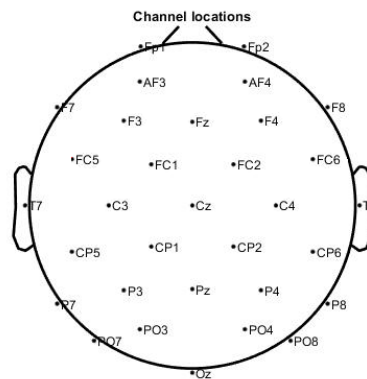


Figure 6.1. Channels locations according to the 10-20 EEG system.

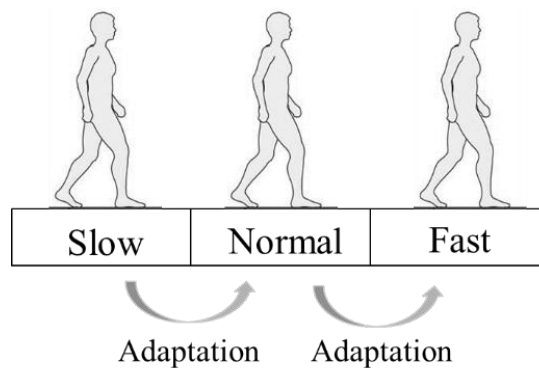


Figure 6.2. Experimental design. Participants walk freely according to a musical tone that switches randomly between three modes (slow, normal and fast).

6.2 Analysis

6.2.1 Gait Features Extraction

To extract gait features from the data, the first step is to epoch the EEG signal into segments according to left/right heel strikes. In order to discriminate between left and right heel strikes, it was used both the camera recordings and the acceleration data of the EEG system.

6.2.1.1 Gait Features Extraction based on a single camera

Camera recordings were processed with OpenPose, a real-time approach that uses deep neural networks to track the joints of multiple-persons. The output consists in a 2D skeleton, with the coordinates of human joints, as shown in figure 6.3 [148] [149] [150]. To extract the gait events of right and left heel strikes, the Euclidean distance between the left and right ankle coordinates was estimated, assuming that the camera was in a vertical position. Considering, left and right ankle coordinates, each foot contact is represented by a peak.

To denoise the signal and to improve the detection of the peaks, singular spectrum analysis (SSA) was applied. After the SSA, a peak detection method (Appendix B) was used to detect heel strikes. In this method, a point is considered a maximum peak if it has the maximal value and was preceded (to the left) by a value lower than delta ($\delta = 0.1$).

6.2.1.2 Gait Features Extraction based on acceleration data

The acceleration data was processed with Principal Component Analysis (PCA) to derive the dominant signal variation, due to gait. Here, the first components were used to reconstruct the observations. Singular spectrum analysis and peak detection ($\delta = 0.05$) were also applied to detect heel strikes. Both PCA and SSA were performed with Matlab functions, `pca.m` and `ssa.m`, respectively.

The main goal of the acceleration data is to ensure that the EEG signal and the video timeline are completely synchronized.

Figure 6.4 illustrates the peak detection method, both on video poses and acceleration, where each peak corresponds to a heel strike. It is also possible to visualize the markers representing each musical tone (slow, normal and fast).

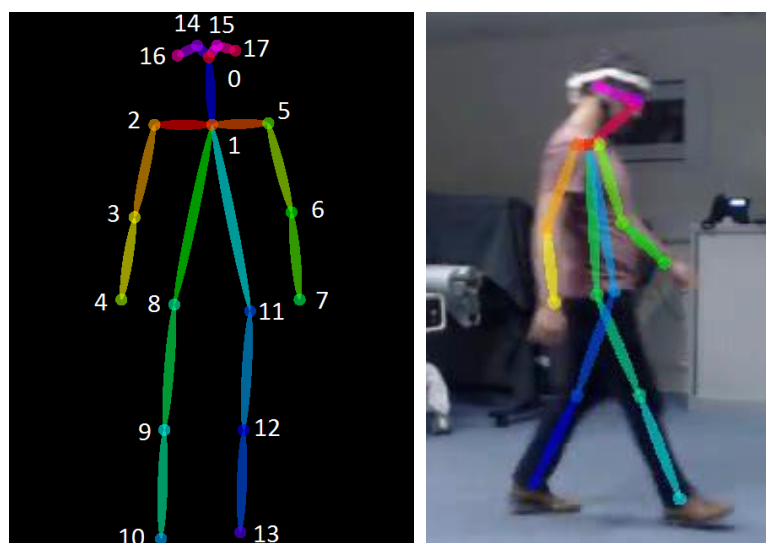


Figure 6.3. (Left) OpenPose output. (Right) OpenPose 2D keypoint detection.

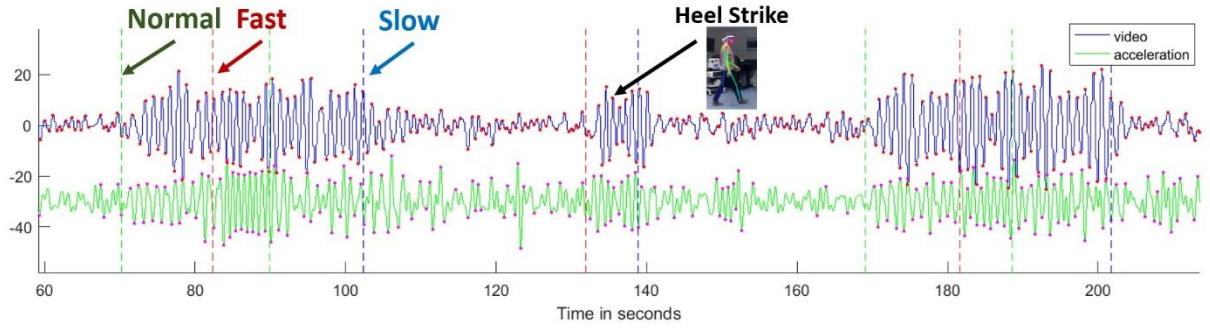


Figure 6.4. Gait feature extraction: The video-based gait signal and the acceleration-based gait signal are plotted in blue and green lines, respectively after SSA processing. The extrema points represent left and right heel strikes, respectively. Adaptation events are represented as vertical lines in green, red and blue colours that represent, normal, fast and slow speed, respectively.

6.2.1.3 Singular spectrum analysis

As previously said, SSA was used to denoise the signal and improve the peak detection, both on video and acceleration data. This technique is based on time series analysis that incorporate multivariate statistics, multivariate geometry, dynamical systems and signal processing. This technique can be applied to a time series data in order to decompose it into a number of orthogonal components, such as slowly varying trend, oscillatory components and a noise. The SSA algorithm comprises two different stages: decomposition and reconstruction [151].

Decomposition is subdivided in embedding and singular value decomposition. During embedding, a one-dimensional time series s of length n is transferred into a multidimensional matrix ($l \times k$), called trajectory matrix:

$$X = [x_{ij}] = [x_1, x_2, \dots, x_k] \quad (6.1)$$

Where $k = n - l + 1$ and l is the window length or embedding dimension. Singular value decomposition, calculates the singular value decomposition of the trajectory matrix, representing it as a sum of rank-one bi-orthogonal elementary matrices. Considering $S = XX^T$ and assuming that $\lambda_1, \lambda_2, \dots, \lambda_l$ are eigenvalues of S , the corresponding eigenvectors are u_1, u_2, \dots, u_l . If $v_i = X^T u_i / \sqrt{\lambda_i}$, it is possible to write the trajectory matrix as:

$$X = X_1 + X_2 + \dots + X_d \quad (6.2)$$

Where $d = \text{argmax}_i \{\lambda_i > 0\}$ and $X_i = \sqrt{\lambda_i} u_i v_i^T$. Each principle component is given by the projection of the time series into the direction of each eigenvector

Therefore, reconstruction is subdivided in grouping and diagonal averaging. The grouping step, splits the elementary matrices X_i into several groups and sums the matrices within each group. The elementary matrices of each group are represented by:

$$X_{I_j} = X_{i_{j1}} + \dots + X_{i_{jp}} \quad (6.3)$$

Where $I_j = i_{j1}, \dots, i_{jp}$ represents the indices for each group. The original matrix can be written as the sum of all the resulted matrices X_{I_j} :

$$X = X_{I_1} + \dots + X_{I_m} \quad (6.4)$$

The last step of the SSA algorithm (diagonal averaging) transforms the final elementary matrix into a time-series of length n . The elements of the resultant time series are computed using the average of the matrix elements over the diagonal elements.

6.2.1.4 Principal Component Analysis

PCA is a statistical technique that analyses data representing observations described by several dependent variables. In this study, PCA was used to derive the dominant signal variation (gait). The main goal of PCA is to extract the significant information from the data and express this information as a set of new orthogonal and uncorrelated variables, called principal components.

Mathematically, PCA transforms the data to a new coordinate system such that the greatest variance by some projection of the data comes to lie on the first coordinate (first principal component).

The first principal component is the linear combination of n -variables that has maximum variance, among all linear combinations, explaining as much of the variability in the data as possible [152].

6.2.2 Movement Artefact Removal

It is known that EEG-data acquisition is very sensitive to motion artefacts. As shown in chapter three, in order to eliminate the influence of motion, the EEG signal was filtered based on a bandpass impulse response filter of 3-45 Hz (figure 3.2). Subsequently, ICA was used to remove the influence of motion components [140]. Artefactual components were removed, and the EEG signal were reconstructed without their interference, like is shown in chapter 3, figures 3.8-3.10. In this study, an average of 24.17 ± 3.55 independent components were left after ICA decomposition.

6.2.3 EEG Feature Extraction

This study focuses on two classification problems: right versus left gait cycle classification and adaptation versus non-adaptation steps (two classes classification).

According to the adaptation versus non-adaptation steps classification, EEG feature extraction is formulated by a classification problem of whether a step is an adaptation step or not. Adaptation steps are based on the reaction time (RT) between the change of the rhythmic tone and the step to match the average step of the session. On the other hand, non-adaptation steps are chosen from the middle of the trial to match the number of the adaptation steps.

6.2.3.1 Feature Extraction based on Common Spatial Patterns

Similarly, to the previous chapter, to extract classification features from the EEG data, it was used the Common Spatial Pattern algorithm. The CSP training was performed with the function `learnCSP.m`, developed by Lotte et al [81].

6.2.3.2 Feature Extraction based on Regularised Common Spatial Patterns (RCSP)

To minimize the influence of outliers in extracting features based on the CSP algorithm it was used the regularization, particularly, with the Ledoit and Wolf's method [86]. The CSP training was performed with the function `learn_DL_CSPLagrangian_auto.m`, also developed by Lotte et al.

6.2.4 Classification

Like the previous chapter, for the classification process, it was used both SVM based on radial basis function and LDA. SVM and LDA algorithms were implemented with the Matlab proper functions, `fitsvm.m` and `fitcdiscr.m`, respectively.

6.3 Results

As previously mentioned, the investigation of gait and gait adaptation is based on two EEG classification experiments: Right vs left gait cycle classification and adaptation vs non-adaptation steps. For each adaptation type, it was estimated the step duration, the adaptation time and the number of adaptation steps, also called, reaction time. Reaction time is estimated as the time between the change of the rhythmic tone and the time when the step matches the average step of the session within the standard deviation limit. Table 6.1 summarises the behavioural analysis for each adaptation type.

Table 6.1. Behavioural analysis of adaptation. Steps statistics (step duration, adaptation time and number of adaptation steps) according to the music tone frequency (slow, normal or fast).

Adaptation Time	Steps Statistics		
	Step duration (secs)	Adaptation time (secs)	Number of adaptation Steps
Slow	0.57 ± 0.13	1.29 ± 0.62	2.24 ± 0.96
Normal	0.56 ± 0.01	2.01 ± 0.26	3.53 ± 0.46
Fast	0.45 ± 0.02	1.47 ± 0.33	3.26 ± 0.79

According to table 6.1, the adaptation time was the lowest (1.29 ± 0.62 seconds) when participants tried to adapt their walking to the slowest musical tone, resulting in the smallest number of adaptation steps (2.24 ± 0.96 steps). On the other hand, the highest adaptation time (2.01 ± 0.26 seconds) was verified when participants adapted their walking to the normal musical tone, and, subsequently, the number of adaptation steps was the highest (3.53 ± 0.46 steps). As expected, in terms of steps duration, the highest mean value was verified for the slow musical tone and the lowest value for the fastest tone.

The classification results for the right versus left gait cycles and for the adaptation versus non-adaptation, steps are summarized in table 6.2 and illustrated in figure 6.5. Figure 6.5 demonstrates the testing accuracy of the classifications results of left versus right (L/R) steps and adaptation versus non-adaptation (A/NA) steps, based on CSP and RCSP feature extraction. The results are shown across different sizes of sliding window (w) with a range from 90 samples to 60 samples, where 90 samples correspond to 0.36 seconds, whereas the event duration is taken to be 0.4 seconds.

Table 6.2. Classification results for the right versus left gait cycles and for the adaptation versus non-adaptation steps, based on CSP and RCSP. The results are shown across different sizes of sliding window (w) with a range from 90 to 60 samples.

	Testing Accuracy (%)			
	L/R (CSP)	L/R (RCSP)	A/NA (CSP)	A/NA (RCSP)
SVM (w=90)	63.71 ± 6.86	78.57 ± 6.45	86.32 ± 7.43	90.26 ± 5.39
SVM (w=80)	63.54 ± 6.53	76.43 ± 5.77	85.51 ± 6.08	90.13 ± 2.83
SVM (w=70)	63.41 ± 6.24	76.24 ± 5.38	84.30 ± 5.15	88.90 ± 3.60
SVM (w=60)	62.96 ± 5.40	74.53 ± 5.76	82.47 ± 4.90	87.17 ± 4.63
LDA (w=90)	60.29 ± 2.49	61.41 ± 2.44	73.75 ± 2.57	74.13 ± 3.75

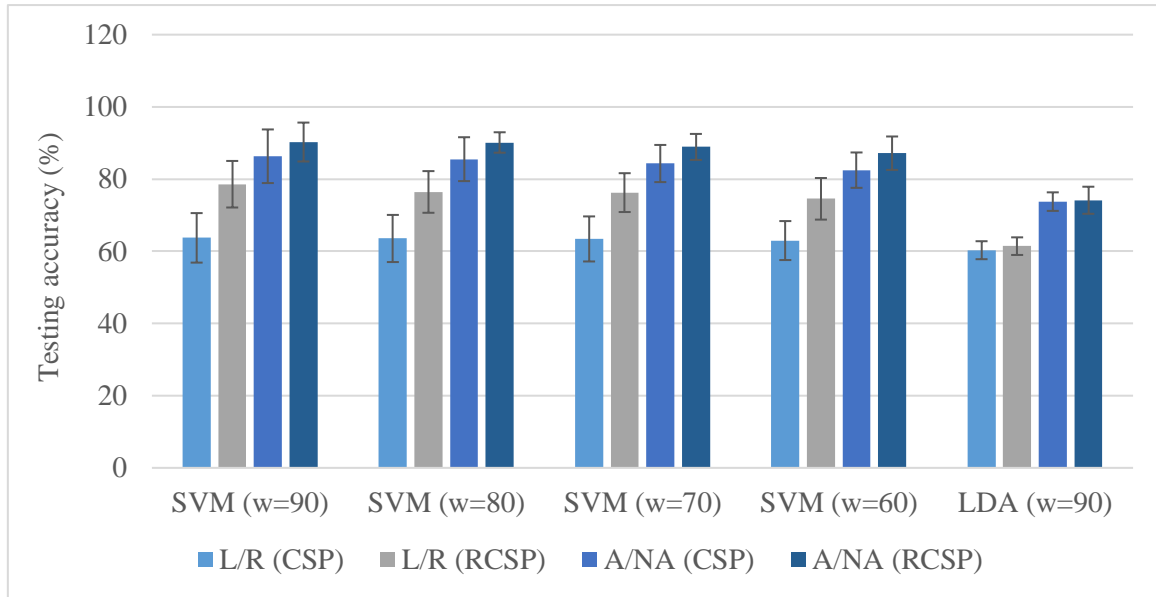


Figure 6.5. Average testing accuracy of the classifications results of left versus right (L/R) steps and adaptation versus non-adaptation (A/NA) steps, based on CSP and RCSP feature extraction. The results are shown across different sizes of sliding window (w) with a range from 90 to 60 samples

According to table 6.2 and figure 6.5, in terms of adaptation versus non-adaptation, the highest classification (90.26 ± 5.39 %) was obtained when using the SVM method with a sliding window of 90 samples, based on RCSP algorithm. Regarding the right-left steps classification, the highest classification was also obtained with the same method, although the accuracy is significantly lower (78.57 ± 6.45 %).

The 10-fold cross-validation generalization loss of the classifications results for the right versus left gait cycles and for the adaptation versus non-adaptation steps are summarized in table 6.3 and illustrated in figure 6.6. Figure 6.6 demonstrates the generalization loss of the classifications results of left versus right (L/R) steps and adaptation versus non-adaptation (A/NA) steps, based on CSP and RCSP feature extraction. The results are shown across different sizes of sliding window (w) with a range from 90 samples to 60 samples, where 90 samples correspond to 0.36 seconds, whereas the event duration is taken to be 0.4 seconds

Table 6.3. 10-fold cross-validation generalization loss of the classifications results for the right versus left gait cycles and for the adaptation versus non-adaptation steps, based on CSP and RCSP. The results are shown across different sizes of sliding window (w) with a range from 90 to 60 samples.

	Generalisation Loss			
	L/R (CSP)	L/R (RCSP)	A/NA (CSP)	A/NA (RCSP)
SVM (w=90)	0.19 ± 0.10	0.14 ± 0.03	0.09 ± 0.04	0.06 ± 0.04
SVM (w=80)	0.24 ± 0.04	0.17 ± 0.03	0.10 ± 0.04	0.06 ± 0.02
SVM (w=70)	0.26 ± 0.02	0.17 ± 0.03	0.11 ± 0.04	0.07 ± 0.02
SVM (w=60)	0.25 ± 0.04	0.19 ± 0.03	0.12 ± 0.03	0.09 ± 0.03
LDA (w=90)	0.40 ± 0.03	0.38 ± 0.02	0.39 ± 0.06	0.25 ± 0.04

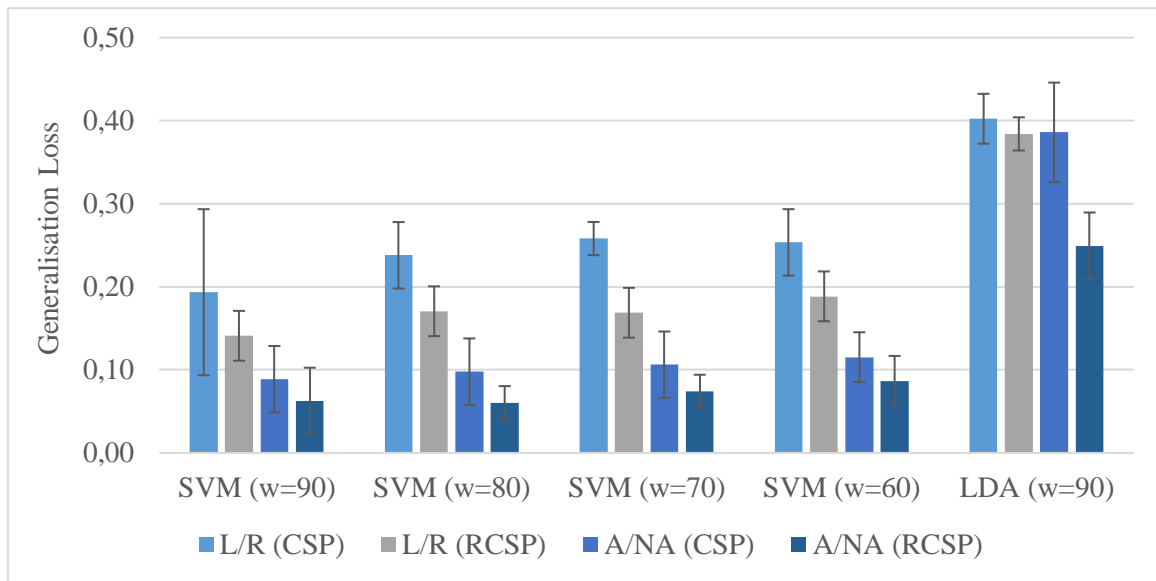


Figure 6.6. 10-fold cross-validation generalization loss of the classifications results of left versus right (L/R) steps and adaptation versus non-adaptation (A/NA) steps, based on CSP and RCSP feature extraction. The results are shown across different sizes of sliding window (w) with a range from 90 to 60 samples.

Considering table 6.3 and figure 6.6, the lowest generalisation loss, in terms of adaptation versus non-adaptation, was obtained when using the SVM method with a sliding window of 90 and 80 samples, based on RCSP algorithm (0.06 ± 0.04 and 0.06 ± 0.02). Regarding the right-left steps classification, the lowest generalisation loss was also obtained when using the SVM method with a sliding window of 90, also based on the RCSP algorithm (0.14 ± 0.03).

Figure 6.7 - 6.10 evaluate the influence of the number of components to the classification accuracy, in terms of adaptation/non-adaptation and right/left steps. Figure 6.7 shows the average across subjects, 10-fold cross-validation, generalisation loss more CSP components are chosen from the most significant to less significant eigenvalues. Figure 6.8 shows the average testing accuracy across subjects as more CSP components are chosen from the most significant to less significant eigenvalues.

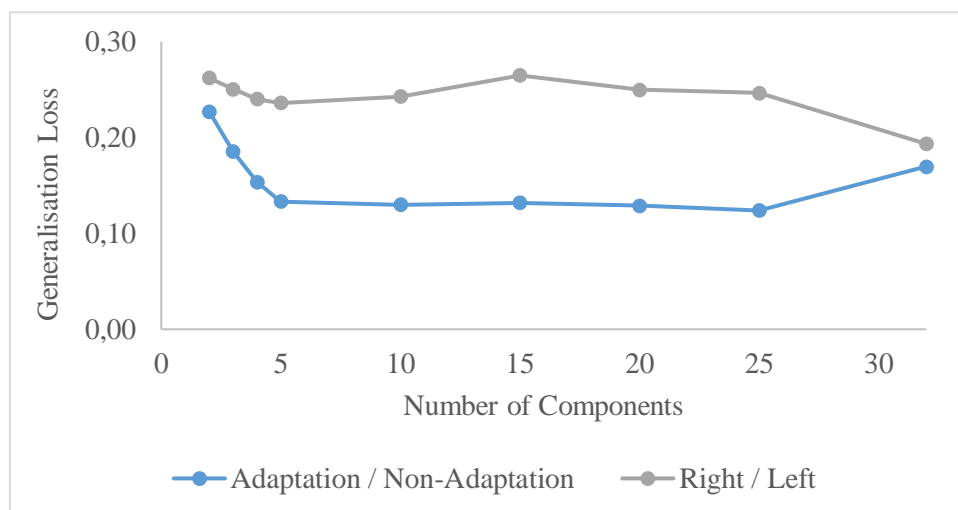


Figure 6.7. Generalisation loss for different numbers of CSP components, from the most significant to less significant eigenvalues.

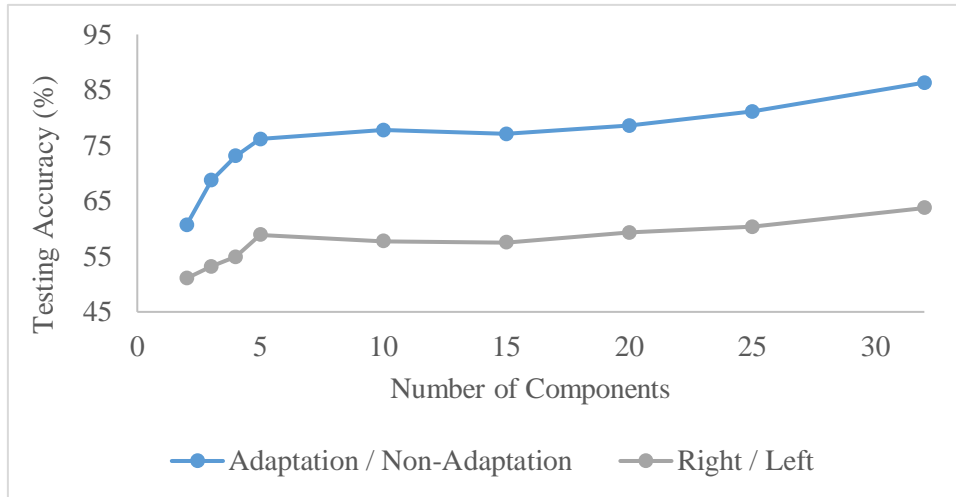


Figure 6.8. Average testing accuracy across subjects as more CSP components are chosen from the most significant to less significant eigenvalues.

Evaluating figure 6.7, it is possible to note that that for both type classifications, the error drops significantly for the first five components but it remains the same or even increases when more components are incorporated. According to figure 6.8, it is possible to infer that 5 out of 32 components are enough to achieve high accuracy, although the accuracy increases with the number of components incorporated.

Figure 6.9 shows the average across subjects, 10-fold cross-validation, generalisation loss as more RCSP components are chosen from the most significant to less significant eigenvalues. We note that for both type of two-class classification the error drops significantly for the first five components, but it remains the same or even increases when more components are incorporated. Figure 6.10 shows the average testing accuracy across subjects as more RCSP components are chosen from the most significant to less significant eigenvalues.

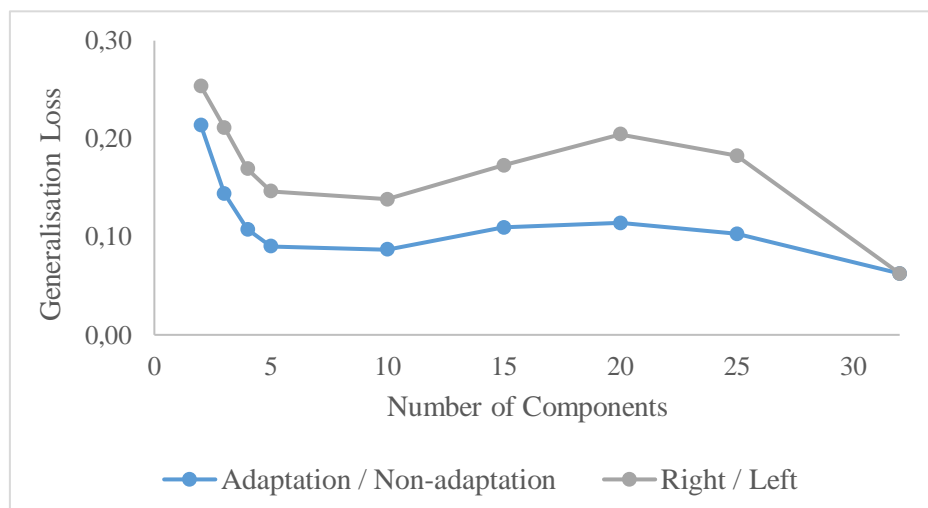


Figure 6.9. Generalisation loss for different numbers of RCSP components, from the most significant to less significant eigenvalues.

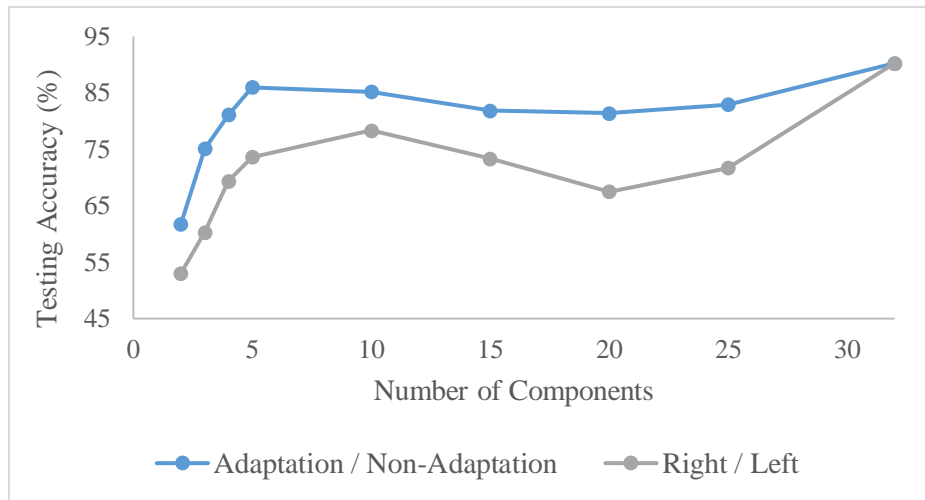


Figure 6.10. Average testing accuracy across subjects as more RCSP components are chosen from the most significant to less significant eigenvalues.

Evaluating figure 6.9 and 6.10 it is possible to verify the same similar behaviour as with the CSP method, for both the testing accuracy and generalisation loss, when the number of components incorporated varies.

Finally, figure 6.11 shows the spatial distribution of the five most significant RCSP components for one of the subjects. The top row shows the RCSP filters associated with adaptation/non-adaptation classification, whereas the bottom row shows the RCSP filters associated with right/left classification.

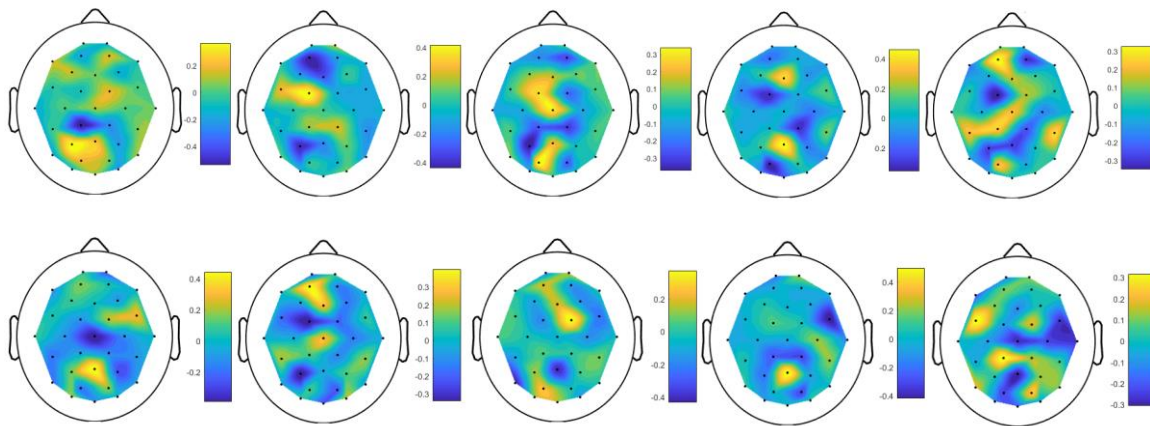


Figure 6.11. RCSP filters for the five most significant components of one of the subjects. Top row shows the RCSP filters associated with adaptation/non-adaptation classification. Bottom row shows the RCSP filters associated with right/left classification.

To compare the methods used (LDA and SVM with different values of sliding windows) based on CSP and RCSP, it was performed a paired t-test.

Table 6.4. Paired t-test to compare the methods used (LDA and SVM with different values of sliding windows) based on CSP and RCSP.

	Paired t-test	
	A / NA	L/R
SVM (w=90) CSP / SVM (w=90) RCSP	0.0489	0.0004
SVM (w=80) CSP / SVM (w=80) RCSP	0.0071	0.0001
SVM (w=70) CSP / SVM (w=70) RCSP	0.0056	0.0001
SVM (w=60) CSP / SVM (w=60) RCSP	0.0072	0.0001
LDA (w=90) CSP / LDA (w=90) RCSP	0.0010	0.0454

Considering the previous table, it is possible to verify that the p-value is lower than 0.05 in all cases, which means that it is possible to assume that a significant difference exists, between both methods (CSP and RCSP).

6.4 Discussion

According to the previous results, there is a significant improvement in the classification accuracy and generalisation loss, based on the RCSP filters for all types of classification. It is also noted that, for both experiments (left/right and adaptation/non-adaptation), that five out of 32 components are enough to achieve a high accuracy. Furthermore, the spatial distribution of the RCSP components seems to be of physiological origin.

7. Conclusions

In order to develop robust brain computer interface environments for neuro-rehabilitation of patients and robotic prosthesis control, motor imagery is an important technique. Several studies showed that MI activates partially the same brain regions as the performance of the real task and it can increase motor performance and, therefore, it is widely used in rehabilitation. To bring this technology to everyday use, relatively new EEG acquisition systems have been developed. These systems are highly portable, wireless and they are based on dry and active electrodes, which does not require the use of conductive gel. As a result, they are more prone to interference and their signal-to-noise ratio may be low. In chapter five, the classification performance of a dry 16-channel and a wet, 32-channel, wireless EEG system is compared based on a number of MI tasks along with actual movements of the limbs. According to the results, it is possible to conclude that the combination of a beta bandpass filter with a RCSP filter and the SVM classifier has shown the best classification rate (97.84 ± 1.18 % for the dry electrodes and 100.00 ± 0.00 % for the wet electrodes). These results show the feasibility of home use of dry electrode systems with a small number of sensors, making EEG systems user-friendly and more reliable.

Gait is an important activity of daily life, which requires the activation of the nervous and musculoskeletal systems and has an important role in the quality of life and independence of people. Gait adaptation plays a significant role in the ability of humans to walk and maintain their balance. In the elderly and people with neurological problems, it is an index of their health progression. Consequently, assistive robotic devices should consider this adaptation and be able to sense and adjust to gait changes. This requires the decoding of neural signals while people walk, especially in their natural environments.

Contrary to the adaptation studies today, which are based on specialized equipment, chapter six focusses on gait adaptation in natural settings. The subjects walk in a room following a tone that changes between three modes of slow, normal and fast pace, randomly. EEG signal is recorded wirelessly, and gait characteristics are extracted based on a single RGB camera. The EEG signal is pre-processed based on a bandpass filter, followed by ICA to identify and remove motion-related artefacts. Later, the extracted gait characteristics are used to epoch the EEG signal and to formulate two classification problems of intention detection in gait adaptation: i) right versus left step and ii) adaptation steps versus non-adaptation steps. Subsequently, CSP and RCSP are used to extract EEG features that maximize the discriminability between two classes. Finally, this study shows the influence of the number of components to the classification accuracy and their spatial distribution. Accordingly, to the results, participants showed the lowest adaptation time when participants adapted their walking to the normal musical tone. The classification results showed that there is a significant improvement in the classification accuracy and generalisation loss when a RCSP filter is used, both for left/right and adaptation/non-adaptation classification. Additionally, it was showed that that five out of 32 components are enough to achieve a high accuracy. Furthermore, the spatial distribution of the RCSP components seems to be of physiological origin.

In terms of challenges and limitations, there are several challenges associated with the detection of motor intention in imagery movement tasks of the legs and hands. The number and placement of EEG electrodes plays a critical role. The use of fewer channels helps to decrease the computational complexity and develop methods that allow real-time feedback to the user. The type of EEG electrodes is also quite important, since electrodes can be either wet or dry. Wet electrodes require the application of conductive gel, which improves the signal quality. However, they require long preparation times and impede the use of the technology at everyday scenarios. Dry electrodes may overcome this problem, reducing montage times and subject discomfort but the signal quality is poorer.

Another limitation of the present study, it the fact that the BCI presented is not a closed-loop BCI, which means that the user does not receive real-time feedback of the neural activity.

Artefact removal is the main challenge in intention detection, since the EEG data is highly corrupted with noise, especially when the subjects are performing motor actions. Although the literature in artefact removal is very extensive, researches haven't agreed in an optimal method to clean the EEG signal. In the past few years, artefact removal during walking and running has also been studied, but there is still not an accepted method to denoise the signal, which is highly contaminated due to the motor actions. Most of the methods developed for artefact removal during walking are based on channel-based templates, which may remove neurophysiological data.

Even though there is not a standard solution for the removal of EEG artefacts, and especially motion artefacts, ICA is one of the most used techniques to remove gait-related movement artefacts. Chapter three shows that ICA seems to be useful to remove artefacts from the EEG data, both in the motor imagery and gait adaptation studies. This technique is used mainly to remove the influence of motion and gait-related components, suggesting that motion artefacts can be minimized using ICA and filtering techniques, for posterior use with BCI analysis.

Since artefact detection and removal is an ongoing problem and there is not a standard and accepted solution, future work should focus in a more efficient removal of motion artefacts. Additionally, the system can also be designed as an open-loop BCI, in order to provide real-time feedback, allowing the user to verify if the system has the desired output and making it easier to use in real life environments.

8. References

- [1] M. R. Whittle, J.; Levine, D., *Whittle's Gait Analysis*. London, United Kingdom: Elsevier Health Sciences, 2012.
- [2] S. Lobet, C. Detrembleur, F. Massaad, and C. Hermans, "Three-dimensional gait analysis can shed new light on walking in patients with haemophilia," *ScientificWorldJournal*, vol. 2013, p. 284358, 2013.
- [3] G. A. Cavagna, F. P. Saibene, and R. Margaria, "External work in walking," *J Appl Physiol*, vol. 18, pp. 1-9, Jan 1963.
- [4] G. A. Cavagna and R. Margaria, "Mechanics of walking," *J Appl Physiol*, vol. 21, pp. 271-8, Jan 1966.
- [5] F. L. Buczek, K. M. Cooney, M. R. Walker, M. J. Rainbow, M. C. Concha, and J. O. Sanders, "Performance of an inverted pendulum model directly applied to normal human gait," *Clin Biomech (Bristol, Avon)*, vol. 21, pp. 288-96, Mar 2006.
- [6] S. Kajita, F. Kanehiro, K. Kaneko, K. Fujiwara, K. Yokoi, and H. Hirukawa, "Biped walking pattern generation by a simple three-dimensional inverted pendulum model," *Advanced Robotics*, vol. 17, pp. 131-147, 2003/01/01 2003.
- [7] J. B. Saunderson, V. T. Inman, and H. D. Eberhart, "The major determinants in normal and pathological gait," *Journal of Bone and Joint Surgery*, vol. 35, pp. 543-558, 1953.
- [8] P. Mahrkecht, S. Kiechl, B. R. Bloem, J. Willeit, C. Scherfler, A. Gasperi, *et al.*, "Prevalence and Burden of Gait Disorders in Elderly Men and Women Aged 60-97 Years: A Population-Based Study," *Plos One*, vol. 8, Jul 24 2013.
- [9] K. Koster. (30 October). *Physiopedia - Gait*. Available: <https://www.physio-pedia.com/Gait>
- [10] W. Pirker and R. Katzenschlager, "Gait disorders in adults and the elderly A clinical guide," *Wiener Klinische Wochenschrift*, vol. 129, pp. 81-95, Feb 2017.
- [11] S. Ghousayni, C. Stevens, S. Durham, and D. Ewins, "Assessment and validation of a simple automated method for the detection of gait events and intervals," *Gait & Posture*, vol. 20, pp. 266-272, Dec 2004.
- [12] A. Moevus, M. Mignotte, J. A. de Guise, and J. Meunier, "A perceptual map for gait symmetry quantification and pathology detection," *Biomedical Engineering Online*, vol. 14, Oct 29 2015.
- [13] T. Marasovic, M. Cecic, and V. Zanchi, "Ground Reaction Forces in Gait: Statistical Analysis and Interpretation," *Proceedings of the 9th Wseas International Conference on Simulation, Modelling and Optimization*, pp. 108-+, 2009.
- [14] A. Forner Cordero, H. J. F. M. Koopman, and F. C. T. van der Helm, "Use of pressure insoles to calculate the complete ground reaction forces," *Journal of Biomechanics*, vol. 37, pp. 1427-1432, 2004/09/01/ 2004.
- [15] D. T. Fong, Y. Y. Chan, Y. Hong, P. S. Yung, K. Y. Fung, and K. M. Chan, "Estimating the complete ground reaction forces with pressure insoles in walking," *J Biomech*, vol. 41, pp. 2597-601, Aug 7 2008.
- [16] E. Jovanov, A. Milenkovic, C. Otto, and P. C. de Groen, "A wireless body area network of intelligent motion sensors for computer assisted physical rehabilitation," *J Neuroeng Rehabil*, vol. 2, p. 6, Mar 1 2005.
- [17] S. J. M. Bamberg, A. Y. Benbasat, D. M. Scarborough, D. E. Krebs, and J. A. Paradiso, "Gait analysis using a shoe-integrated wireless sensor system," *Ieee Transactions on Information Technology in Biomedicine*, vol. 12, pp. 413-423, Jul 2008.

- [18] A. Sant' Anna, N. Wickström, H. Eklund, R. Zügner, and R. Tranberg, "Assessment of Gait Symmetry and Gait Normality Using Inertial Sensors: In-Lab and In-Situ Evaluation," Berlin, Heidelberg, 2013, pp. 239-254.
- [19] C. Tunca, N. Pehlivan, N. Ak, B. Arnrich, G. Salur, and C. Ersoy, "Inertial Sensor-Based Robust Gait Analysis in Non-Hospital Settings for Neurological Disorders," *Sensors*, vol. 17, Apr 2017.
- [20] P. Piriyaarasarth, M. E. Morris, A. Winter, and A. E. Bialocerkowski, "The reliability of knee joint position testing using electrogoniometry," *Bmc Musculoskeletal Disorders*, vol. 9, Jan 22 2008.
- [21] G. Dominguez, E. Cardiel, S. Arias, and P. Rogeli, "A Digital Goniometer Based on Encoders for Measuring Knee-Joint Position in an Orthosis," *2013 World Congress on Nature and Biologically Inspired Computing (Nabib)*, pp. 1-4, 2013.
- [22] D. Jarchi, C. Wong, R. M. Kwasnicki, B. Heller, G. A. Tew, and G. Z. Yang, "Gait Parameter Estimation From a Miniaturized Ear-Worn Sensor Using Singular Spectrum Analysis and Longest Common Subsequence," *IEEE Transactions on Biomedical Engineering*, vol. 61, pp. 1261-1273, Apr 2014.
- [23] L. Atallah, A. Wiik, G. G. Jones, B. Lo, J. P. Cobb, A. Amis, *et al.*, "Validation of an ear-worn sensor for gait monitoring using a force-plate instrumented treadmill," *Gait & Posture*, vol. 35, pp. 674-676, Apr 2012.
- [24] F. Deligianni, C. Wong, B. Lo, and G. Z. Yang, "A fusion framework to estimate plantar ground force distributions and ankle dynamics," *Information Fusion*, vol. 41, pp. 255-263, May 2018.
- [25] C. Yang, U. C. Ugbohue, A. Kerr, V. Stankovic, L. Stankovic, B. Carse, *et al.*, "Autonomous Gait Event Detection with Portable Single-Camera Gait Kinematics Analysis System," *Journal of Sensors*, 2016.
- [26] X. Gu, F. Deligianni, B. Lo, W. Chen, and G. Z. Yang, "Markerless gait analysis based on a single RGB camera," in *2018 IEEE 15th International Conference on Wearable and Implantable Body Sensor Networks (BSN)*, 2018, pp. 42-45.
- [27] M. H. Thaut and M. Abiru, "Rhythmic Auditory Stimulation in Rehabilitation of Movement Disorders: A Review Of Current Research," *Music Perception: An Interdisciplinary Journal*, vol. 27, pp. 263-269, 2010.
- [28] M. Roerdink, C. J. Lamoth, J. van Kordelaar, P. Elich, M. Konijnenbelt, G. Kwakkel, *et al.*, "Rhythm perturbations in acoustically paced treadmill walking after stroke," *Neurorehabil Neural Repair*, vol. 23, pp. 668-78, Sep 2009.
- [29] T. E. Howe, B. Lovgreen, F. W. Cody, V. J. Ashton, and J. A. Oldham, "Auditory cues can modify the gait of persons with early-stage Parkinson's disease: a method for enhancing parkinsonian walking performance?," *Clin Rehabil*, vol. 17, pp. 363-7, Jul 2003.
- [30] M. Roerdink, C. J. Lamoth, G. Kwakkel, P. C. van Wieringen, and P. J. Beek, "Gait coordination after stroke: benefits of acoustically paced treadmill walking," *Phys Ther*, vol. 87, pp. 1009-22, Aug 2007.
- [31] S. Grillner, "The motor infrastructure: From ion channels to neuronal networks," *Nature Reviews Neuroscience*, vol. 4, pp. 573-586, Jul 2003.
- [32] C. H. Wang, Y. Y. Wai, B. C. Kuo, Y. Y. Yeh, and J. J. Wang, "Cortical control of gait in healthy humans: an fMRI study," *Journal of Neural Transmission*, vol. 115, pp. 1149-1158, Aug 2008.
- [33] W. T. Thach and A. J. Bastian, "Role of the cerebellum in the control and adaptation of gait in health and disease," *Brain Mechanisms for the Integration of Posture and Movement*, vol. 143, pp. 353-366, 2004.

- [34] (29-01). *PhysiologyWeb – Neural Action Potentials – Refractory Periods*. Available: http://www.physiologyweb.com/lecture_notes/neuronal_action_potential/neuronal_action_potential_refractory_periods.html
- [35] J. Xu, S. Mitra, C. Van Hoof, R. F. Yazicioglu, and K. A. A. Makinwa, "Active Electrodes for Wearable EEG Acquisition: Review and Electronics Design Methodology," *IEEE Rev Biomed Eng*, vol. 10, pp. 187-198, 2017.
- [36] E. R. Kandel, J. H. Schwartz, T. M. Jessell, S. A. Siegelbaum, and A. J. Hudspeth, *Principles of Neural Science, Fifth Edition*: McGraw-Hill Education, 2012.
- [37] G. R. Muller-Putz, D. Zimmermann, B. Graimann, K. Nestinger, G. Korisek, and G. Pfurtscheller, "Event-related beta EEG-changes during passive and attempted foot movements in paraplegic patients," *Brain Research*, vol. 1137, pp. 84-91, Mar 16 2007.
- [38] M. Wieser, J. Haefeli, L. Butler, L. Jancke, R. Riener, and S. Koeneke, "Temporal and spatial patterns of cortical activation during assisted lower limb movement," *Experimental Brain Research*, vol. 203, pp. 181-191, May 2010.
- [39] A. Presacco, R. Goodman, L. Forrester, and J. L. Contreras-Vidal, "Neural decoding of treadmill walking from noninvasive electroencephalographic signals," *Journal of Neurophysiology*, vol. 106, pp. 1875-1887, Oct 2011.
- [40] G. Pfurtscheller and F. H. L. da Silva, "Event-related EEG/MEG synchronization and desynchronization: basic principles," *Clinical Neurophysiology*, vol. 110, pp. 1842-1857, Nov 1999.
- [41] T. Gilbertson, E. Lalo, L. Doyle, V. Di Lazzaro, B. Cioni, and P. Brown, "Existing motor state is favored at the expense of new movement during 13-35 Hz oscillatory synchrony in the human corticospinal system," *Journal of Neuroscience*, vol. 25, pp. 7771-7779, Aug 24 2005.
- [42] M. Seeber, R. Scherer, J. Wagner, T. Solis-Escalante, and G. R. Muller-Putz, "High and low gamma EEG oscillations in central sensorimotor areas are conversely modulated during the human gait cycle," *Neuroimage*, vol. 112, pp. 318-326, May 15 2015.
- [43] F. Deligianni, M. Centeno, D. W. Carmichael, and J. D. Clayden, "Relating resting-state fMRI and EEG whole-brain connectomes across frequency bands," *Frontiers in Neuroscience*, vol. 8, Aug 28 2014.
- [44] A. R. Sipp, J. T. Gwin, S. Makeig, and D. P. Ferris, "Loss of balance during balance beam walking elicits a multifocal theta band electrocortical response," *Journal of Neurophysiology*, vol. 110, pp. 2050-2060, Nov 2013.
- [45] J. Haefeli, S. Vogeli, J. Michel, and V. Dietz, "Preparation and performance of obstacle steps: interaction between brain and spinal neuronal activity," *European Journal of Neuroscience*, vol. 33, pp. 338-348, Jan 2011.
- [46] J. Wagner, S. Makeig, M. Gola, C. Neuper, and G. Muller-Putz, "Distinct beta Band Oscillatory Networks Subserving Motor and Cognitive Control during Gait Adaptation," *Journal of Neuroscience*, vol. 36, pp. 2212-2226, Feb 17 2016.
- [47] M. Suzuki, I. Miyai, T. Ono, I. Oda, I. Konishi, T. Kochiyama, *et al.*, "Prefrontal and premotor cortices are involved in adapting walking and running speed on the treadmill: an optical imaging study," *Neuroimage*, vol. 23, pp. 1020-1026, Nov 2004.
- [48] K. L. M. Koenraadt, E. G. J. Roelofsen, J. Duysens, and N. L. W. Keijsers, "Cortical control of normal gait and precision stepping: An fNIRS study," *Neuroimage*, vol. 85, pp. 415-422, Jan 15 2014.
- [49] H. Fukuyama, Y. Ouchi, S. Matsuzaki, Y. Nagahama, H. Yamauchi, M. Ogawa, *et al.*, "Brain functional activity during gait in normal subjects: a SPECT study," *Neurosci Lett*, vol. 228, pp. 183-6, Jun 13 1997.

- [50] L. Alcock, B. Galna, J. M. Hausdorff, S. Lord, and L. Rochester, "Gait & Posture Special Issue: Gait adaptations in response to obstacle type in fallers with Parkinson's disease," *Gait Posture*, vol. 61, pp. 368-374, Mar 2018.
- [51] S. M. Bruijn, J. H. Van Dieen, and A. Daffertshofer, "Beta activity in the premotor cortex is increased during stabilized as compared to normal walking," *Front Hum Neurosci*, vol. 9, p. 593, 2015.
- [52] P. C. Dixon, K. H. Schutte, B. Vanwanseele, J. V. Jacobs, J. T. Dennerlein, and J. M. Schiffman, "Gait adaptations of older adults on an uneven brick surface can be predicted by age-related physiological changes in strength," *Gait Posture*, vol. 61, pp. 257-262, Mar 2018.
- [53] L. Fernandez, N. Albein-Urios, M. Kirkovski, J. L. McGinley, A. T. Murphy, C. Hyde, *et al.*, "Cathodal Transcranial Direct Current Stimulation (tDCS) to the Right Cerebellar Hemisphere Affects Motor Adaptation During Gait," *Cerebellum*, vol. 16, pp. 168-177, Feb 2017.
- [54] D. Martelli, V. Vashista, S. Micera, and S. K. Agrawal, "Direction-Dependent Adaptation of Dynamic Gait Stability Following Waist-Pull Perturbations," *IEEE Trans Neural Syst Rehabil Eng*, vol. 24, pp. 1304-1313, Dec 2016.
- [55] J. M. Belda-Lois, S. Mena-del Horno, I. Bermejo-Bosch, J. C. Moreno, J. L. Pons, D. Farina, *et al.*, "Rehabilitation of gait after stroke: a review towards a top-down approach," *J Neuroeng Rehabil*, vol. 8, p. 66, Dec 13 2011.
- [56] A. H. Do, P. T. Wang, C. E. King, A. Schombs, S. C. Cramer, and Z. Nenadic, "Brain-computer interface controlled functional electrical stimulation device for foot drop due to stroke," *2012 Annual International Conference of the Ieee Engineering in Medicine and Biology Society (Embc)*, pp. 6414-6417, 2012.
- [57] A. Ramos-Murguialday, D. Broetz, M. Rea, L. Laer, O. Yilmaz, F. L. Brasil, *et al.*, "Brain-Machine Interface in Chronic Stroke Rehabilitation: A Controlled Study," *Annals of Neurology*, vol. 74, pp. 100-108, Jul 2013.
- [58] C. Neuper, M. Wortz, and G. Pfurtscheller, "ERD/ERS patterns reflecting sensorimotor activation and deactivation," *Event-Related Dynamics of Brain Oscillations*, vol. 159, pp. 211-222, 2006.
- [59] G. Pfurtscheller, C. Brunner, A. Schlogl, and F. H. L. da Silva, "Mu rhythm (de)synchronization and EEG single-trial classification of different motor imagery tasks," *Neuroimage*, vol. 31, pp. 153-159, May 15 2006.
- [60] M. Takahashi, K. Takeda, Y. Otaka, R. Osu, T. Hanakawa, M. Gouko, *et al.*, "Event related desynchronization-modulated functional electrical stimulation system for stroke rehabilitation: A feasibility study," *Journal of Neuroengineering and Rehabilitation*, vol. 9, Aug 16 2012.
- [61] J. W. Wolpaw, E. W., *Brain-Computer Interfaces: Principles and Practice*: Oxford University Press, USA, 2012.
- [62] J. J. Vidal, "Real-Time Detection of Brain Events in Eeg," *Proceedings of the Ieee*, vol. 65, pp. 633-641, 1977.
- [63] J. K. Chapin, K. A. Moxon, R. S. Markowitz, and M. A. L. Nicolelis, "Real-time control of a robot arm using simultaneously recorded neurons in the motor cortex," *Nature Neuroscience*, vol. 2, pp. 664-670, Jul 1999.
- [64] M. A. N. Lebedev, M. A., "Brain-machine interfaces: past, present and future.," *Trends Neuroscience*, vol. 29, pp. 536-546, 2006.
- [65] L. A. Farwell and E. Donchin, "Talking Off the Top of Your Head - toward a Mental Prosthesis Utilizing Event-Related Brain Potentials," *Electroencephalography and Clinical Neurophysiology*, vol. 70, pp. 510-523, Dec 1988.

- [66] J. R. Wolpaw, D. J. McFarland, G. W. Neat, and C. A. Forneris, "An Eeg-Based Brain-Computer Interface for Cursor Control," *Electroencephalography and Clinical Neurophysiology*, vol. 78, pp. 252-259, Mar 1991.
- [67] F. Galan, M. Nuttin, E. Lew, P. W. Ferrez, G. Vanacker, J. Philips, *et al.*, "A brain-actuated wheelchair: Asynchronous and non-invasive Brain-computer interfaces for continuous control of robots," *Clinical Neurophysiology*, vol. 119, pp. 2159-2169, Sep 2008.
- [68] J. R. Wolpaw, N. Birbaumer, D. J. McFarland, G. Pfurtscheller, and T. M. Vaughan, "Brain-computer interfaces for communication and control," *Clin Neurophysiol*, vol. 113, pp. 767-91, Jun 2002.
- [69] J. D. Bayliss and D. H. Ballard, "A virtual reality testbed for brain-computer interface research," *IEEE Trans Rehabil Eng*, vol. 8, pp. 188-90, Jun 2000.
- [70] R. Sitaram, A. Caria, R. Veit, T. Gaber, G. Rota, A. Kuebler, *et al.*, "fMRI brain-computer interface: a tool for neuroscientific research and treatment," *Comput Intell Neurosci*, p. 25487, 2007.
- [71] J. Mellinger, G. Schalk, C. Braun, H. Preissl, W. Rosenstiel, N. Birbaumer, *et al.*, "An MEG-based brain-computer interface (BCI)," *Neuroimage*, vol. 36, pp. 581-93, Jul 1 2007.
- [72] S. M. Coyle, T. E. Ward, and C. M. Markham, "Brain-computer interface using a simplified functional near-infrared spectroscopy system," *Journal of Neural Engineering*, vol. 4, pp. 219-226, Sep 2007.
- [73] L. R. Hochberg, M. D. Serruya, G. M. Friehs, J. A. Mukand, M. Saleh, A. H. Caplan, *et al.*, "Neuronal ensemble control of prosthetic devices by a human with tetraplegia," *Nature*, vol. 442, pp. 164-171, Jul 13 2006.
- [74] E. C. Leuthardt, G. Schalk, J. R. Wolpaw, J. G. Ojemann, and D. W. Moran, "A brain-computer interface using electrocorticographic signals in humans," *Journal of Neural Engineering*, vol. 1, pp. 63-71, Jun 2004.
- [75] D. J. Krusienski, G. Schalk, D. J. McFarland, and J. R. Wolpaw, "A mu-rhythm matched filter for continuous control of a brain-computer interface," *IEEE Trans Biomed Eng*, vol. 54, pp. 273-80, Feb 2007.
- [76] S. P. Kelly, E. C. Lalor, C. Finucane, G. McDarby, and R. B. Reilly, "Visual spatial attention control in an independent brain-computer interface," *IEEE Trans Biomed Eng*, vol. 52, pp. 1588-96, Sep 2005.
- [77] D. P. Burke, S. P. Kelly, P. de Chazal, R. B. Reilly, and C. Finucane, "A parametric feature extraction and classification strategy for brain-computer interfacing," *IEEE Trans Neural Syst Rehabil Eng*, vol. 13, pp. 12-7, Mar 2005.
- [78] L. Qin and B. He, "A wavelet-based time-frequency analysis approach for classification of motor imagery for brain-computer interface applications," *J Neural Eng*, vol. 2, pp. 65-72, Dec 2005.
- [79] Q. Wei, Y. Wang, X. Gao, and S. Gao, "Amplitude and phase coupling measures for feature extraction in an EEG-based brain-computer interface," *J Neural Eng*, vol. 4, pp. 120-9, Jun 2007.
- [80] H. Ramoser, J. Muller-Gerking, and G. Pfurtscheller, "Optimal spatial filtering of single trial EEG during imagined hand movement," *IEEE Transactions on Rehabilitation Engineering*, vol. 8, pp. 441-446, Dec 2000.
- [81] F. Lotte and C. T. Guan, "Regularizing Common Spatial Patterns to Improve BCI Designs: Unified Theory and New Algorithms," *IEEE Transactions on Biomedical Engineering*, vol. 58, pp. 355-362, Feb 2011.
- [82] B. Reuderink and M. Poel, "Robustness of the common spatial patterns algorithm in the BCI-pipeline," 2008.

- [83] H. P. Lu, K. N. Plataniotis, and A. N. Venetsanopoulos, "Regularized Common Spatial Patterns with Generic Learning for EEG Signal Classification," *2009 Annual International Conference of the IEEE Engineering in Medicine and Biology Society, Vols 1-20*, pp. 6599+, 2009.
- [84] H. Kang, Y. Nam, and S. Choi, "Composite Common Spatial Pattern for Subject-to-Subject Transfer," *IEEE Signal Processing Letters*, vol. 16, pp. 683-686, Aug 2009.
- [85] F. G. Lotte, C., "Spatially Regularized Common Spatial Patterns for EEG Classification. ," presented at the International Conference on Pattern Recognition (ICPR), Istanbul, Turkey, 2010.
- [86] O. Ledoit and M. Wolf, "A well-conditioned estimator for large-dimensional covariance matrices," *Journal of Multivariate Analysis*, vol. 88, pp. 365-411, Feb 2004.
- [87] B. Blankertz, M. Kawanabe, R. Tomioka, F. U. Hohlefeld, V. Nikulin, K.-R. M, *et al.*, "Invariant common spatial patterns: alleviating nonstationarities in Brain-computer Interfacing," presented at the Proceedings of the 20th International Conference on Neural Information Processing Systems, Vancouver, British Columbia, Canada, 2007.
- [88] A. N. Tikhonov, "Regularization of Incorrectly Posed Problems," *Soviet Mathematics Doklady*, vol. 4, pp. 1624-1627, 1963.
- [89] S. Lemm, C. Schafer, and G. Curio, "BCI competition 2003 - Data set III: Probabilistic modeling of sensorimotor mu rhythms for classification of imaginary hand movements," *IEEE Transactions on Biomedical Engineering*, vol. 51, pp. 1077-1080, Jun 2004.
- [90] S. N. Solhjoo, M. A.; Golpayegani, H., "Classification of chaotic signals using HMM classifiers:EEG-based mental task classification," *2005 13th European Signal Processing Conference*, pp. 1-4, 2005.
- [91] F. Lotte, L. Bougrain, A. Cichocki, M. Clerc, M. Congedo, A. Rakotomamonjy, *et al.*, "A review of classification algorithms for EEG-based brain-computer interfaces: a 10 year update," *J Neural Eng*, vol. 15, p. 031005, Jun 2018.
- [92] P. Shenoy, M. Krauledat, B. Blankertz, R. P. Rao, and K. R. Muller, "Towards adaptive classification for BCI," *J Neural Eng*, vol. 3, pp. R13-23, Mar 2006.
- [93] L. Deng and D. Yu, *Deep Learning: Methods and Applications*: Now Publishers, 2014.
- [94] Y. Renard, F. Lotte, G. Gibert, M. Congedo, E. Maby, V. Delannoy, *et al.*, "OpenViBE: An Open-Source Software Platform to Design, Test, and Use Brain-Computer Interfaces in Real and Virtual Environments," *Presence-Teleoperators and Virtual Environments*, vol. 19, pp. 35-53, Feb 2010.
- [95] G. Schalk, D. J. McFarland, T. Hinterberger, N. Birbaumer, and J. R. Wolpaw, "BCI2000: a general-purpose brain-computer interface (BCI) system," *IEEE Transactions on Biomedical Engineering*, vol. 51, pp. 1034-1043, 2004.
- [96] (April). *TOBI : Tools for Brain-Computer Interaction*. Available: <http://archiveweb.epfl.ch/www.tobi-project.org/>
- [97] C. Andreas Kothe and S. Makeig, *BCILAB: A platform for Brain-Computer interface development* vol. 10, 2013.
- [98] P. Perego, L. Maggi, S. Parini, and G. Andreoni, *BCI++: A New Framework for Brain Computer Interface Application*, 2009.
- [99] I. P. Susila, S. i. Kanoh, K.-i. Miyamoto, and T. Yoshinobu, *xBCI: A Generic Platform for Development of an Online BCI System* vol. 5, 2010.
- [100] L. Bianchi, F. Babiloni, F. Cincotti, S. Salinari, and M. G Marciani, *Introducing BF++: A C++ framework for cognitive bio-feedback systems design* vol. 42, 2003.
- [101] B. Venthur, S. Scholler, J. Williamson, S. Dahne, M. S. Treder, M. T. Kramarek, *et al.*, "Pyff - a pythonic framework for feedback applications and stimulus presentation in neuroscience," *Front Neurosci*, vol. 4, p. 179, 2010.

- [102] C. Vidaurre, T. H. Sander, and A. Schlogl, "BioSig: the free and open source software library for biomedical signal processing," *Comput Intell Neurosci*, vol. 2011, p. 935364, 2011.
- [103] M. Jeannerod, "The Representing Brain - Neural Correlates of Motor Intention and Imagery," *Behavioral and Brain Sciences*, vol. 17, pp. 187-202, Jun 1994.
- [104] T. Hanakawa, I. Immisch, K. Toma, M. A. Dimyan, P. Van Gelderen, and M. Hallett, "Functional properties of brain areas associated with motor execution and imagery," *Journal of Neurophysiology*, vol. 89, pp. 989-1002, Feb 2003.
- [105] G. Pfurtscheller and C. Neuper, "Motor imagery and direct brain-computer communication," *Proceedings of the Ieee*, vol. 89, pp. 1123-1134, Jul 2001.
- [106] A. Kubler, F. Nijboer, J. Mellinger, T. M. Vaughan, H. Pawelzik, G. Schalk, *et al.*, "Patients with ALS can use sensorimotor rhythms to operate a brain-computer interface," *Neurology*, vol. 64, pp. 1775-1777, May 24 2005.
- [107] R. Scherer, A. Mohapp, P. Grieshofer, G. Pfurtscheller, and C. Neuper, "Sensorimotor EEG patterns during motor imagery in hemiparetic stroke patients," vol. 9, 2007.
- [108] M. Bakker, F. P. de Lange, J. A. Stevens, I. Toni, and B. R. Bloem, "Motor imagery of gait: a quantitative approach," *Experimental Brain Research*, vol. 179, pp. 497-504, May 2007.
- [109] J. Decety, D. Perani, M. Jeannerod, V. Bettinardi, B. Tadary, R. Woods, *et al.*, "Mapping Motor Representations with Positron Emission Tomography," *Nature*, vol. 371, pp. 600-602, Oct 13 1994.
- [110] S. Hetu, M. Gregoire, A. Saimpont, M. P. Coll, F. Eugene, P. E. Michon, *et al.*, "The neural network of motor imagery: An ALE meta-analysis," *Neuroscience and Biobehavioral Reviews*, vol. 37, pp. 930-949, Jun 2013.
- [111] R. Dickstein, A. Dunskey, and E. Marcovitz, "Motor imagery for gait rehabilitation in post-stroke hemiparesis," *Physical Therapy*, vol. 84, pp. 1167-1177, Dec 2004.
- [112] K. M. Oostra, A. Oomen, G. Vanderstraeten, and G. Vingerhoets, "Influence of Motor Imagery Training on Gait Rehabilitation in Sub-Acute Stroke: A Randomized Controlled Trial," *Journal of Rehabilitation Medicine*, vol. 47, pp. 204-209, Mar 2015.
- [113] I. Navarro, F. Sepulveda, and B. Hubais, "A comparison of time, frequency and ICA based features and five classifiers for wrist movement classification in EEG signals," *2005 27th Annual International Conference of the Ieee Engineering in Medicine and Biology Society, Vols 1-7*, pp. 2118-2121, 2005.
- [114] F. S. Ghani, H.; Anwar, D.; Farooq, O.; Khan, Y., "Classification of Wrist Movements Using EEG Signals," *Journal of Next Generation Information Technology (JNIT)*, vol. 4, pp. 29-39, 2013.
- [115] S. Boudet, L. Peyrodie, P. Gallois, and C. Vasseur, "Filtering by optimal projection and application to automatic artifact removal from EEG," *Signal Processing*, vol. 87, pp. 1978-1992, 2007/08/01/ 2007.
- [116] S. Boudet, L. Peyrodie, G. Forzy, A. Pinti, H. Toumi, and P. Gallois, "Improvements of Adaptive Filtering by Optimal Projection to filter different artifact types on long duration EEG recordings," *Comput Methods Programs Biomed*, vol. 108, pp. 234-49, Oct 2012.
- [117] G. Gratton, M. G. H. Coles, and E. Donchin, "A New Method for Off-Line Removal of Ocular Artifact," *Electroencephalography and Clinical Neurophysiology*, vol. 55, pp. 468-484, 1983.
- [118] M. K. Islam, A. Rastegarnia, and Z. Yang, "Methods for artifact detection and removal from scalp EEG: A review," *Neurophysiologie Clinique-Clinical Neurophysiology*, vol. 46, pp. 287-305, Nov 2016.
- [119] J. A. Uriguen and B. Garcia-Zapirain, "EEG artifact removal-state-of-the-art and guidelines," *Journal of Neural Engineering*, vol. 12, Jun 2015.

- [120] C. J. James and C. W. Hesse, "Independent component analysis for biomedical signals," *Physiological Measurement*, vol. 26, pp. R15-R39, Feb 2005.
- [121] T. P. Jung, C. Humphries, T. W. Lee, S. Makeig, M. J. McKeown, V. Iragui, *et al.*, "Extended ICA removes artifacts from electroencephalographic recordings," *Advances in Neural Information Processing Systems 10*, vol. 10, pp. 894-900, 1998.
- [122] J. Iriarte, E. Urrestarazu, M. Valencia, M. Alegre, A. Malanda, C. Viteri, *et al.*, "Independent component analysis as a tool to eliminate artifacts in EEG: A quantitative study," *Journal of Clinical Neurophysiology*, vol. 20, pp. 249-257, Jul-Aug 2003.
- [123] P. Berg and M. Scherg, "Dipole modelling of eye activity and its application to the removal of eye artefacts from the EEG and MEG," *Clin Phys Physiol Meas*, vol. 12 Suppl A, pp. 49-54, 1991.
- [124] T. D. Lagerlund, F. W. Sharbrough, and N. E. Busacker, "Spatial filtering of multichannel electroencephalographic recordings through principal component analysis by singular value decomposition," *J Clin Neurophysiol*, vol. 14, pp. 73-82, Jan 1997.
- [125] M. Unser and A. Aldroubi, "A review of wavelets in biomedical applications," *Proceedings of the IEEE*, vol. 84, pp. 626-638, Apr 1996.
- [126] N. E. Huang, Z. Shen, S. R. Long, M. L. C. Wu, H. H. Shih, Q. N. Zheng, *et al.*, "The empirical mode decomposition and the Hilbert spectrum for nonlinear and non-stationary time series analysis," *Proceedings of the Royal Society a-Mathematical Physical and Engineering Sciences*, vol. 454, pp. 903-995, Mar 8 1998.
- [127] D. Iatsenko, P. V. E. McClintock, and A. Stefanovska, "Nonlinear mode decomposition: A noise-robust, adaptive decomposition method," *Physical Review E*, vol. 92, Sep 29 2015.
- [128] V. J. Krishnaveni, S.; Aravind, S.; Hariharasudhan, V.; Ramadoss, K., "Automatic Identification and Removal of Ocular Artifacts from EEG using Wavelet Transform," *Measurement Science Review*, vol. 6, 2006.
- [129] M. Akhtar, W. Mitsuhashi, and C. James, *Employing spatially constrained ICA and wavelet denoising, for automatic removal of artifacts from multichannel EEG data* vol. 92, 2012.
- [130] D. Looney, L. Li, T. M. Rutkowski, D. P. Mandic, and A. Cichocki, "Ocular Artifacts Removal from EEG Using EMD," Dordrecht, 2008, pp. 831-835.
- [131] M. K. Molla, T. Tanaka, T. Rutkowski, and A. Cichocki, *Separation of EOG artifacts from EEG signals using bivariate EMD*, 2010.
- [132] D. Safieddine, A. Kachenoura, L. Albera, G. Birot, A. Karfoul, A. Pasnicu, *et al.*, "Removal of muscle artifact from EEG data: comparison between stochastic (ICA and CCA) and deterministic (EMD and wavelet-based) approaches," *EURASIP Journal on Advances in Signal Processing*, vol. 2012, p. 127, July 02 2012.
- [133] B. Mijovic, M. De Vos, I. Gligorijevic, J. Taelman, and S. Van Huffel, "Source separation from single-channel recordings by combining empirical-mode decomposition and independent component analysis," *IEEE Trans Biomed Eng*, vol. 57, pp. 2188-96, Sep 2010.
- [134] N. P. Castellanos and V. A. Makarov, "Recovering EEG brain signals: artifact suppression with wavelet enhanced independent component analysis," *J Neurosci Methods*, vol. 158, pp. 300-12, Dec 15 2006.
- [135] K. L. Snyder, J. E. Kline, H. J. Huang, and D. P. Ferris, "Independent Component Analysis of Gait-Related Movement Artifact Recorded using EEG Electrodes during Treadmill Walking," *Frontiers in Human Neuroscience*, vol. 9, Dec 1 2015.
- [136] J. T. Gwin, K. Gramann, S. Makeig, and D. P. Ferris, "Removal of Movement Artifact From High-Density EEG Recorded During Walking and Running," *Journal of Neurophysiology*, vol. 103, pp. 3526-3534, Jun 2010.

- [137] A. S. Oliveira, B. R. Schlink, W. D. Hairston, P. Konig, and D. P. Ferris, "A Channel Rejection Method for Attenuating Motion-Related Artifacts in EEG Recordings during Walking," *Front Neurosci*, vol. 11, p. 225, 2017.
- [138] B. H. Kim and S. Jo, "Real-time motion artifact detection and removal for ambulatory BCI," in *The 3rd International Winter Conference on Brain-Computer Interface*, 2015, pp. 1-4.
- [139] A. Delorme and S. Makeig, "EEGLAB: an open source toolbox for analysis of single-trial EEG dynamics including independent component analysis," *Journal of Neuroscience Methods*, vol. 134, pp. 9-21, Mar 15 2004.
- [140] S. Makeig, A. J. Bell, T. P. Jung, and T. J. Sejnowski, "Independent component analysis of electroencephalographic data," *Advances in Neural Information Processing Systems* 8, vol. 8, pp. 145-151, 1996.
- [141] T. W. Lee, M. Girolami, and T. J. Sejnowski, "Independent component analysis using an extended infomax algorithm for mixed subgaussian and supergaussian sources," *Neural Comput*, vol. 11, pp. 417-41, Feb 15 1999.
- [142] G. Pfurtscheller, C. Neuper, G. R. Muller, B. Obermaier, G. Krausz, A. Schlogl, *et al.*, "Graz-BCI: State of the art and clinical applications," *IEEE Transactions on Neural Systems and Rehabilitation Engineering*, vol. 11, pp. 177-180, Jun 2003.
- [143] D. H. Brainard, "The psychophysics toolbox," *Spatial Vision*, vol. 10, pp. 433-436, 1997.
- [144] D. G. Pelli, "The VideoToolbox software for visual psychophysics: Transforming numbers into movies," *Spatial Vision*, vol. 10, pp. 437-442, 1997.
- [145] M. Kleiner, D. Brainard, and D. Pelli, "What's new in Psychtoolbox-3?," *Perception*, vol. 36, pp. 14-14, 2007.
- [146] J. Andreu-Perez, F. Cao, H. Hagaras, and G. Z. Yang, "A Self-Adaptive Online Brain-Machine Interface of a Humanoid Robot Through a General Type-2 Fuzzy Inference System," *IEEE Transactions on Fuzzy Systems*, vol. 26, pp. 101-116, Feb 2018.
- [147] I. Domingos, F. Deligianni, and G. Yang, "Dry versus Wet EEG electrode systems in Motor Imagery Classification.", UK RAS: Robotics and Autonomous Systems, Bristol, United Kingdom, 2017
- [148] Z. Cao, T. Simon, S. E. Wei, and Y. Sheikh, "Realtime Multi-Person 2D Pose Estimation using Part Affinity Fields," *30th Ieee Conference on Computer Vision and Pattern Recognition (Cvpr 2017)*, pp. 1302-1310, 2017.
- [149] T. Simon, H. Joo, I. Matthews, and Y. Sheikh, "Hand Keypoint Detection in Single Images using Multiview Bootstrapping," *30th IEEE Conference on Computer Vision and Pattern Recognition (Cvpr 2017)*, pp. 4645-4653, 2017.
- [150] S. E. Wei, V. Ramakrishna, T. Kanade, and Y. Sheikh, "Convolutional Pose Machines," *2016 IEEE Conference on Computer Vision and Pattern Recognition (Cvpr)*, pp. 4724-4732, 2016.
- [151] H. Hassani, "Singular Spectrum Analysis: Methodology and Comparison," *Journal of Data Science*, vol. 5, pp. 239-257, 2007.
- [152] H. Abdi and L. J. Williams, "Principal component analysis," *Wiley Interdisciplinary Reviews: Computational Statistics*, vol. 2, pp. 433--459, 2010.

9. Appendix

A. Preprocessing for BCI

```
% -----  
%                               Preprocessing for BCI  
% -----  
  
close all; clear all; clc;  
  
eeglabDir = 'C:\SOFTWARE\software\eeglab_current\eeglab14_1_1b';  
mainEEGdir = 'C:\DATA\Adaptation Data\Subject 1';  
capInfo = '\\icnas3.cc.ic.ac.uk\id1016\downloads\Standard-10-20-Cap81.ced';  
eegfile = 'sub1-eeg.csv';  
[~,namef,ext] = fileparts(eegfile);  
setname = strcat(namef, '_eeglab');  
filtered_file = strcat(namef, '_eeglab', '_ica');  
  
eegData = readtable( fullfile(mainEEGdir,eegfile) , 'Delimiter', ';',  
    'ReadVariableNames', true );  
data = table2array(eegData);  
time = data(1,:);  
restCh = data(34:end,:);  
data = data(2:33,:);  
  
%Initialize eeglab and load the data  
currentPath = pwd;  
cd(eeglabDir);  
[ALLEEG EEG CURRENTSET ALLCOM] = eeglab;  
cd(currentPath);  
  
% Load the dataset  
EEG = pop_importdata('data', data, 'srate', 250);  
  
% Save dataset  
[ALLEEG EEG CURRENTSET] = pop_newset(ALLEEG, EEG, CURRENTSET, 'setname', setname,  
    'savenew', setname);  
  
% Store the dataset into EEGLAB  
[ALLEEG EEG CURRENTSET] = eeg_store(ALLEEG, EEG);  
  
eeglab redraw;  
  
% Import channel locations  
EEG.chanlocs = readlocs(capInfo);  
pop_eegplot(EEG, 1, 1, 1);  
  
% EEG filtering  
EEG = pop_eegfiltnew(EEG, 1, 30);  
  
% ICA  
EEG = pop_runica(EEG, 'extended', 1, 'interrupt', 'on');  
  
% Scalp maps  
pop_topoplot(EEG, 0, 1:32);  
pop_selectcomps(EEG, 1:32);  
  
% Components to remove  
EEG = pop_subcomp(EEG);  
  
% Save new dataset  
[ALLEEG EEG CURRENTSET] = pop_newset(ALLEEG, EEG, CURRENTSET, 'setname',  
    filtered_file, 'savenew', filtered_file);  
  
[ALLEEG EEG CURRENTSET] = eeg_store(ALLEEG, EEG);  
  
varNames = eegData.Properties.VariableNames;  
data2save = [time' EEG.data' restCh];
```

```
table2save = array2table(data2save);
tmpnames = table2save.Properties.VariableNames;

for i=1:length(tmpnames)
    table2save.Properties.VariableNames(tmpnames(i)) = varNames(i);
end

outputfile = strcat('filtered_file','.txt');
export(table2dataset(table2save),'file',outputfile,'delimiter',';');
```

B. Analysis of EEG signals based on time locked events

```
%-----  
%                               Analysis of EEG data  
%-----  
  
close all; clear all; clc;  
  
eeglabDir = 'C:\Program Files\eeglab_current\eeglab14_1_2b';  
mainEEGdir = 'C:\Users\Data\Motor Imagery\Wet Cap\Movement\subject 3';  
capInfo = '\\icnas3.cc.ic.ac.uk\id1016\downloads\Standard-10-20-Cap81.ced';  
eegfile = 'filtered_file.txt';  
[~,namef,ext] = fileparts(eegfile);  
setname = 'EEG Analysis';  
filtered_file = strcat(namef, '_eeglab', '_ica');  
  
eegData = readtable( fullfile(mainEEGdir,eegfile) , 'Delimiter', ';',  
    'ReadVariableNames', true );  
data = table2array(eegData);  
time = data(1,:);  
restCh = data(34:end,:);  
data = data(2:33,:);  
  
% Initialize eeglab and load the data  
currentPath = pwd;  
cd(eeglabDir);  
[ALLEEG EEG CURRENTSET ALLCOM] = eeglab;  
cd(currentPath);  
  
% Load the dataset  
EEG = pop_importdata('data', data, 'srate', 250);  
  
% Import channels locations  
EEG.chanlocs = readlocs(capInfo);  
  
% Import events  
cd(mainEEGdir);  
[EEG, eventnumbers] = pop_importevent(EEG, 'event', 'stimulations.txt', 'fields', ...  
    {'latency', 'type', 'duration'}, 'append', 'no', 'timeunit', 1);  
  
pop_eegplot( EEG, 1, 1, 1);  
  
% Save dataset  
[ALLEEG EEG CURRENTSET] = pop_newset(ALLEEG, EEG, CURRENTSET, 'setname', setname,  
    'savenew', setname);  
  
% Store the dataset into EEGLAB  
[ALLEEG EEG CURRENTSET ] = eeg_store(ALLEEG, EEG);  
  
eeglab redraw;  
  
pop_saveset(EEG)  
  
% Extract epochs from data  
EEG = pop_epoch( EEG, {'769'}, [0 3], 'newname', 'epochs_left', 'epochinfo',  
    'yes');  
EEG = pop_epoch( EEG, {'770'}, [0 3], 'newname', 'epochs_right', 'epochinfo',  
    'yes');  
  
% Plot channel spectra and maps  
% Change dataset to epochs_left or epochs_right  
figure;  
pop_spectopo(EEG, 1, [0 3000], 'EEG', 'freq', [4 8 14 26], 'fregrange', [2  
30], 'electrodes', 'on');
```

C. Peak Detection method

```
function [maxtab, mintab]=peakdet(v, delta, x)

% PEAKDET Detect peaks in a vector
% [MAXTAB, MINTAB] = PEAKDET(V, DELTA) finds the local maxima and minima ("peaks")
% in the vector V.
% Eli Billauer, 3.4.05 (Explicitly not copyrighted).

maxtab = [];
mintab = [];

v = v(:);

if nargin < 3
    x = (1:length(v))';
else
    x = x(:);
    if length(v)~= length(x)
        error('Input vectors v and x must have same length');
    end
end

if (length(delta(:))>1)
    error('Input argument DELTA must be a scalar');
end

if delta <= 0
    error('Input argument DELTA must be positive');
end

mn = Inf; mx = -Inf;
mnpos = NaN; mxpos = NaN;

lookformax = 1;

for i=1:length(v)
    this = v(i);
    if this > mx, mx = this; mxpos = x(i); end
    if this < mn, mn = this; mnpos = x(i); end

    if lookformax
        if this < mx-delta
            maxtab = [maxtab ; mxpos mx];
            mn = this; mnpos = x(i);
            lookformax = 0;
        end
    else
        if this > mn+delta
            mintab = [mintab ; mnpos mn];
            mx = this; mxpos = x(i);
            lookformax = 1;
        end
    end
end
end
```